FABRICATION AND CHARACTERISATION OF SOLID-PHASE CRYSTALLISED PLASMA-DEPOSITED SILICON THIN FILMS ON GLASS FOR PHOTOVOLTAIC APPLICATIONS

AVISHEK KUMAR

NATIONAL UNIVERSITY OF SINGAPORE

2014

FABRICATION AND CHARACTERISATION OF SOLID-PHASE CRYSTALLISED PLASMA-DEPOSITED SILICON THIN FILMS ON GLASS FOR PHOTOVOLTAIC APPLICATIONS

AVISHEK KUMAR

(B.Eng., MSc-Microelectronics)

A THESIS SUBMITTED

FOR THE DEGREE OF DOCTOR OF PHILOSOPHY

DEPARTMENT OF ELECTRICAL AND COMPUTER ENGINEERING

NATIONAL UNIVERSITY OF SINGAPORE

2014

DECLARATION

I hereby declare that the thesis is my original work and it has been written by me in its entirety.
I have duly acknowledged all the sources of information which have been used in the thesis.

The thesis has also not been submitted for any degree in any university previously.

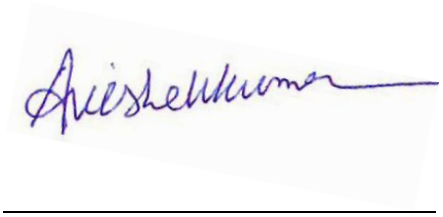

Avishek KUMAR

14th December 2014

ACKNOWLEDGEMENTS

Before I proceed further, I would like to extend my thanks to the people, who helped me to make through my PhD research journey.

Firstly, I would like to express my heartfelt gratitude and appreciation to my supervisors Prof. Armin G. Aberle, Dr. P. I. Widenborg and Dr. Goutam K. Dalapati for their valuable insights and patience in guiding me throughout the course of this research.

I am grateful to Prof. Armin Aberle for giving me an opportunity to work at the Solar Energy Research Institute of Singapore (SERIS) and for his valuable feedback on my research progress and journal publications. I thank Dr. Per Widenborg for accepting me in the Poly-Si Thin-Film group and for his patience in guiding me through my PhD. I would also like to thank Dr. Goutam Dalapati for giving me an opportunity to work in his lab and for his valuable guidance during this work. I would like to thank Dr. Bram Hoex for his scientific advice.

I thank Dr. Hidayat for his assistance with the ECV and Suns-V_{oc} characterization techniques. I am grateful to Dr. Felix Law for training me on EBSD and for his valuable insight about crystallization kinetics of poly-Si thin film. I am grateful to Dr. Sandipan Chakraborty, Selven Virasawmy and Cangming Ke for their contributions to the metallization of poly-Si thin-film solar cells. I appreciate Cangming's help with EQE measurements and Dr. Jidong Long for his assistance with the PECVD cluster tool. I would also like to extend my appreciation to

Ms. Gomathy Sandhya Subramanian for training and assistance on the Raman equipment and Saeid Masudy Panah for training me on various other equipment at IMRE. I would like to thank Nasim Sahraei for giving valuable feedback on my scientific presentations. A special thanks to Aditi Sridhar for helping me with her Photoshop skills and proof reading.

The journey at SERIS would not have been the same without the friends who made the PhD life colourful. I would like to thank Hidayat, Ziv, Kishan, Ankit, Felix, Shubham, Jai Prakash, Baochen, Johnson, Juan Wang, Wilson, and Licheng for going through the thick and thin together. A special mention goes to Pooja Chaturvedi and Dr. Swapnil Dubey for their valuable advice and sumptuous dinners at their homes. I extend my thanks to Pavithra and Aditi for filling the workspace with fun. I would also like to thank Ann Roberts and Maggie Keng for their admin support; Dr. Rolf Stangl, Dr. Thomas Mueller and Dr. Prabir Basu for enlightening and enthusiastic discussions. I would like to give special thanks to all my fellow peers and staff at SERIS who have helped me in one way or another during this journey.

Last but not the least, I would like to thank my wife, family and friends, especially Gautam, Sanglap, Saurabh, Priyanka and Swapnil for their encouragement and heartfelt support during the course of my PhD research work. This journey would not have been complete without them.

Table of Contents

Summary

Polycrystalline silicon prepared from solid-phase crystallisation (SPC) of PECVD (plasma-enhanced chemical vapour deposition) a-Si:H thin films is a promising semiconductor for the photovoltaic (PV) industry. However, poor material quality of poly-Si thin films, which acts as a bottleneck in achieving higher PV efficiency, and the relatively low deposition rate (~30 nm/min) of standard PECVD, which significantly adds to the cost of poly-Si thin-film solar cells, are two major factors that presently prevent the commercialization of this technology.

This thesis investigates the impact of the poly-Si material quality on the performance of poly-Si thin-film solar cells and extensively explores the process parameter space of a-Si:H deposition to achieve a high deposition rate for SPC poly-Si thin-film solar cells. Towards this, *n*-type poly-Si films with very large grains, exceeding 30 μm in width, and with high Hall mobility of about 71.5 cm^2/Vs are successfully prepared on glass by the SPC technique through control of the PH_3(2% in H_2)/SiH_4 gas flow ratio. A significant improvement in the efficiency of *p*-type poly-Si thin-film solar cells is demonstrated through the improvement of the material quality of the n^+ emitter layer. Furthermore, a high-rate (> 140 nm/min) conformal PECVD a-Si:H deposition process is established for the SPC method. SPC poly-Si thin films prepared from high rate deposited (146 nm/min) a-Si:H films are shown to have the same (or even slightly better) crystal quality as those deposited at a low deposition rate of ~20 nm/min.

In addition, this research work also explores new materials which have high photosensitivity, to achieve high PV efficiency at low cost. Towards this, a highly absorbing *p-type* β-$FeSi_2$(Al) semiconductor is successfully integrated with *n*-type SPC poly-Si on glass for the first time. A promising open-circuit voltage (V_{oc}) of 320 mV with pseudo fill factor (*pFF*) of 67 % is obtained for the β-$FeSi_2$(Al)/*n*-poly-Si test structure, with a scope of further improvement by inter-facial engineering and thickness optimization.

List of Tables

List of Figures

List of Symbols

C	capacitance
I_{SC}	short-circuit current
J_{SC}	short-circuit current density
ehp	electron-hole pairs
ε_0	permittivity of free space
ε_r	relative permittivity
FF	fill factor
J_o	diode saturation current density
k	Boltzmann constant
N_A	Avogadro constant
ρ	resistivity
pFF	pseudo fill factor
R_S	series resistance
R_{SH}	shunt resistance
R_{Sheet}	sheet resistance
q	elementary charge
T_{RTA}	peak temperature during the RTA process
T_S	substrate temperature
V_{OC}	open-circuit voltage

Nomenclature

a-Si	amorphous silicon
ABF	ammonium bi-fluoride
AIT	aluminium-induced texturing
AIC	aluminium induced crystallisation
BSF	back surface field
C-V	capacitance-voltage
CVD	chemical vapour deposition
e-beam	electron beam method of deposition
EBSD	electron backscatter diffraction
ECV	electrochemical capacitance-voltage
GAM	grain average misorientation
GNDs	geometrically necessary dislocations
HAADF	high angle annular dark field
HRTEM	high-resolution transmission electron microscopy
HYD	hydrogenation
IAD	ion assisted deposition
KAM	Kernel average misorientation
PECVD	plasma-enhanced chemical vapour deposition
poly-Si	polycrystalline silicon
RTA	rapid thermal annealing
RTP	rapid thermal processing
SAD	selected-area diffraction
SEM	scanning electron microscopy

SIMS	secondary ion mass spectroscopy
SPC	solid phase crystallisation
SSDs	statistically stored dislocations
STEM	scanning tunnelling electron microscopy
TEM	transmission electron microscopy
WBDF	weak beam dark-field

Chapter 1

Chapter 1- Introduction

1.1. Need for renewable energy

1.2. Photovoltaics: an effective solution

1.3. Overview of PV technologies

1.4. Poly-Si thin film solar cell

1.5. Poly-Si thin film as a template for other earth abundant materials

1.6. Organization of thesis

1.1 Need for renewable energy

More than 85% of our current global energy needs are met by fossil fuels [1]. This massive consumption has raised questions regarding the sustainability of the use of these fuels for our daily lives. Fossil fuels are not only limited in nature, but also produce greenhouse gases and toxic chemicals such as nitrogen oxides, sulphur dioxide, and volatile organic compounds as their by-products. These greenhouse gases are the main contributors of climate change as billions of tonnes of gases are released into the environment due to our global annual consumption. An imbalance in nature has thus been created due to the tremendous increase in greenhouse gases. This imbalance in nature is clearly visible in terms of an alarming increase in natural disasters such as draught, floods, hurricanes etc. Such effects of global warming are more evident than ever, with reports suggesting an accelerated melting of glaciers [2]. The melting of glaciers will result in an increase in the sea level and thus will have severe consequences. Thus, it has never been more urgent to look into alternative energy sources that are not detrimental to the environment.

Furthermore, a rapid growth in the world population over the decades has resulted in an exponential increase in consumption of fossil fuels to support the energy demands of our lifestyles. This rapid growth has, in turn, caused a shortage in energy availability for all. Recent reports state that nearly one fifth of the world population has no access to reliable electricity [3] and the energy prices are set to rise due to the limited nature of fossil fuels. This also means the world's poor will

remain alien to electricity if alternate sources of electricity are not considered [3]. The use of renewable energy is no more a choice but a necessity for the mankind. Renewable energy will, in the coming decades, not only play a key role in restoring a balance in nature, but will also provide better energy security to the world.

1.2 Photovoltaics - an effective renewable technology

Wind, solar, hydropower, geothermal, ocean and bio energy are various renewable technologies which are promising for alternative forms of energy generation [4]. Every year, the solar insolation reaching earth's surface amounts to roughly 10,000 times of mankind's total global energy consumption. This means that even if we only succeed in converting 0.1 % of the available sunlight into energy, we will have much more clean energy than we need. In addition, solar energy is one of the most abundant and widely distributed free natural resources available on earth [5, 6]. Photovoltaics (PV), the direct conversion of sunlight into electricity, is one of the most efficient ways to extract energy from the sun. However, today only ~0.1 % of the global electricity comes from PV [6]. According to the International Energy Agency (IEA), PV is expected to provide up to 11 % of total electricity by 2050 [6]. This means nearly a 100 times increase in PV capacity of what we have today. This can only be achieved through dedicated research focused on cost reduction of PV technologies and its scalability for large-scale deployment [6].

Over the last two decades the PV industry has grown at an annual rate of

30-40 % and crystalline silicon (c-Si) technology has emerged as a major driving force behind this. To make this high growth rate sustainable, it is desired to significantly reduce the cost of c-Si technology and look for other emerging PV technologies. The cost reduction in producing PV technologies can be achieved by increasing the conversion efficiency of the PV devices and by reducing the thickness of the materials.

1.3 Overview of PV technologies

Till today, traditional crystalline silicon has been used as the light absorbing semiconductor for most of the solar cells. So far, it has proven to be an effective choice and yields stable solar cells with industrial efficiencies of 16-19 % [7, 8] whereby the theoretical maximum is about 31 % for a single-junction solar cell. The highest reported efficiency for a c-Si solar cell is 25.6 %, achieved by Panasonic Corporation in its world-record HIT solar cells [7]. This technology is material intensive and traditionally uses 150- 250 cm^2 Si wafers with a thickness in the range of 180-250 µm. The PV industry is hence moving towards thinner large-area wafers to reduce the cost. However, the thickness of the wafer acts as a bottleneck for further scaling of wafer based Si solar cell technology. Further reduction in the wafer thickness below 100 µm will result in the increase in wafer breakage rate and thus yield losses [9]. In addition, a thinner wafer also suffers from a higher kerf loss [9]. Thus, in order to bring the PV system cost further down to below 1 €/W_p and compete with fossil fuel based energy, it is desired to look into alternative materials and thin-film solar cell technologies [9].

There are several materials like amorphous silicon (a-Si), cadmium telluride (CdTe), copper indium diselenide (CIS), beta iron silicide (β-$FeSi_2$) and epitaxial gallium arsenide (GaAs) on germanium (Ge), which are very strong light absorbers and therefore only need a relatively thin absorber layer for efficient solar cells, thereby reducing the material cost significantly. However, this thesis focuses on another promising c-Si based thin-film technology named poly-crystalline silicon (poly-Si) that combines the robustness of the c-Si wafer-based technology with the advantages of thin films [10]. Specifically, the thesis focuses on poly-Si thin films produced by solid phase crystallization (SPC) of amorphous silicon. This technology benefits from technical know-how from the five decade old c-Si wafer industry and from the availability of the associated production equipment.

1.4 Poly-Si thin-film technology

Thin-film SPC poly-Si is a promising semiconductor for the PV industry, mainly due to its properties (such as a standard and optimized fabrication process, robustness, scalability, excellent stability and environmental friendliness) which make it advantageous to be used as a solar cell. It is mainly composed of silicon and hydrogen, both of which are non-toxic and present in great abundance on earth. SPC poly-Si is formed from amorphous silicon (a-Si) by a standard process of deposition of a-Si on glass by plasma-enhanced chemical vapour deposition (PECVD) and then by baking it in a conventional nitrogen-purged atmospheric pressure furnace at a temperature of about 600 °C for about 12 hours.

The best efficiencies achieved so far for poly-Si thin-film solar cells on glass are 10.4 % for a 94-cm^2 mini-module using the SPC technique [11] and a record efficiency of 11.7 % for a 1-cm^2 cell using the diode laser crystallisation technique [12]. Poly-Si thin films prepared by the SPC technique seem to be more relevant for the PV industry and SPC remains so far as the only technique that has been commercialised (by CSG Solar in 2006) [13].

Significantly higher PV efficiencies seem possible for SPC poly-Si PV modules by (i) further improving the material quality of the individual layers of the poly-Si thin film ($n^+/p^-/p^+$), (ii) optimising the inter- and intra-grain defects in the poly-Si thin film, (iii) optimising the doping profiles of the n^+ and p^+ poly-Si layers (thereby improving their electronic properties), and (iv) by improving the light trapping properties of the devices. In addition, the slow deposition rate by the traditional PECVD process adds to the cost of the poly-Si thin-film solar cell production and makes the process slow. There is tremendous scope to enhance the deposition rate of amorphous Si films without significantly degrading the efficiency of the SPC poly-Si thin-film solar cells. This thesis demonstrates the fabrication and characterization of large-grain *n*-type poly-Si thin films for emitter layer applications. The impact of this emitter layer on the performance of the *p*-type poly-Si thin film is investigated in detail. A high-rate (> 140 nm/min) PECVD a-Si:H deposition process is developed that is suitable for the SPC process. A detailed investigation is performed to understand the relationships between the material quality of the SPC poly-Si thin film and the corresponding high-rate a-Si characteristics.

1.5 Poly-Si thin film as a crystalline template for other earth abundant materials

Poly-Si thin films have good stability and don't degrade over time [14]. In addition, doped poly-Si thin films are found to have very high mobilities for electrons and holes [15]. Most of the present thin-film solar cell technologies are based on earth abundant semiconductors such as β-$FeSi_2$ [16-18], Cu_2O [19], CuO [20] and amorphous Si [21] which use expensive transparent conductive oxides (TCOs) as an electrode. In some cases, TCOs are even used as *n*-type emitter layers for the formation of a *p*-*n* junction in a solar cell [19]. TCOs are not only expensive, but also have poor thermal stability and low carrier mobility. In the literature, even c-Si wafers are being used as a crystalline template to the earth abundant semiconductors and as an emitter for the formation of thin-film solar cells [17, 20]. The use of c-Si wafers is good for the demonstration of a concept, but it is not economical and finds no application at the commercial level. Thin poly-Si films (< 1 μm) with high Hall mobility and good thermal stability are technically capable of replacing both TCOs and c-Si wafers in thin-film solar cell technologies. It is also quite easy to fabricate both *n*-type and *p*-type poly-Si thin films, unlike TCOs, which are generally *n*-type in nature. Unfortunately, there are no reports in the literature where a poly-Si thin film was integrated with another earth abundant semiconductor for the formation of the solar cell. In this thesis, we demonstrate a successful integration of poly-Si thin films with one of the earth abundant materials, β-$FeSi_2$, for application in solar cells.

1.6 Organization of thesis

This thesis is sub-divided into 8 chapters.

Chapter 1 highlights the need and urgency to look into our renewable resources for energy generation and, in particular, photovoltaics as the most promising alternative source. The chapter introduces the motivation to work in the field of thin-film solar cells and the choice to focus on poly-Si on glass solar cell technology. The challenges and opportunities for poly-Si thin-film technology are also addressed in this chapter. Finally, the chapter explores the properties of poly-Si thin films that can benefit other thin-film technologies and highlights the importance of the integration of poly-Si thin films with earth abundant materials like β-$FeSi_2$. The chapter ends with an overview of the layout of this thesis.

Chapter 2 gives an overview of the background and status of the poly-Si thin-film solar cell technology. A brief overview of the process sequence adopted by SERIS for the fabrication of poly-Si on glass thin-film solar cells on glass is presented. The chapter then describes the PECVD deposition technique and other equipment used for the fabrication of the poly-Si thin-film solar cells on glass. Finally, the Chapter presents an overview of the characterisation techniques that are used in this PhD research work.

Chapter 3 presents a method to fabricate and characterise extremely large-grain *n*-type poly-Si thin films. It also presents a detailed study of the properties of the large-grained poly-Si thin films. In this chapter, *n*-type poly-Si

films with very large grains, exceeding 30 µm in width, and with high Hall mobility of about 71.5 cm^2/Vs are successfully prepared by the solid-phase crystallization (SPC) technique on glass, through the control of the PH_3 (2% in H_2)/SiH_4 gas flow ratio. The effect of this gas flow ratio on the electronic and structural quality of the *n*-type poly-Si thin film is systematically investigated using Hall Effect measurements, Raman microscopy, electron backscatter diffraction (EBSD) and high-resolution transmission electron microscopy (HRTEM).

Chapter 4 introduces a process and mechanism to improve the material quality of large-grained n-type poly-Si thin films through the control of stress in the films. In this chapter, *n*-type SPC poly-Si thin films with large grains and high crystal quality are successfully made on planar glass by controlling the stress and intra-grain misorientation in the films. The stress in the films is found to exceed 650 MPa, with a high intra-grain misorientation of up to 5°. The stress is successfully engineered to values below 130 MPa through the control of the a-Si:H deposition temperature and the PH_3 (2% in H_2)/SiH_4 gas flow ratio. The stress and intra-grain misorientations in the SPC poly-Si films are found to affect their crystal quality. The effects of the PH_3 (2% in H_2)/SiH_4 gas flow ratio and the a-Si:H deposition temperature on the material quality of the *n*-type SPC poly-Si thin films are systematically investigated using Raman microscopy and electron backscatter diffraction.

Chapter 5 presents a study on the impact of the n^+ emitter layer on the

structural and electrical properties of the *p*-type poly-Si thin-film solar cells. In this Chapter, the effect of the phosphine (PH_3) flow rate on the doping profile, in particular the peak doping concentration of the n^+ emitter layer, of SPC poly-Si thin-film solar cells on glass is investigated by electrochemical capacitance-voltage profiling. The impact of the PH_3 flow rate on the crystal quality of the poly-Si films is analysed using ultraviolet (UV) reflectance and UV/visible Raman spectroscopy. The impact of the PH_3 flow rate on the efficiency of poly-Si thin-film solar cells is investigated using electrical measurements. The best fabricated poly-Si thin-film solar cell is found to also have the highest crystal quality factor, based on both Raman and UV reflectance measurements.

Chapter 6 focuses on the optimization of PECVD process parameters space for 13.56 MHz frequency to significantly increase the deposition rate to > 150 nm/min of the a-Si:H to be used as an absorber layer in a poly-Si thin film solar cell using SPC technique. In this Chapter, the impact of the deposition parameters gas flow (sccm) and RF plasma power density (mW/cm^2) on the deposition rate of a-Si:H films is studied. A relationship between the deposition rate and the material quality of the poly-Si thin film is established. A high deposition rate of 146 nm/min is obtained through the optimization of the gas flow and the power density.

Chapter 7 highlights the advantages of the integration of poly-Si thin films with another earth abundant material. In this Chapter, aluminium-alloyed polycrystalline *p*-type *β*-phase iron disilicide *p*-*β*-$FeSi_2$(Al) films with different

thicknesses are successfully integrated with *n*-type poly-Si films on glass for thin-film solar cell applications. A sharp and high-quality interface is formed between 49 nm thick β-$FeSi_2$(Al) and poly-Si through the formation of a thin layer (~7 nm) of Al-doped p^+ epitaxial Si. The structural and photovoltaic characteristics of the *p*-type β-$FeSi_2$/p^+ Si/n^- Si/n^+ Si solar cell samples are investigated in detail.

Chapter 8 presents a summary of the PhD research work along with the author's original contributions. The chapter ends with a brief discussion of the challenges and recommendations for future work on poly-Si on glass thin-film solar cells.

References of Chapter 1

[1] J. Smith. Power up: Future energy solutions. Available: http://www.corbisimages.com/content/energy/pdf/report.noam.pdf.

[2] J. Nandi, "Glacier feeding Indus tributary melting fast, JNU study says," in *The Times of India*, ed, 1st June 2014.

[3] S. Singer, *The energy report: 100% renewable energy by 2050*: Ecofys bv, 2010.

[4] C. C. Mitigation, "IPCC special report on renewable energy sources and climate change mitigation," 2011.

[5] C. Honsberg and S. Bowden. *PVCDROM*. *2014*. Available: http://www.pveducation.org/pvcdrom.

[6] P. Frankl and S. Nowak, *Technology roadmap: solar photovoltaic energy*: OECD/IEA, 2010.

[7] M. A. Green, K. Emery, Y. Hishikawa, W. Warta, and E. D. Dunlop, "Solar cell efficiency tables (version 44)," *Progress in Photovoltaics: Research and Applications*, vol. 22, pp. 701-710, 2014.

[8] T. Saga, "Advances in crystalline silicon solar cell technology for industrial mass production," *NPG Asia Materials*, vol. 2, pp. 96-102, 2010.

[9] A. G. Aberle and P. I. Widenborg, "Crystalline Silicon Thin-Film Solar Cells via High-Temperature and Intermediate-Temperature Approaches," in *Handbook of Photovoltaic Science and Engineering*, ed: John Wiley & Sons, Ltd, 2011, pp. 452-486.

[10] A. G. Aberle, "Fabrication and characterisation of crystalline silicon thin-film materials for solar cells," *Thin Solid Films*, vol. 511–512, pp. 26-34, 2006.

[11] M. A. Green, K. Emery, Y. Hishikawa, and W. Warta, "Solar cell efficiency tables (version 35)," *Progress in Photovoltaics: Research and Applications*, vol. 18, pp. 144-150, 2010.

[12] J. Dore, D. Ong, S. Varlamov, R. Egan, and M. A. Green, "Progress in Laser-Crystallized Thin-Film Polycrystalline Silicon Solar Cells: Intermediate Layers, Light Trapping, and Metallization," *IEEE Journal of Photovoltaics*, vol. 4, pp. 33-39, 2014.

[13] P. A. Basore, "CSG-1: Manufacturing a New Polycrystalline Silicon PV Technology," in Proc. *4th IEEE World Conference on Photovoltaic Energy Conversion*, pp. 2089-2093, 2006.

[14] P. A. Basore, "Pilot production of thin-film crystalline silicon on glass modules," in Proc. 29th *IEEE Photovoltaic Specialists Conference*, pp. 49-52, 2002.

[15] A. Kumar, P. I. Widenborg, H. Hidayat, Q. Zixuan, and A. G. Aberle, "Impact of rapid thermal annealing and hydrogenation on the doping concentration and carrier mobility in solid phase crystallized poly-Si thin films," *MRS Online Proceedings Library*, vol. 1321, 2011.

[16] Z. Liu, S. Wang, N. Otogawa, Y. Suzuki, M. Osamura, Y. Fukuzawa, *et al.*, "A thin-film solar cell of high-quality β-$FeSi_2$/Si heterojunction prepared by sputtering," *Solar Energy Materials and Solar Cells*, vol. 90, pp. 276-282, 2006.

[17] G. K. Dalapati, S. L. Liew, A. S. W. Wong, Y. Chai, S. Y. Chiam, and D. Z. Chi, "Photovoltaic characteristics of *p*-β-$FeSi_2$(Al)/n-Si(100) heterojunction solar cells and the effects of interfacial engineering," *Applied Physics Letters*, vol. 98, p. 013507, 2011.

[18] N. Momose, J. Shirai, H. Tahara, Y. Todoroki, T. Hara, and Y. Hashimoto, "Toward the β-$FeSi_2$ *p-n* homo-junction structure," *Thin Solid Films*, vol. 515, pp. 8210-8215, 2007.

[19] A. T. Marin, D. Muñoz-Rojas, D. C. Iza, T. Gershon, K. P. Musselman, and J. L. MacManus-Driscoll, "Novel Atmospheric Growth Technique to Improve Both Light Absorption and Charge Collection in ZnO/Cu_2O Thin Film Solar Cells," *Advanced Functional Materials*, vol. 23, pp. 3413-3419, 2013.

[20] S. Masudy-Panah, G. K. Dalapati, K. Radhakrishnan, A. Kumar, H. R. Tan, E. Naveen Kumar, *et al.*, "*p*-CuO/*n*-Si heterojunction solar cells with high open circuit voltage and photocurrent through interfacial engineering," *Progress in Photovoltaics: Research and Applications*, 2014.

[21] J. Yang, A. Banerjee, and S. Guha, "Triple-junction amorphous silicon alloy solar cell with 14.6 % initial and 13.0 % stable conversion efficiencies," *Applied Physics Letters*, vol. 70, pp. 2975-2977, 1997.

Chapter 2

Chapter 2- Background, Fabrication and Characterization of Poly-Si Thin-Film Solar Cells

2.1. Background

2.2. Fabrication of poly-Si thin-film solar cells

2.3. Major characterization techniques

2.1 Background

More than 90 % of today's photovoltaic market is dominated by crystalline silicon (c-Si) wafer solar cells [1]. However this technology is material and energy intensive, which acts as bottleneck for further cost reductions. High-efficiency poly-Si thin-film solar modules could be a promising alternative technology to reduce the cost further.

Poly-Si thin-film solar cells on glass have the potential to reach low fabrication cost due to several reasons, such as the use of relatively inexpensive large-area glass substrates, monolithic series interconnections of the solar cells to form PV modules, and the elimination of transparent conductive oxides (TCOs) from the manufacturing process. In addition, the following properties make poly-Si thin films an interesting material for research in the quest to achieve high efficiency at low cost:

1. Capable of achieving a high efficiency of > 13 % with a single-junction device [2]. An improvement in the bulk material quality along with the reduction of the inter- and intra-grain defect density in the poly-Si thin films and an optimized light trapping scheme are expected to give such high efficiencies. This seems possible since the properties of thin-film poly-Si can be quite close to those of crystalline silicon wafers (c-Si) [3].
2. Poly-Si thin-film solar cells have good stability and don't degrade over time [4], unlike a-Si:H cells which suffer a deterioration in their performance due to light induced degradation.

3. High carrier mobility of the n^+ emitter and the p^+ back surface field (BSF) [3] allows the poly-Si thin-film technology to eliminate the need of expensive transparent conductive oxides (TCOs). TCO layers are essential but non-ideal in many thin-film solar cell technologies as they have significant optical absorption but are unavoidable in many thin-film solar cells.
4. Poly-Si thin-film solar cell modules consist of hydrogenated Si, aluminium, silicon nitride (SiN), and glass, all of which are abundant and non-toxic materials. This will further help to keep the costs of the modules in check.

Thus, all these properties make thin-film poly-Si indeed a promising PV material that combines the durability of c-Si with the benefits of thin films [5].

The solid phase crystallised (SPC) poly-Si thin-film solar cell technology was pioneered by Sanyo in the 1990s [6]. The company managed to achieve an efficiency of 9.2 % for small-area (1 cm^2) solar cells using an ITO/*p*-type a-Si/ *n*-type poly-Si/n^+-type poly-Si thin-film heterostructure fabricated on metal substrates [7]. In the 2000s, CSG Solar developed a SPC poly-Si thin-film solar cell on glass technology [8] and in 2007 managed to achieve a record efficiency of 10.4 % for a 94-cm^2 mini-module using a simple $p^+/p^-/n^+$ poly-Si homojunction solar cell [9].

There are several ways to prepare poly-Si films, such as liquid phase epitaxy (LPE) [10], epitaxial growth on Si wafers (or crystalline Si seed layers) by chemical vapour deposition (CVD) [11, 12] ion assisted deposition [13, 14]

[10,11] and from the crystallisation of the deposited a-Si:H film using SPC [6, 7, 15, 16], diode laser [17, 18] or flash lamp annealing techniques [19]. The electrical and crystalline material quality of the poly-Si films depends on a number of factors such as fabrication method, deposition parameters and the substrate temperature. The poly-Si film with best material quality to date was prepared in a thermal CVD system using a high-temperature epitaxial thickening approach on Si wafer [20]. The poly-Si thin-film solar cells fabricated from these films had efficiencies as high as 17.6 % [20]. However, this technology didn't offer any advantage over the traditional c-Si wafer cell technology which proved to be a cheaper and simpler technology option. Many researchers have since then tried to bring the cost of this technology down by growing poly-Si films epitaxially on high-quality c-Si wafers via a separation layer (oxide, porous Si, etc), thus enabling the poly-Si films to be separated from the wafers and be transferred to cheaper substrates. The best efficiencies achieved using this approach was in the range of 13-16 % for small-area solar cells [21, 22]. The scaling of this technology became an issue and it was deemed unfit with the current technology for MW scale production. However, poly-Si thin-film technology using a direct deposition approach on non-wafer-substrates remained of great interest. This approach offers great flexibility with process scalability and cost reduction. The University of New South Wales (UNSW) has explored and pioneered several such technologies for the fabrication of poly-Si thin-film solar cells on glass substrates [14, 16, 23-26].

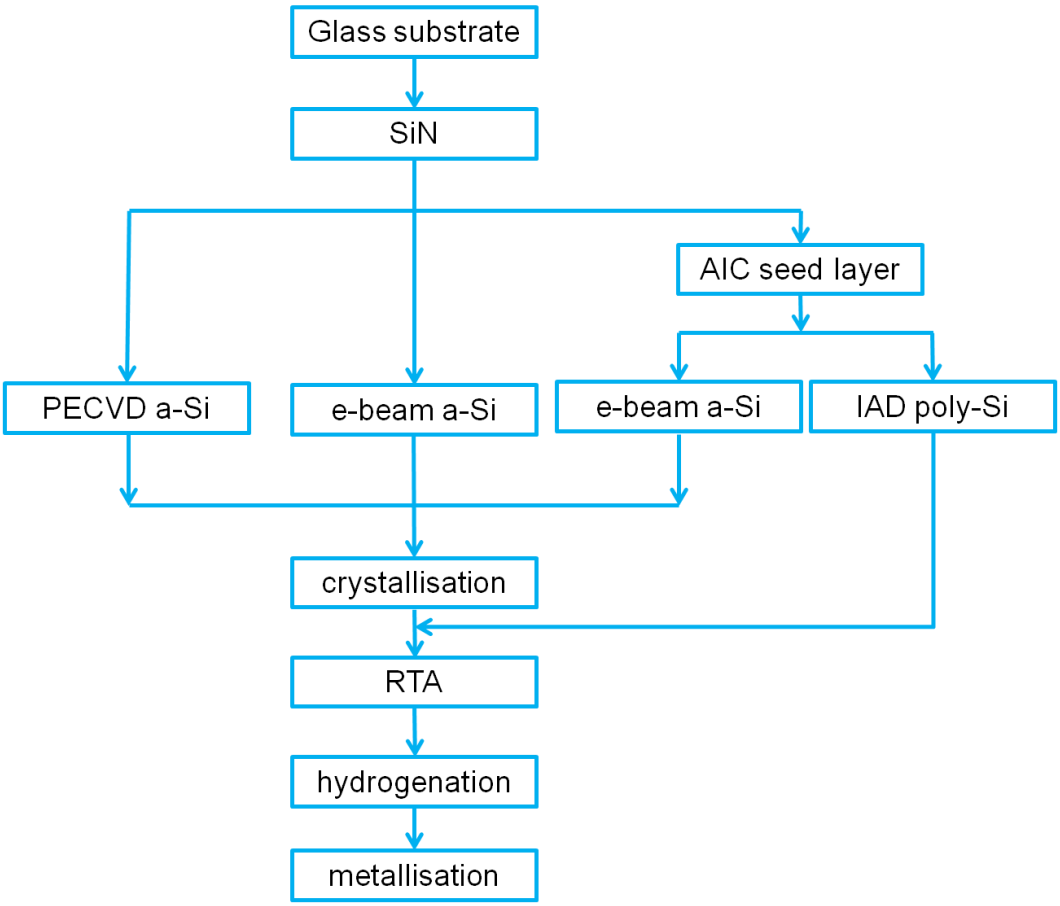

Figure 2.1: *Processing sequence of the various kinds of poly-Si on glass solar cells investigated at UNSW in recent years [23, 27, 28].*

Figure 2.1 describes the various technologies and processing steps developed at UNSW for the fabrication of the poly-Si thin-film solar cells. It can be seen that two different approaches were investigated at UNSW for the fabrication of the poly-Si thin films. One was the seed layer approach in which a thin seed layer was formed first using aluminium induced crystallization (AIC), which yielded large (> 5 µm) columnar grains, followed by epitaxial growth of the poly-Si film using ion assisted deposition (IAD). The other approach involved the solid phase crystallization (SPC) technique to fabricate poly-Si thin-film solar cells from a-Si:H films. The a-Si:H films were mainly deposited using plasma-

enhanced chemical vapour deposition (PECVD) and e-beam evaporation techniques. The reason for these technologies to emerge as the preferred deposition method at UNSW could be due to their capability of conformal deposition of a-Si:H films at high rate. However, based on the process simplicity and capability of MW scaling, poly-Si solar cells made from the SPC of PECVD a-Si:H films emerged as a technology for commercialization [29]. In addition, this technology greatly benefited from the advancement in PECVD equipment capability for large-area industrial deposition of a-Si films on glass for the liquid crystal display (LCD) industry.

CSG Solar commercialized its SPC poly-Si on glass technology in 2006 [29] and was able to achieve a world record conversion efficiency of 10.5 % for a 94-cm^2 mini-module, with an average cell V_{oc} of 492 mV, J_{sc} of 29.7 mA/cm^2 and a *FF* of 72.1% [30]. Several research groups had since then tried to fabricate poly-Si thin-film solar cells using different approaches [11, 31-36]. However no efficiency improvements were reported until recently, where two groups reported record efficiencies of *about* 11.5 to 11.7 % for small-area poly-Si thin-film solar cells prepared with liquid phase crystallization (LPC) techniques [18, 37]. While the LPC approach has emerged as a promising alternate technology for the fabrication of poly-Si thin film solar cells, its scalability and commercial viability remains a topic for further research. The thin-film poly-Si on glass solar cells prepared by SPC remains the only technique commercialised as yet [29] and has the potential to reach high efficiencies at low cost.

A significantly higher efficiency (> 13%) is possible with this technology by targeting $V_{oc,}$ J_{sc} and *FF* values of 570 mV, 35 mA/cm^2 and > 70%, respectively, which can possibly be achieved by a careful study and implementation of the following:

1. Further improvement in the material quality of the poly-Si thin film.
2. Control of the inter- and intra-grain defects in the poly-Si thin film.
3. Optimisation of the doping profiles of the n^+ and p^+ poly-Si layers (thereby improving their electronic properties).
4. Implementation of innovative light trapping schemes in the poly-Si thin-film solar cell devices.

In addition, there is a tremendous scope to bring down the cost of this technology by increasing the deposition rate of the PECVD a-Si:H films. All these promising features of SPC poly-Si thin films encouraged us to pursue further research on this technology.

The aim of this thesis is to understand the nature of the defects in SPC poly-Si thin films and to improve the material quality. In addition, the scope of this work is to significantly increase the deposition rate of PECVD a-Si:H films, without impacting the material quality of the resulting SPC poly-Si thin films and maintaining a good thickness uniformity over large area.

2.2 Fabrication process of poly-Si thin film solar cells at SERIS

This section explains the approach and process flow adopted by the Poly-Si thin-film solar cell group at the Solar Energy Research Institute of Singapore (SERIS) for the fabrication of SPC poly-Si thin-film solar cells. SERIS focuses on the research of SPC poly-Si thin-film solar cells using PECVD deposition on planar/textured glass ('PLASMA' cells). The process sequence of poly-Si thin-film solar cell fabrication at SERIS is illustrated in Figure 2.2.

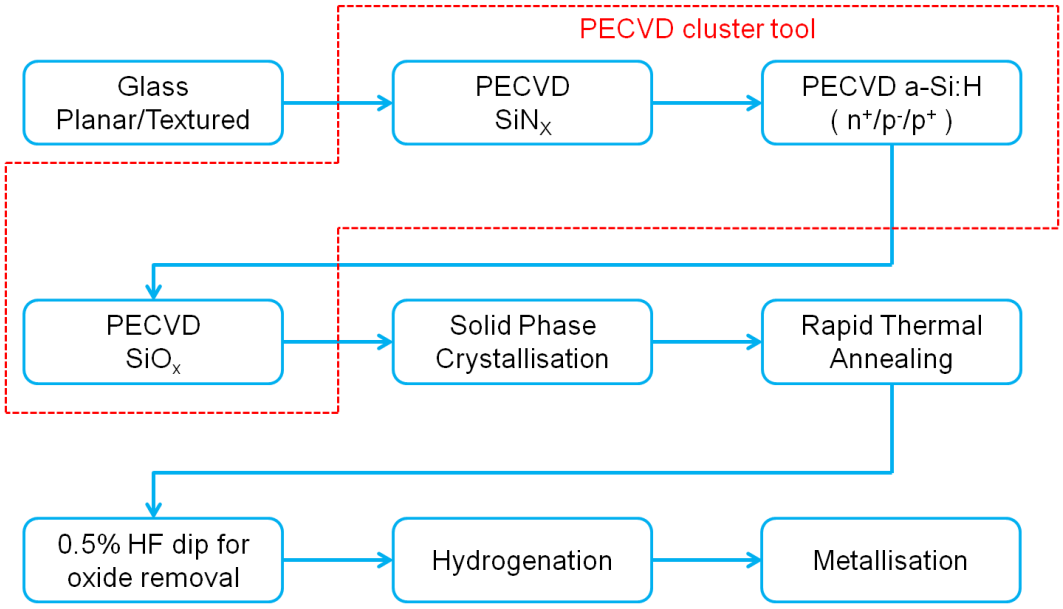

Figure 2.2: *Fabrication process of poly-Si thin-film silicon on glass solar cells at SERIS.*

2.2.1 Glass texturing

Glass texturing is required to enhance the light trapping in the poly-Si thin-film solar cells. SERIS' Poly-Si group has adopted the aluminium-induced glass texturing method ('AIT' [38]) to enhance light trapping in the poly-Si thin-film solar cells. Figure 2.3 describes the steps involved in the AIT process.

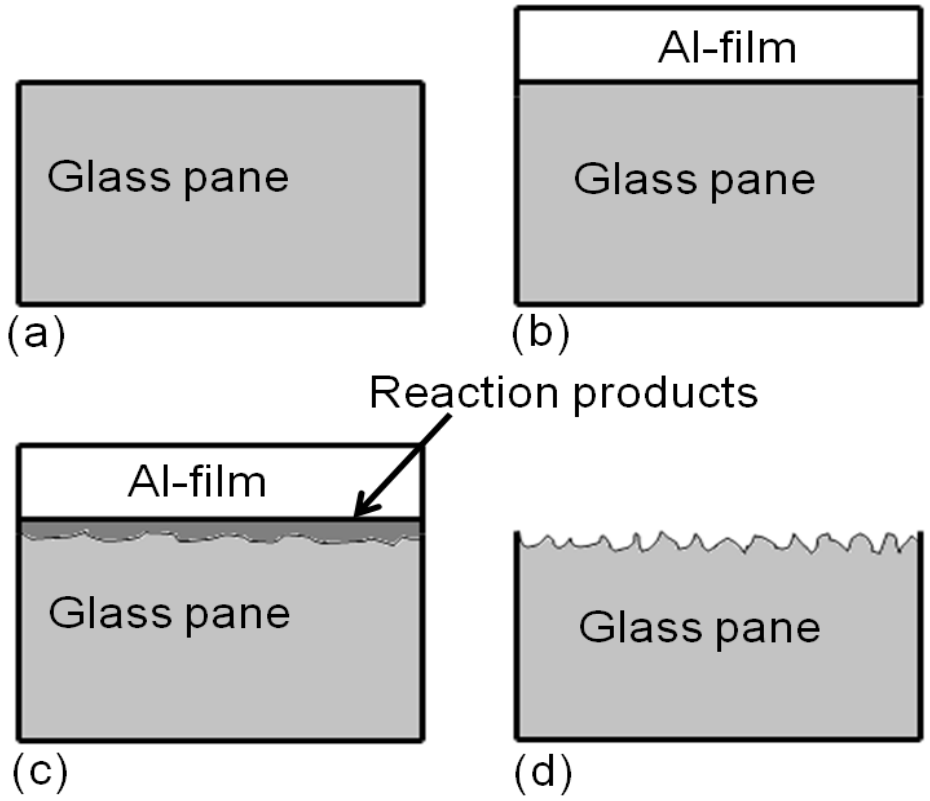

Figure 2.3: *Process sequence of the AIT technology. (a) Chemically cleaned glass pane; (b) Al deposition onto the glass pane; (c) Al reaction with glass during thermal annealing; (d) wet etching removes the reaction products, exposing the textured glass surface [39].*

The mechanism and further details on the AIT process can be found in the literature [39, 40]. AIT is a promising technique and has successfully demonstrated very good light trapping capabilities and antireflective benefits [41, 42]. The AIT surface also has very good thermal tolerance capability [38]. Figure 2.4 is a focused ion beam (FIB) microscope image of the surface of a poly-Si thin film solar cell made on an AIT glass sheet, clearly revealing the surface topography.

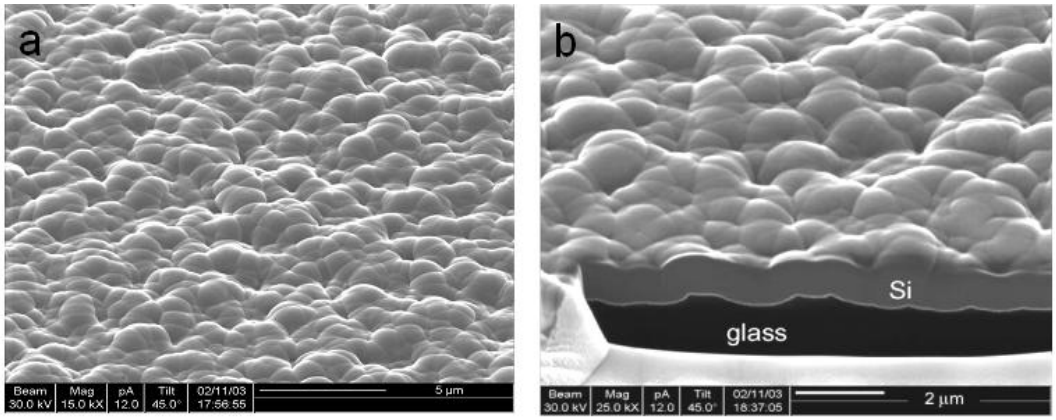

Figure 2.4: *Focus ion beam microscope images of (a) the surface morphology and (b) the cross section of a poly-Si film formed on SiN-coated AIT glass. The poly-Si film was formed by SPC of PECVD a-Si:H films. Note that the images have different scales - image a) shows a 22 µm wide region, image b) a 13 µm wide region [27].*

2.2.2 PECVD cluster tool deposition

This section first introduces the PECVD cluster tool equipment which was extensively used in this work. The section then briefly discusses the working principles of PECVD deposition techniques. The section ends with a discussion of the process flow and the standard recipe used for the fabrication of baseline diodes.

(a) Overview of the PECVD cluster tool at SERIS

A specially designed PECVD cluster tool from MV Systems, USA was used extensively in this work for the deposition of thin films on glass. The tool was capable of deposition of various kinds of inorganic films (a-Si:H, SiN_x, SiO_x, TCOs etc.) on relatively large-area (30 × 40 cm^2) glass sheets. Figure 2.5(a) shows the layout of the PECVD cluster tool used at SERIS. The tool consisted of four specially designed PECVD chambers (PL2 - PL5), a RF sputter chamber (PL8), a load lock, a parking station (PL7) and a central isolation and transfer zone (ITZ) chamber located at the centre of the tool (see Figure 2.5(b)). Figure

2.5(b) shows the top view of the ITZ chamber along with the substrate transfer system (the "Robotic Arm"). The substrates were loaded in the load lock chamber and the robotic arm was used to transfer the substrates between the load lock and the different chambers in the cluster tool. Chamber PL7 was used as a parking chamber, as well as for preheating each glass substrate before the deposition of the first PECVD layer. When not in use, all PECVD chambers were kept at a very low base pressure of ~10^{-8} mTorr. Thus, a preheating of the glass substrates was performed to reduce their moisture contents, before loading them into one of the PECVD chambers. PL2 to PL5 were the PECVD chambers, while PL8 was used for sputter deposition TCO and aluminium films. The ITZ and robotic arm ensured that substrates could be transported from one process chamber to any other without breaking the vacuum.

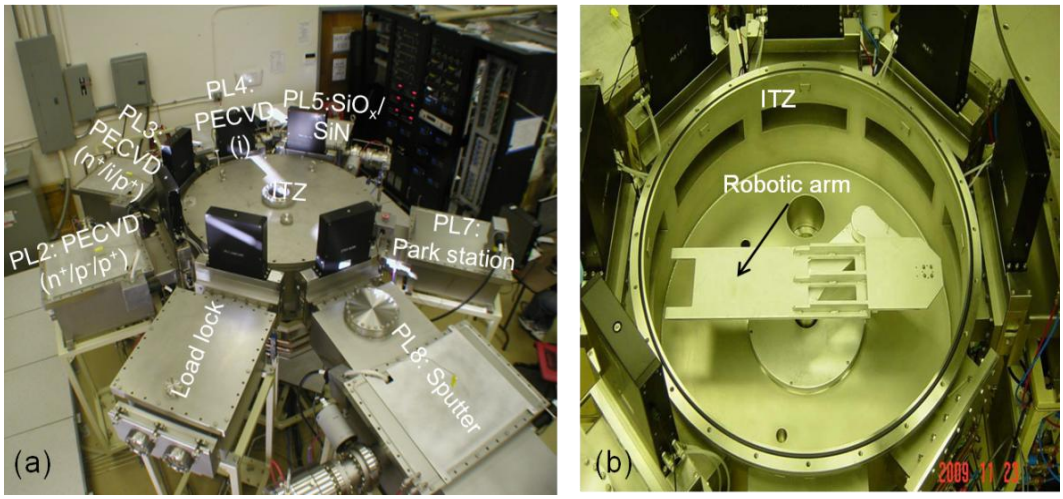

Figure 2.5: *(a) PECVD cluster tool layout, (b) Substrate transfer system.*

Furthermore, the PECVD chambers in the cluster tool were designed such that the substrate is located at the top of the chamber and the driven electrode at the bottom. This arrangement minimises the deposition of dust particles onto the

deposited film, which helps to keep the formation of pinholes in the deposited a-Si:H films under control. Figure 2.6 shows a schematic diagram of the PECVD chambers used in the cluster tool at SERIS. The substrate rests above the top electrode through the help of two dedicated tracks. The distance between the substrate and the lower electrode ('RF electrode') is controlled via adjustable legs. Figure 2.7 shows a top-view photograph of one the PECVD chambers of the cluster tool.

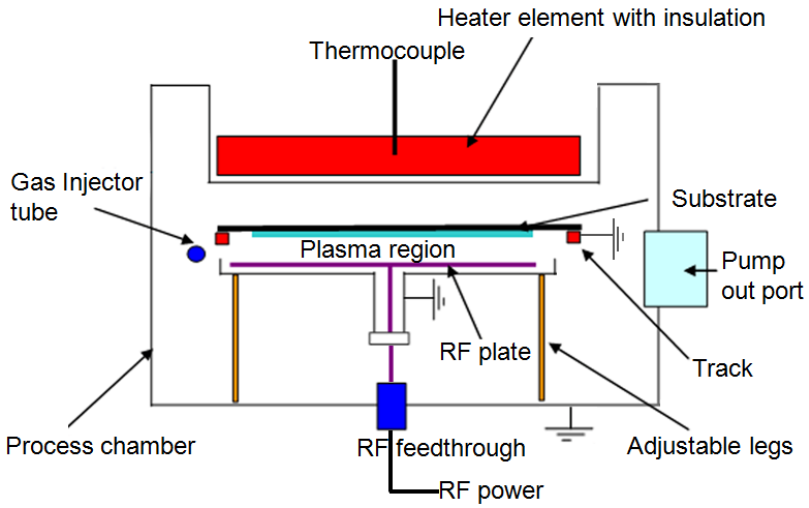

Figure 2.6: *Schematic of a typical PECVD processing chamber used in the cluster tool.*

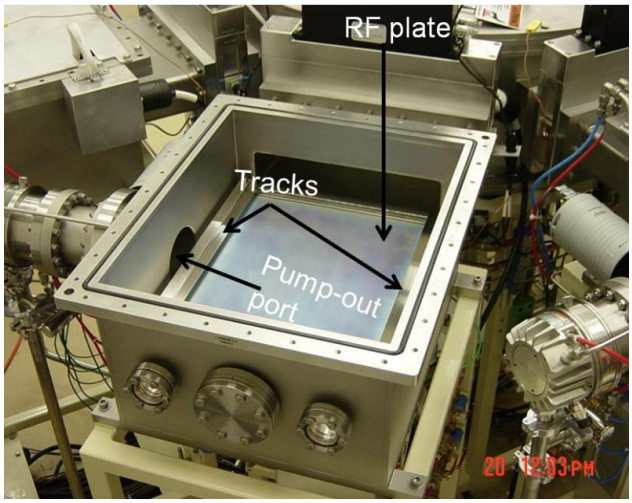

Figure 2.7: *Photograph (top view) of one of the PECVD chambers of the cluster tool.*

(b) Working principle of plasma-enhanced chemical vapour deposition

PECVD is a glow discharge technique where precursor gasses (such as SiH_4, PH_3, B_2H_6) are injected into a vacuum reactor chamber. An electric field is applied between the two electrodes which initiate the glow discharge (plasma) while a process pressure of 0.1 - 3 Torr is maintained inside the vacuum chamber. In the case of a-Si:H deposition, the whole PECVD deposition process can be broken down into four steps [42, 43]:

1. Electrical energy is transferred to the gas mixture, which results in electron impact excitation, dissociation and ionization of SiH_4 molecules. The plasma at this stage consists of molecules, neutral radicals, positive and negative ions, and electrons.
2. The reactive neutral species then approach the substrate by diffusion and the positive ions bombard the growing film while the negative ions are trapped within the sheath, which may finally form dust or small particles. The electronic and structural properties of the deposited a-Si:H film are determined in this step.
3. The third step consists of surface reactions, which include radical diffusion, chemical bonding and hydrogen abstraction.
4. Finally, there is a relaxation of the formed silicon matrix and a release of hydrogen molecules.

Figure 2.8 describes the complete PECVD deposition process of a-Si:H in a simple schematic diagram.

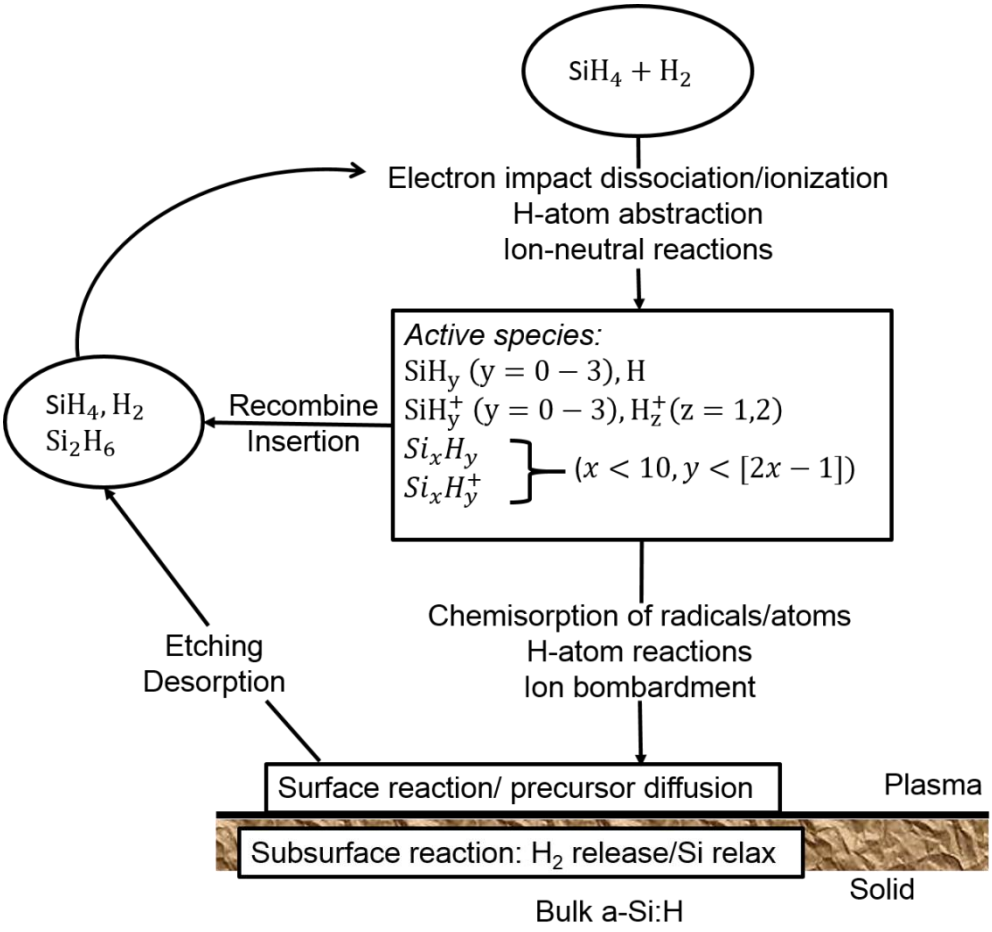

Figure 2.8: *Schematic representation of the PECVD deposition process [43].*

Furthermore, PECVD process parameters such as excitation frequency, incident power density, gas flow rate, substrate temperature, process pressure and the electrode spacing determine the deposition rate and the quality of the deposited films. Thus, these parameters need to be studied carefully to understand the relationship between deposition rate, film quality and conformity over large area. The film quality is usually established in steps 1 & 2, as described above. The dependence of these parameters on the deposition rate and the material quality of the films will be discussed in detail in Chapter 6.

PECVD offers several advantages over other deposition techniques, which

makes it commercially more attractive. Currently, PECVD is the dominant technology for the industrial deposition of a-Si:H films. Some of the properties which make it so attractive for industry and research are: (i) ability of conformal film deposition onto textured substrates, (ii) flexibility of gas purification in liquid as well solid forms, (iii) relatively low substrate temperatures, (iv) reproducibility of the process, and (v) the ability to deposit high-quality conformal a-Si:H films over very large areas (up to 10 m^2). However, the low deposition rate of the conventional PECVD technique acts as a bottleneck for further reductions of the production costs of thin-film poly-Si solar cells and modules. One of the aims of this research is thus to explore the process parameter space of the PECVD deposition method and achieve a high-rate deposition of a-Si:H films without significantly impacting the material quality of the SPC poly-Si thin films (see Chapter 6).

(c) Fabrication of a typical baseline diode in the cluster tool

A 3.3 mm thick planar or textured glass substrate was cleaned and then loaded into the load lock (LL) of the PECVD cluster tool. The glass substrate was then transferred to the parking chamber (PL7), where it was preheated for 15 min at 150 °C to remove the moisture from the glass. The glass substrate was then transferred to a PECVD chamber (PL5) designed for silicon nitride (SiN) and silicon dioxide (SiO_x) deposition. An about 70 nm thick SiN film was deposited onto the glass substrate in this chamber. The SiN nitride coated glass sheet was then transferred to another PECVD chamber (PL2) designed for the deposition of doped a-Si:H films. Three doped layers of a-Si:H films($n^+/p^-/p^+$) were sequentially deposited onto the SiN-coated glass substrate, in the sequence shown in Fig. 2.9.

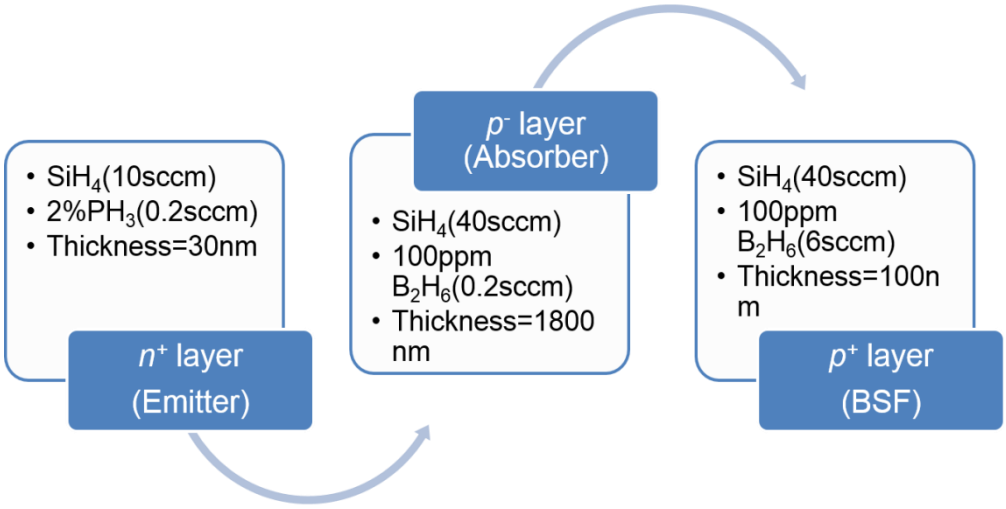

Figure 2.9: *Process sequence and the recipe for the deposition of the doped a-Si:H films.*

A 100 nm thick SiO_x film was then deposited onto the doped a-Si:H films in PL5. This SiO_x layer acts as a capping layer for impurities entering the film from the ambient during the SPC and RTA processes. Table 2.1 summarises the recipe used for the fabrication of our standard baseline samples.

Table 2.1: *Recipe used for the fabrication of the baseline diode at SERIS.*

Process condition	SiN_x	n^+ layer	p^- layer	p^+ layer	SiO_x
SiH_4 (sccm)	12	10	40	40	10
2% PH_3:H_2 (sccm)	0	0.2	0	0	0
100 ppm B_2H_6:H_2 (sccm)	0	0	0.2	6	0
NH_3 (sccm)	20	0	0	0	0
N_2 (sccm)	143	0	0	0	0
N_2O (sccm)	0	0	0	0	50
Time (s)	636	960	4905	795	200
Substrate temperature (°C)	350	380	380	380	350
Pressure (Pa)	80	80	107	107	80
RF power density (mW/cm^2)	8	8	33	33	8

2.2.3 Solid phase crystallization (SPC) of a-Si:H films

After the PECVD deposition, the a-Si:H coated glass sheets were taken out of the cluster tool and loaded into an atmospheric-pressure oven (Nabertherm, N 120/65HAC furnace, Germany) to achieve the transformation of the a-Si:H films from the amorphous to the crystalline phase. The samples were annealed in a N_2 atmosphere for 12 hours, using a defined temperature profile. Figure 2.10 shows the temperature profile used to achieve the SPC of the a-Si:H films. The a-Si:H coated glass sheets were first annealed at 450 ^{o}C for one hour to remove most of the hydrogen from the a-Si:H films. This is necessary because a large hydrogen content would create cracks in the film during the SPC process. The temperature is then ramped to 610 °C where the a-Si:H films are crystallised to poly-Si films. The temperature is kept constant at 610 °C for 10 hours, followed by natural cooling in an N_2 atmosphere. Further details about the crystallisation kinetics and the impact of the SPC annealing temperature on the properties of SPC poly-Si thin films can be found in the literature [44 - 46].

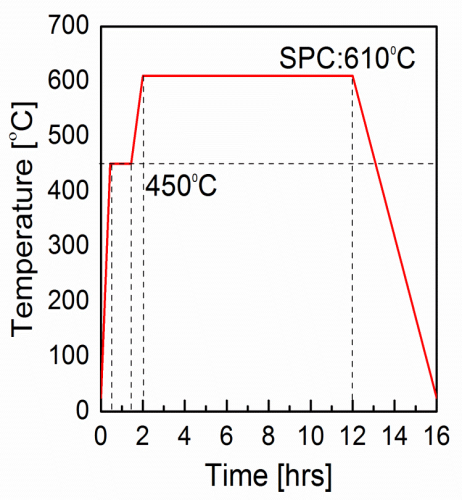

Figure 2.10: *Temperature profile used for the solid phase crystallization of the a-Si:H films.*

2.2.4 Rapid thermal annealing of poly-Si thin films

After the SPC process, the poly-Si thin films were loaded into an RTA system (RTA, CVD Equipment, USA). The RTA system was capable of processing large-area samples of up to 1200 cm^2. The poly-Si thin films were subjected to an RTA process for 1 minute at a peak temperature of 1000 ºC, using an N_2 atmosphere and a temperature profile as shown in Fig. 2.11.

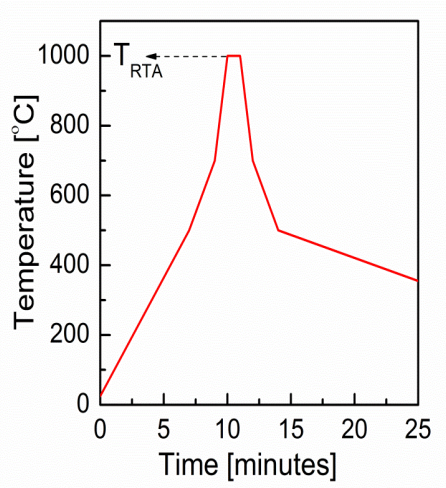

Figure 2.11: *Temperature profile used in the RTA process.*

The RTA step is required to remove crystallographic defects from the SPC poly-Si thin films and to activate the dopants. Figure 2.12 shows Hall measurement results for several n^+ poly-Si thin-film samples. The Hall mobility and the resistivity as a function of the majority carrier concentration after the SPC and RTA processes are shown in Figs. 2.12(a) and 2.12(b), respectively. A Hall mobility of 40 cm^2/Vs was obtained for an n^+ poly-Si film at a carrier concentration of 2.19×10^{19} cm^{-3}. This value increased to 71 cm^2/Vs due to the RTA process. The significant mobility increase (~77%) and the associated decrease in the resistivity confirm that the RTA process removes a substantial fraction of the

crystallographic defects and activates a large fraction of the dopants in the SPC poly-Si film. Further details about the RTA process and its impact on the structural and electrical properties of the poly-Si thin films can be found in the literature [47 - 49].

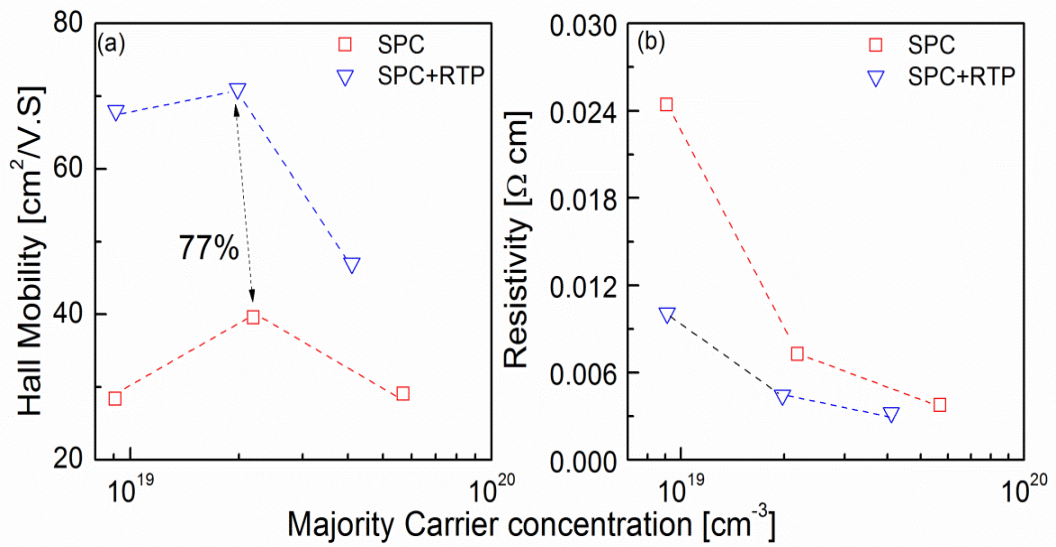

Figure 2.12: *(a) Hall mobility of n^+ poly-Si thin films as a function of the majority carrier concentration, (b) Resistivity of n^+ poly-Si thin films as a function of the majority carrier concentration.*

2.2.5 Hydrogenation of the poly-Si thin film

After the RTA process, the samples were cleaned in a diluted (5%) HF solution to remove the capping SiO_x layer, rinsed in DI water, dried with a nitrogen gun, and then immediately loaded into a single-chamber linear microwave-powered plasma system (AK800 system, Roth & Rau, Germany). The poly-Si thin-film samples were then hydrogenated in a hydrogen plasma at a substrate temperature of 475 °C. This hydrogenation step passivates the grain boundaries and defects. More details about the hydrogenation process can be found in a recent PhD thesis completed at SERIS [47]. Figure 2.13 gives a

schematic diagram of a typical baseline poly-Si thin-film diode formed using the process sequence described above.

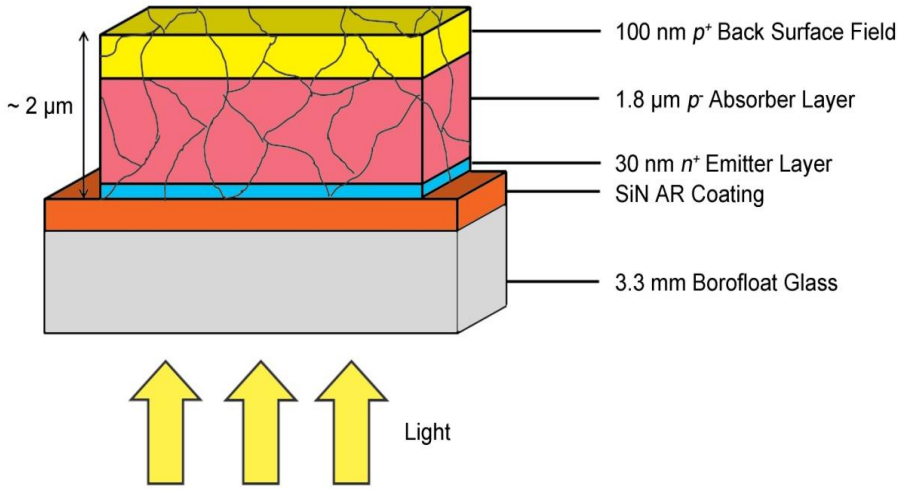

Figure 2.13: *Structure of a p-type poly-Si thin-film solar cell on planar glass.*

2.2.6 Metallisation of poly-Si thin-film diodes

After the hydrogenation process, the poly-Si thin-film diodes were metallised using an interdigitated comb-like scheme developed at UNSW [50, 51]. The metallisation scheme of fully metallised SPC poly-Si thin-film solar cells is illustrated in Figure 2.14. The final cell structure with metal fingers and busbars is shown in Fig. 2.14(a). Figure 2.14(b) shows a detailed cross-sectional view of the finger region.

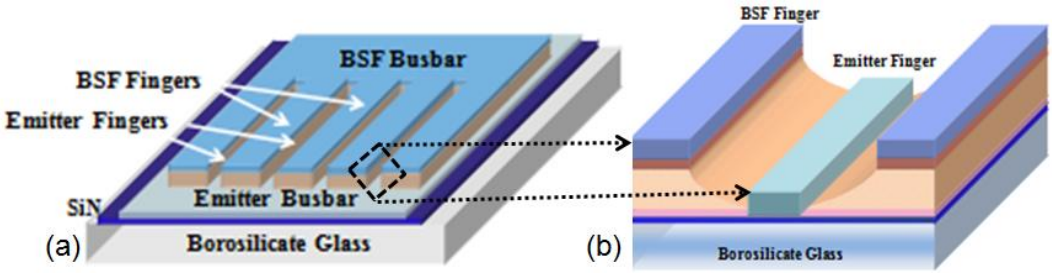

Figure 2.14: *(a) Schematic representation of the interdigitated metallisation scheme of poly-Si thin-film solar cells on glass. (b) Schematic cross-section of an emitter finger, the sloped sidewalls, and parts of two BSF fingers.*

2.3 Characterisation Techniques

Advances with various characterization techniques have played a key role in improving the efficiencies of various photovoltaic technologies. A number of ways and methods to characterise a solar cell can be found in the literature [52]. Moreover, this section particularly focuses on specific characterization techniques that have been used in this thesis to study the properties of poly-Si thin film solar cells. These techniques are divided into two sections: structural and electrical characterization.

2.3.1 Structural characterisation

2.3.1.1 Spectrophotometer

A spectrophotometer (PerkinElmer, Lambda 950, UV/Vis/NIR spectrometer) was extensively used in this work to measure the reflectance and transmission of the poly-Si thin films, in substrate as well as in superstrate configuration. Several important properties such as thickness, material quality and absorbance were extracted from these measurements.

(a) Deposition rate fitting using W.V.A.S.E

Figure 2.15 shows the reflectance data of a poly-Si thin film in the superstrate configuration (i.e., the light enters the poly-Si film through the glass sheet). The thickness of the poly-Si film is obtained by curve fitting of the measured reflectance data using the W.V.A.S.E software.

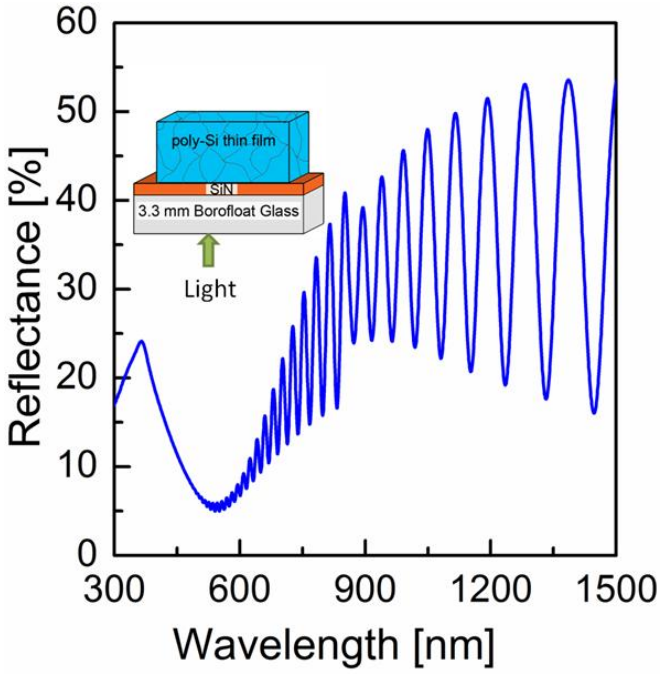

Figure 2.15: *Reflectance spectrum of an ~2 µm thick poly-Si thin film in superstrate configuration. Inset: Schematic of the measured sample.*

(b) Structural quality of poly-Si thin film (Q_r)

The structural quality of the poly-Si film can be obtained from reflectance measurements in substrate configuration at short wavelengths (UV, 250-400 nm), by comparing the measured UV reflectance with that of a polished single-crystalline Si wafer (c-Si). Two characteristic peaks closely related to the optical transition in c-Si [53] appear in the UV reflectance measurement at wavelengths of ~ 360 nm and ~275 nm (*Re1* and *Re2*, respectively). Defects in the silicon material lead to the decrease and broadening of these peaks [54]. Figure 2.16 shows the measured UV reflectance of an about 2 µm thick poly-Si thin film measured from the air side. Also shown, for comparison, is the UV reflectance measured on a polished single-crystalline Si wafer.

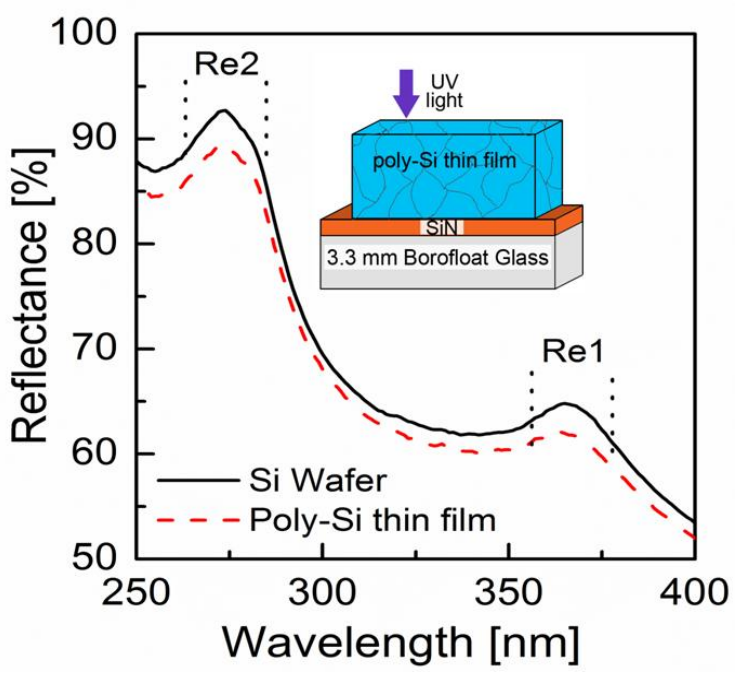

Figure 2.16: *Hemispherical UV reflectance measured on a polished single-crystalline Si wafer and a poly-Si thin film. Inset: Schematic of the measured poly-Si thin-film sample.*

A rough estimate of the crystal quality of the poly-Si film can be obtained from this graph by taking the reflectance spectra of c-Si as a reference. Furthermore, it is possible to quantify the structural quality of the poly-Si thin film by defining a crystal quality factor Q_r. The UV reflectance based crystal quality factor is derived by fitting the absolute heights of the *Re1* and *Re2* UV peaks using the following equation [55]:

$$Q_r = \frac{1}{2}\left[\frac{Re1}{Re1.cSi} + \frac{Re2}{Re2.cSi}\right]. \qquad 2.1$$

The UV-Vis-NIR measurement at wavelengths below 300 nm has a small signal-to-noise ratio. Therefore, we exclude the *Re2* to get the following equation:

$$Q_r = \frac{Re1}{Re1.cSi}. \qquad 2.2$$

The quality factor Q_r quantifies how closely the UV reflectance of a single-crystalline Si wafer is mimicked by a particular poly-Si thin-film sample and thus

provides a qualitative measure of its area-averaged crystal quality [55]. This technique is used extensively in this work to quantify the structural quality of the near-surface region of SPC poly-Si thin films.

2.3.1.2 Raman spectroscopy

Raman spectroscopy is another non-destructive characterization technique that was extensively used in this work to characterize stress and defects in polycrystalline silicon films [56 - 58]. A Witec Alpha 300R confocal Raman microscope system equipped with a 532-nm Nd:YAG laser and LabRam HR system equipped with a 325 nm (UV) and 488 nm (visible) laser line was used in this study. Typical Raman spectra acquired with the visible (532 nm) laser line on two poly-Si thin films and a single-crystalline high-resistivity FZ-grown silicon wafer (solid line) are shown in Fig. 2.17.

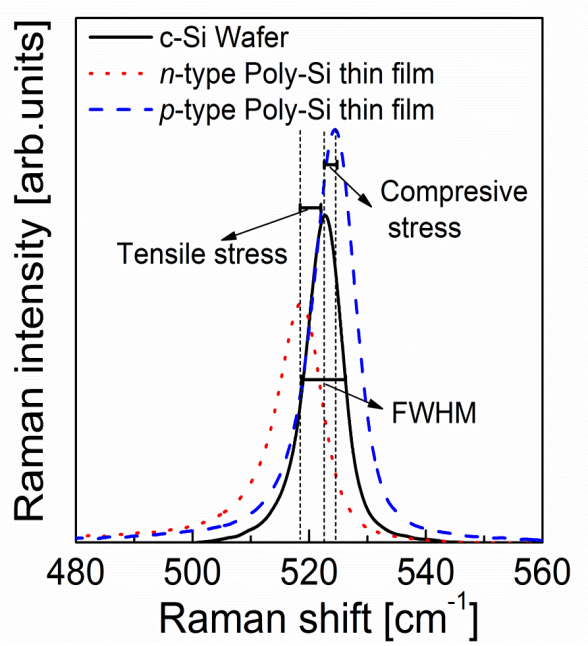

Figure 2.17: *Measured Raman spectra of two selected poly-Si thin films. Also shown, for comparison, is the Raman spectrum measured for a polished single-crystalline Si wafer (solid black line).*

Raman measurements give a single peak at ~522 cm^{-1} for c-Si wafers. This peak position value of c-Si may slightly vary from experiment to experiment, depending on the calibration of the spectrometer and the monochromator. Valuable information such as crystal quality and stress in c-Si films can be obtained from the full width at half maximum (FWHM) of the curve and the position (in cm^{-1}) of the peak. A shift in the peak position of the poly-Si thin-film samples towards lower wavenumbers with respect to a defect-free single-crystal c-Si wafer indicates the presence of tensile stress in the film [59, 60], whereas a shift of the peak towards higher wavenumbers with respect to c-Si indicates the presence of compressive stress [61]. The level of stress in a poly-Si film can be quantified from the shift in wavenumber obtained from the Raman measurements, using the following equation [56, 57, 62]:

$$\sigma = -(250\ MPa\ cm) \times \Delta\omega, \qquad 2.3$$

where σ stands for stress and Δω is the shift in the Raman peak position (wave-number) of the poly-Si film compared to that of unstressed single-crystal Si. Furthermore, an increase in the defect density and disorder in Si thin films leads to a broadening of the peak (FWHM) [56, 58, 63] and hence the FWHM value is frequently used as an indicator for the crystal quality of poly-Si films. A Raman quality factor (R_Q) is defined here, and has been used frequently in this work, as the ratio between the FWHM of single-crystal Si to that of the poly-Si film ($R_Q = \frac{FWHM_{c-Si}}{FWHM_{poly-Si}}$) to quantify the structural quality of a poly-Si film relative to a c-Si wafer.

2.3.1.3 Electron Backscatter diffraction (EBSD)

EBSD is a micro-structural crystallographic technique to examine the crystallographic orientation of many materials. EBSD can be used to index and identify the seven crystal systems, and thus it can be used for crystal orientation mapping, defect studies, phase identification, grain boundary and morphology studies, regional heterogeneity investigations, material discrimination, microstrain mapping, and for physicochemical identification. An EBSD system (Bruker Quantax EBSD CrystAlign, Germany) attached to a SEM (Carl Zeiss, Germany) was used extensively in this work to characterize the grain size, orientation and plastic deformation in SPC poly-Si thin films. It was also used to identify grain boundary defects in poly-Si thin films. Details about the EBSD technique and the set-up used in this work can be found in the literature [64, 65]. Figure 2.18 shows a typical EBSD grain orientation and distribution map of an *n*-type poly-Si thin film. The colour triangle in the top left corner of the graph gives information about the different crystal orientations.

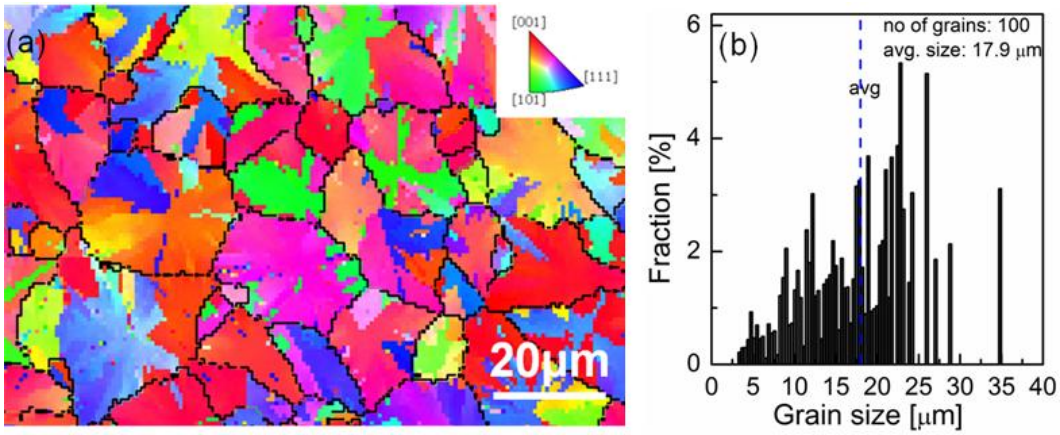

Figure 2.18: *(a) EBSD grain size orientation map, (b) Grain size distribution graph of an n-type poly-Si thin-film sample.*

Furthermore, small rotations in the material can be detected with SERIS' EBSD system. A grain average misorientation (GAM) map can also be generated by the EBSD system, which allows the visualization of misorientation gradients within the material ('plastic deformation'); thus, the accumulated orientation changes relative to the average orientation within a grain can be measured [66 - 68]. First, the grains and subgrains in the poly-Si thin films are detected and identified by the EBSD system based on their diffraction pattern. The EBSD software CrysAlign at SERIS uses the linear intercept method to detect the grains [65]. Once the grain distribution map is obtained, an orientation matrix is generated for every pixel in the map [64]. A transformation matrix between two pixels is called misorientation. Misorientation angle and subsequently misorientation maps are obtained from the transformation matrix [64]. Kernel average misorientation (KAM) and GAM maps are usually used to assess the plastic deformation in the polycrystalline film [69]. The choice of the reference orientation matrix defines the two maps [64]. In a GAM map, the average orientation matrix for a particular grain is chosen as reference orientation matrix, whereas for KAM map, the average of a cluster of eight pixels surrounding the pixel of interest at the centre is chosen as a reference orientation matrix [64]. In this work, GAM map has been extensively used to visualize the plastic deformation (strain) is poly-Si thin film. Figure 2.19 shows a typical grain average misorientation (GAM) map for an *n*-type SPC poly-Si film. A colour code from blue (0°) to red (5°) is used to measure the misorientation between the reference pixel and every other pixel, for each grain. Small amounts of misorientation are represented by blue colour (0-

0.5°), whereas large misorientations (plastic deformations) are represented by red colour (~4-5°). Qualitative and quantitative information about the misorientation (or plastic deformation) present in the poly-Si thin film grains was extracted in this work from EBSD measurements, to better understand the material quality of the film [66, 67, 69, 70].

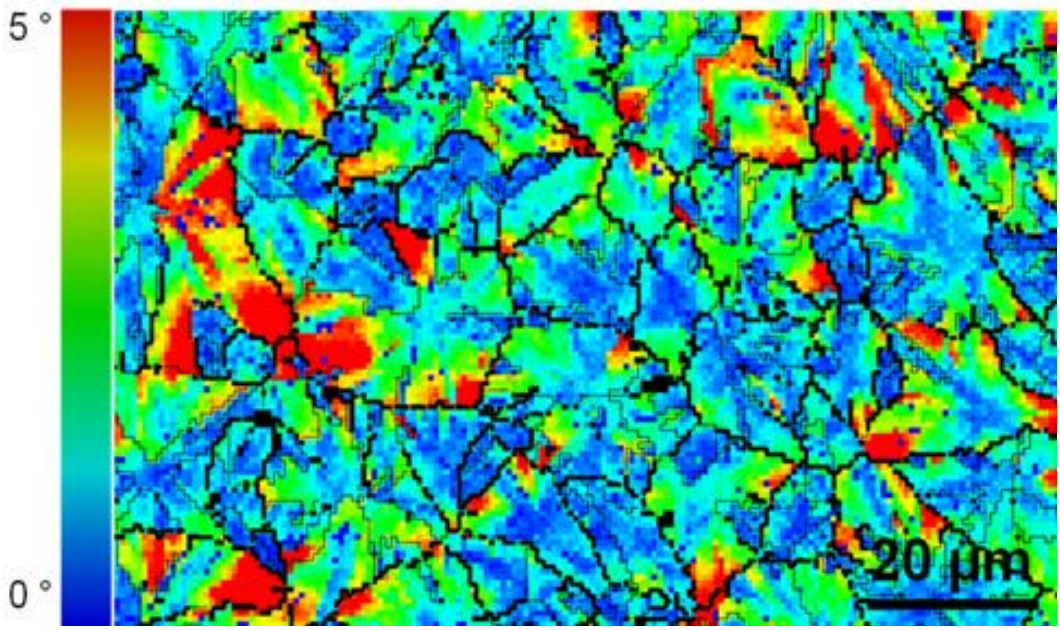

Figure 2.19: *Grain average misorientation map of an n-type SPC poly-Si thin-film sample.*

2.3.1.4 Transmission electron microscopy (TEM)

A transmission electron microscope (TEM, CM300, Philips) was used in this work to examine the interface properties, thickness and microstructure of SPC poly-Si thin films. In addition, dark-field TEM (DF-TEM) and high angle annular dark field scanning tunnelling microscopy (HAADF-STEM) were used to investigate the intra-grain defects and to reveal the dislocations in the poly-Si films. The TEM uses a microscopy technique similar to that of a light microscope; however, an electron beam is used instead of a light source. The short wavelengths of

electrons make TEM capable of high-resolution imaging and hence a very useful tool in materials research.

A TEM is composed of several components, which includes a vacuum system of pressures in the order of 10^{-4} to 10^{-8} kPa to allow the uninterrupted passage of electrons, an electron emission source, a series of intermediate and projector lenses, as well as electrostatic plates. In TEM, a coherent beam of electrons is directed at the specimen, interacting with it as it penetrates through the specimen. The transmitted electrons are then focused by the objective lens into an image, which is then magnified and focused by intermediate and projector lenses onto a phosphor image screen [71]. An image of dark and light contrast is formed due to the different amounts of electrons transmitted through the specimen, which is determined by the density of the specimen at different sites. Both crystallographic information and surface topographic information can, thus, be viewed using the TEM. It is important to note that for TEM, the specimen has to be ultra-thin, to ensure a sufficient number of electrons penetrates the sample. Thinning of samples is done via mechanical polishing and an ion miller using an argon ion beam is used to mill a small hole at interface of very thin samples. Further detailed information on TEM sample preparation and its working principle can be found in the literature [71 - 73]. Figure 2.20 shows a cross-sectional TEM image of about 2 μm thick poly-Si thin-film solar cell. Figure 2.20(a) shows the cross-sectional bright-field (BF) TEM image of the poly-Si thin film. Valuable information such as interface quality, microstructure and thickness of poly-Si thin film can be obtained from this image. Figure 2.20(b) shows the

cross-sectional dark-field (DF) TEM image of the poly-Si thin film. Valuable information about grains, grain boundaries and defects in the poly-Si thin film can be obtained from this image. In TEM imaging, an interpretable amplitude contrast from the electron scatter is obtained by selecting either the direct beam or some of the diffracted beams in the selected-area diffraction (SAD) to form BF and DF images, respectively. The bright field image is formed based on weakening of the direct beam by its interaction with the sample. Mass-thickness and diffraction contrast contribute to the image formation. Thus, thick areas, areas in which heavy atoms are enriched and crystalline areas appear with dark contrast in a BF images. Whereas in DF image, the information is obtained from the diffracted beams which strongly interact with the specimen giving very useful information about defects and particle size. For example, in Figure 2.20(b), a selected grain feature of poly-Si appears bright in the dark field image.

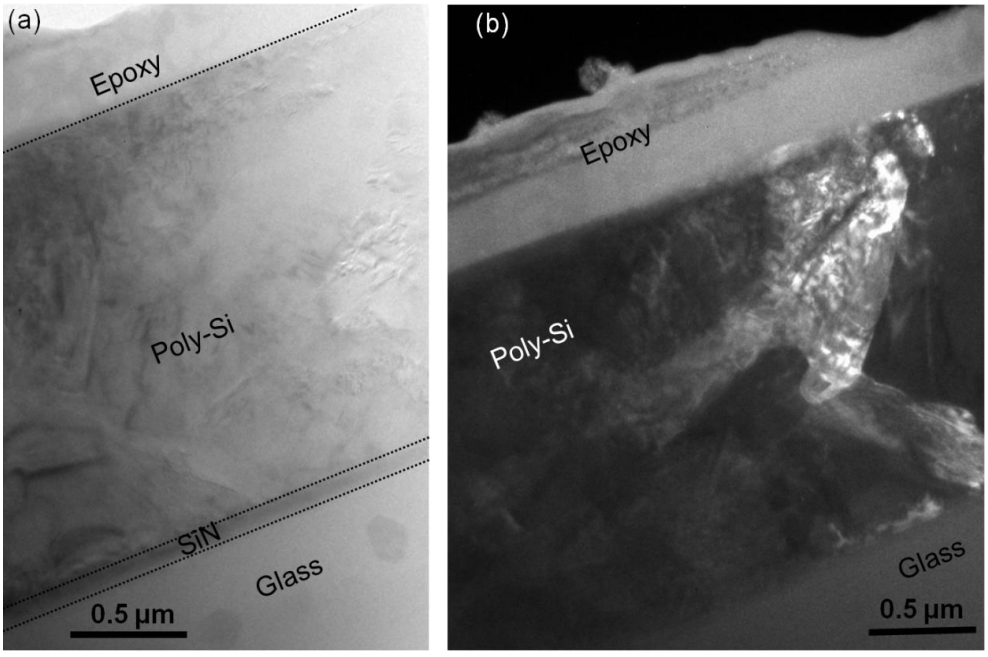

Figure 2.20: *(a) Cross-sectional bright-field TEM image; (b) Cross-sectional dark-field TEM image of a poly-Si thin-film solar cell.*

2.3.1.5 Secondary ion mass spectroscopy (SIMS)

Secondary ion mass spectroscopy (SIMS) is the most sensitive analysis technique used to analyse the composition of thin films. In SIMS, high energy ions are supplied by a primary ion gun and are focused onto the target region of the sample. The focused ion beam (~1-20 keV) ionizes and sputters the atoms off the specimen surface, ejecting secondary ions. These ions are collected by ion extraction lenses and a mass analyser separates the secondary ions by their mass to charge ratio. Hence, the elemental, isotopic and molecular composition of the probed specimen surface can be determined. The SIMS result thus obtained gives the composition versus depth profile of the sample [74]. SIMS analysis is performed in high vacuum with pressures below 10^{-4} Pa to ensure that the ejected secondary ions do not collide with background gases on their way to the detector [74]. SIMS was used in this work to study the chemical composition and dopant profile of Al in β-$FeSi_2$ films (Chapter 7).

2.3.2 Electrical characterization

2.3.2.1 Four point probe

A CRESBOX semi-automatic four point probe sheet resistance/resistivity measurement system was used in this work to determine sheet resistances and for the evaluation of the doping profile of poly-Si thin-film solar cells. Sheet resistances and resistivities are very important parameters for semiconductor materials and devices. They give a lot of valuable information on the free electron (n) and hole (p) densities. Furthermore, valuable information about the electron

and hole mobilities can also be extracted from the resistivity, using the following relationship [75]:

$$\rho = \frac{1}{q(n\mu_n + p\mu_p)} \qquad 2.4$$

The four-point probe measurement is the most standard and accurate technique to measure the resistivity of a semiconductor sample. It is an absolute measurement without the need of calibrated standards and is sometimes used to provide standards for other resistivity measurements [75]. Wire resistance and probe resistance effects are eliminated in the four point probe method, in contrast to the two point probe method [75]. In the four-point probe technique, the probes are generally arranged along a straight line and with equal spacing, as shown in Fig. 2.21. This figure shows a typical four-point probe arrangement for current and voltage measurements. S_1, S_2 and S_3 are the distances between the probes. Two probes carry current, while the other two probes sense a voltage.

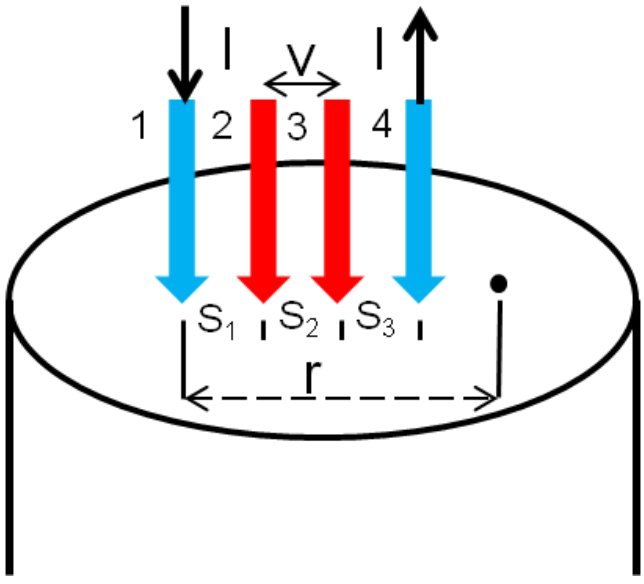

Figure 2.21: *Four-point probe arrangement showing current flow and voltage measurement.*

2.3.2.2 Hall measurement system

Characterisation of a semiconductor using the Hall effect is a simple, yet powerful, technique that measures the resistivity, carrier density and mobility of the sample in one step. Based on its versatility, it has found wide application in the characterization of semiconductor materials. Hall effect works on a simple principle of interaction of electric field and magnetic field placed perpendicular to each other. Consider the case of a *p*-type semiconductor placed in the desired fields. The free majority-carrier holes will experience a Lorentz force due to the magnetic field, which exerts an average upward force on the holes flowing in the x-direction towards the positive y-axis, which in turn results in the accumulation of holes at the top of the sample that give rise to a downward directed electric field. The established electric field is called the Hall field and the voltage drop across the top and bottom is called the Hall voltage. From these obtained parameters, carrier densities and mobility are determined. Details on this method can, for example, be found in the book by D.K. Schroder, "Semiconductor material and device characterization", third edition [75]. We used a Hall measurement system from bio-Rad to determine the carrier concentration and sheet resistance of *n*-type and *p*-type SPC poly-Si thin films. The Hall effect measurements were conducted at a magnetic field of 0.32 T and a sample temperature of 300 K. The system was calibrated with a c-Si reference sample at the identical magnetic field. Details about the sample preparation for the Hall effect measurements can be found in the literature [47]. Figure 2.22 shows the Bio-Rad Hall measurement system used in our experiments. Poly-Si thin films were cut to

small sample sizes of 1 cm × 1 cm and four contacts were then formed at the four corners using a soldering gun and indium wire, as shown in Fig. 2.22(b). The contacted poly-Si thin-film sample was then placed on the sample stage of the Hall system for the measurement.

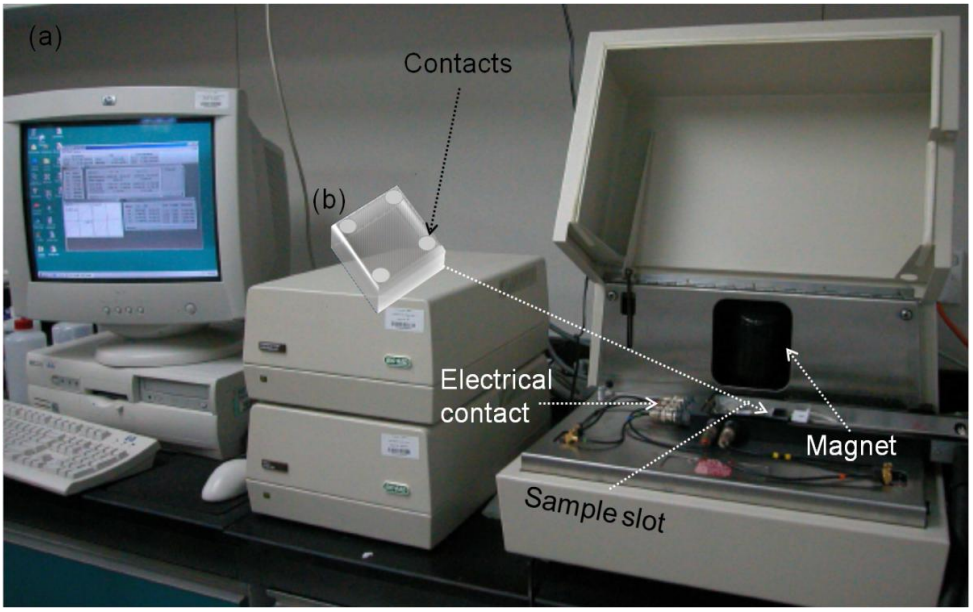

Figure 2.22: *(a) Photograph of the Hall Effect measurement system used in this work (Source: IMRE, A*STAR), (b) Schematic of a typical poly-Si thin-film sample used for Hall measurement.*

2.3.2.3 Suns-V_{OC} method

The electrical quality of poly-Si thin-film diodes and β-$FeSi_2$/poly-Si solar cell test structures was determined by Suns-V_{oc} measurements [76]. The Suns-V_{oc} technique is a powerful method that is frequently used to investigate the material quality and device design of solar cells. The technique offers a great advantage of process control by allowing the operator to measure the performance of the solar cell at various stages of the fabrication process [76 - 78]. The technique doesn't require a metallization of the diode [76 - 78]. The technique was introduced by Sinton and Cuevas [76] and since then is widely used for solar cell characteri-

sation [76 - 78]. In this technique, the short-circuit current (I_{sc}) of the solar cell is not measured at every light intensity but instead, light intensity is measured with a calibrated reference solar cell [76]. Thus, the raw data obtained from this measurement are calibrated light intensity and the V_{oc} of the sample under test. The light intensity is calibrated using a silicon wafer reference solar cell (1 cm^2) located at a fixed distance from the light source. First, the I_{sc} of this reference cell is calculated by measuring the voltage drop across a small load resistances of 1 Ω connected to reference cell. The light intensity is then calculated by dividing the I_{sc} of the reference cell to the I_{sc} at 1 sun obtained independently by a calibrated I-V tester. Therefore, a light I-V curve can be theoretically constructed from Suns-V_{oc} data. This is achieved by assuming a reasonable 1-Sun short-circuit current density (J_{sc}) for the device under test. Generally for poly-Si thin film, a 1-Sun J_{sc} of 30 mA/cm^2 is used [47]. Since this current is not the 'actual' current flowing through the device, this I-V curve is known as a 'pseudo I-V' curve. Important parameter such as the pseudo fill factor (*pFF*) which represents the upper limit of fill factor excluding series resistance (R_s) can be calculated on un-metallised samples from this curve via [78]:

$$pFF = \frac{V_{OC}(MPP) \times J_{norm}(MPP)}{V_{OC}}, \tag{2.5}$$

where V_{oc} is the open-circuit voltage at 1 Sun, V_{oc} (MPP) and J_{norm} (MPP) denotes the open-circuit voltage and the normalized current density at the maximum power point (MPP) of the pseudo-IV curve respectively. *pFF* gives valuable information about the quality of the diode, recombination mechanism and is a very useful parameter for loss analysis in solar cell. Details about the Suns-V_{oc}

set-up used at SERIS for the characterisation of poly-Si thin-film solar cells can be found in the literature [47].

2.3.2.4 Electrochemical capacitance voltage (ECV)

An ECV doping profiler system (CVP21 ECV profiler from WEP Control, Germany) was used in this work for junction location determination and for the estimation of the doping concentrations of each layer ($p^+/p^-/n^+$) in the *p*-type poly-Si thin-film solar cells. ECV is a characterization technique that relies on the measurement of the capacitance of an electrolyte-semiconductor Schottky contact. The method offers several advantages over the conventional capacitance-voltage (C-V) method [79] where a good ohmic contact is required to both the BSF layer and the emitter layer. In contrast, the ECV technique can be applied to non-metalized solar cells, eliminating the need of making a contact to the emitter layer. Making good contact to the emitter layer of SPC poly-Si thin-film diodes can be challenging, as the specific contact resistance of Al on n^+ poly-Si is quite high for the surface doping concentrations encountered in the samples prepared in this thesis ($<\times 10^{20}$ cm^{-3})[80, 81]. In addition, ECV measurements do not need an abrupt *p-n* junction for accurate results, which is required for the analysis of conventional C-V measurements. We used gallium indium (GaIn) eutectic paste to form good ohmic contacts between the sample and the measurement probes. The electrolyte solution was prepared by dissolving 2.89 g of $NH_4F{\cdot}HF$ (ammonium bifluoride, ABF) salt into 500 mL of de-ionised water, giving a 0.1 M solution. The etched area was about 0.100 cm^2. Further details on the ECV method can be found in the literature [82 - 86]. Figure 2.23 shows a simple

schematic of the ECV set-up used in our experiments.

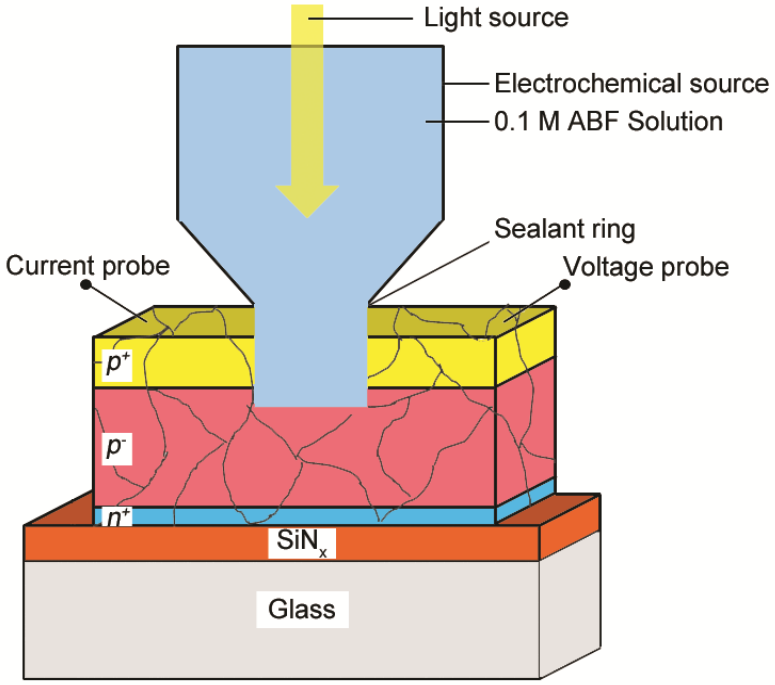

Figure 2.23: *ECV set-up used in this work. Note: The sealant ring defines an area of about 0.100 cm^2 and the light from a halogen lamp is used to assist in the etching process.*

2.3.2.5 Quantum efficiency

The quantum efficiency curve provides valuable information on a solar cell's design and material quality. Important parameters that are required for high-efficiency solar cells, such as base diffusion length and rear surface recombination velocity, can be determined using the external quantum efficiency (EQE) curve. For a given photon wavelength, the "quantum efficiency" (QE) is the ratio of the number of photogenerated carriers collected by the solar cell at short circuit to the number of incoming photons [87]. The quantum efficiency may be given either as a function of wavelength or as energy. Figure 2.24 shows the EQE curve of a typical c-Si wafer solar cell. A Solar Cell Scan 100 system from Zolix

Instruments, China was used in this work to measure the EQE curve of the solar cells and for the calculation of the 1-Sun (AM1.5G) short-circuit current density J_{sc} expected from the measured EQE. The J_{sc} value was calculated from the EQE curve (Zolix system) measured on metallised samples using the following relation:

$$J_{SC}(EQE) = q \int EQE(\lambda)S(\lambda)d(\lambda), \qquad 2.6$$

where J_{SC} is current density (A.m^{-2}), q is the electron charge (A.s), λ is wavelength (nm) and S(λ) is the standard spectral photon density of sunlight at the earth's surface (AM1.5G). It is defined as the number of photon of energy in the range of λ to λ + dλ which are incident on the unit area in unit time (nm^{-1}.m^{-2}.s^{-1}).

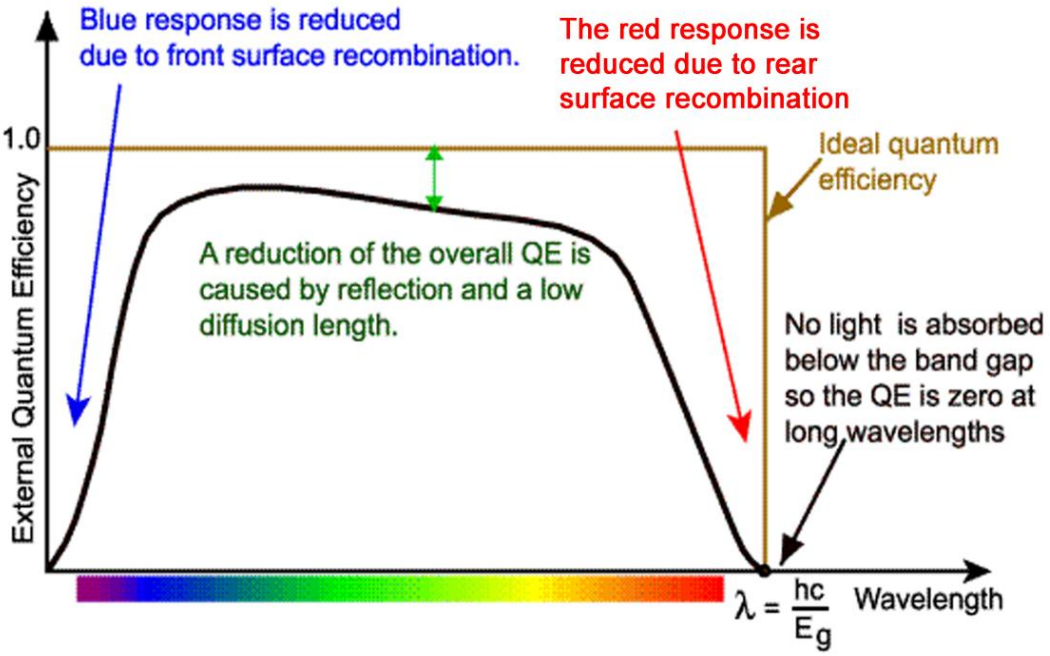

Figure 2.24: *External quantum efficiency curve of a typical c-Si wafer solar cell. The EQE is usually not measured below 350 nm, as the power in the AM1.5 spectrum at these wavelengths is very low [87].*

References of Chapter 2

[1] W. Hirschman, G. Hering and M. Schmela, "Gigawatts - the measure of things to come. Market survey on global solar cell and module production in 2006," *Photon International March 2007*, pp. 136-166.

[2] R.B. Bergmann, "Crystalline Si thin-film solar cells: a review," *Applied Physics A*, vol. 69, pp. 187-194, 1999.

[3] A. Kumar, P.I. Widenborg, H. Hidayat, Q. Zixuan and A.G. Aberle, "Impact of rapid thermal annealing and hydrogenation on the doping concentration and carrier mobility in solid phase crystallized poly-Si thin films," *MRS Online Proceedings Library*, vol. 1321, 2011.

[4] P.A. Basore, "Pilot production of thin-film crystalline silicon on glass modules," in *Photovoltaic Specialists Conference, 2002. Conference Record of the Twenty-Ninth IEEE*, 2002, pp. 49-52.

[5] A.G. Aberle, "Fabrication and characterisation of crystalline silicon thin-film materials for solar cells," *Thin Solid Films*, vol. 511-512, pp. 26-34, 2006.

[6] T. Matsuyama, K. Wakisaka, M. Kameda, M. Tanaka, T. Matsuoka, S. Tsuda *et al.*, "Preparation of high-quality n-type poly-Si films by the solid phase crystallization (SPC) method," *Japanese Journal of Applied Physics*, vol. 29, pp. 2327-2331, 1990.

[7] T. Matsuyama, N. Terada, T. Baba, T. Sawada, S. Tsuge, K. Wakisaka *et al.*, "High-quality polycrystalline silicon thin film prepared by a solid phase crystallization method," *Journal of Non-Crystalline Solids*, vol. 198-200, Part 2, pp. 940-944, 1996.

[8] M.A. Green, P.A. Basore, N. Chang, D. Clugston, R. Egan, R. Evans *et al.*, "Crystalline silicon on glass (CSG) thin-film solar cell modules," *Solar Energy*, vol. 77, pp. 857-863, 2004.

[9] M.J. Keevers, T.L. Young, U. Schubert and M.A. Green, "10% efficient CSG minimodules," in *22nd European Photovoltaic Solar Energy Conference, Milan*, 2007, pp. 235-239.

[10] G.F. Zheng, W. Zhang, Z. Shi, M. Gross, A.B. Sproul, S.R. Wenham *et al.*, "16.4% efficient, thin active layer silicon solar cell grown by liquid phase epitaxy," *Solar Energy Materials and Solar Cells*, vol. 40, pp. 231-238, 1996.

[11] I. Gordon, L. Carnel, D. Van Gestel, G. Beaucarne and J. Poortmans, "Fabrication and characterization of highly efficient thin-film poly-

crystalline-silicon solar cells based on aluminium-induced crystallization," *Thin Solid Films,* vol. 516, pp. 6984-6988, 2008.

[12] E. Schmich, N. Schillinger and S. Reber, "Silicon CVD deposition for low cost applications in photovoltaics," *Surface and Coatings Technology,* vol. 201, pp. 9325-9329, 2007.

[13] L. Oberbeck and R.B. Bergmann, "Electronic properties of silicon epitaxial layers deposited by ion-assisted deposition at low temperatures," *Journal of Applied Physics,* vol. 88, pp. 3015-3021, 2000.

[14] D. Inns, "ALICIA polycrystalline silicon thin-film solar cells," PhD thesis, The University of New South Wales, Sydney, 2007.

[15] D. Song, D. Inns, A. Straub, M.L. Terry, P. Campbell and A.G. Aberle, "Solid phase crystallized polycrystalline thin-films on glass from evaporated silicon for photovoltaic applications," *Thin Solid Films,* vol. 513, pp. 356-363, 2006.

[16] O. Kunz, "Evaporated solid-phase crystallised poly-silicon thin-film solar cell on glass," PhD Thesis, The University of New South Wales, Sydney, 2009.

[17] F. Falk and G. Andrä, "Laser crystallization - a way to produce crystalline silicon films on glass or on polymer substrates," *Journal of Crystal Growth,* vol. 287, pp. 397-401, 2006.

[18] J. Dore, D. Ong, S. Varlamov, R. Egan and M.A. Green, "Progress in laser-crystallized thin-film polycrystalline silicon solar cells: Intermediate layers, light trapping, and metallization," *Photovoltaics, IEEE Journal of,* vol. 4, pp. 33-39, 2014.

[19] K. Ohdaira, T. Fujiwara, Y. Endo, S. Nishizaki and H. Matsumura, "Explosive crystallization of amorphous silicon films by flash lamp annealing," *Journal of Applied Physics,* vol. 106, p. 044907, 2009.

[20] F. R. Faller and A. Hurrle, "High-temperature CVD for crystalline-silicon thin-film solar cells," *Electron Devices, IEEE Transactions on,* vol. 46, pp. 2048-2054, 1999.

[21] H. Tayanaka, K. Yamauchi and T. Matsushita, "Thin-film crystalline silicon solar cells obtained by separation of a porous silicon sacrificial layer," in *Proc. 2nd World Conf. Photovolt. Sol. Energy Conv.*, 1998, pp. 1272-1275.

[22] R. B. Bergmann, C. Berge, T. J. Rinke, J. Schmidt and J. H. Werner, "Advances in monocrystalline Si thin film solar cells by layer transfer," *Solar Energy Materials and Solar Cells,* vol. 74, pp. 213-218, 2002.

[23] A.G. Aberle, "Progress with polycrystalline silicon thin-film solar cells on glass at UNSW," *Journal of Crystal Growth*, vol. 287, pp. 386-390, 2006.

[24] O. Kunz, Z. Ouyang, J. Wong and A.G. Aberle, "Advances in Evaporated Solid-Phase-Crystallized Poly-Si Thin-Film Solar Cells on Glass (EVA)," *Advances in OptoElectronics*, vol. 2008, p. 10, 2009.

[25] O. Kunz, Z. Ouyang, S. Varlamov and A.G. Aberle, "5% efficient evaporated solid-phase crystallised polycrystalline silicon thin-film solar cells," *Progress in Photovoltaics: Research and Applications*, vol. 17, pp. 567-573, 2009.

[26] S. He, "Evaporated polycrystalline silicon thin-film solar cells by aluminium-induced crystallization solid-phase epitaxy," PhD thesis, The University of New South Wales, Sydney, 2009.

[27] A.G. Aberle and P.I. Widenborg, "Crystalline silicon thin-film solar cells via high-temperature and intermediate-temperature approaches," in *Handbook of Photovoltaic Science and Engineering*, ed.: John Wiley & Sons, 2011, pp. 452-486.

[28] J. Wong, "On the recombination mechanisms in poly-silicon thin-film on glass solar cells," PhD thesis, The University of New South Wales, Sydney, 2010.

[29] P. A. Basore, "CSG-1: Manufacturing a new polycrystalline silicon PV technology," in *Photovoltaic Energy Conversion, Conference Record of the 2006 IEEE 4th World Conference on*, 2006, pp. 2089-2093.

[30] M. A. Green, K. Emery, Y. Hishikawa and W. Warta, "Solar cell efficiency tables (version 35)," *Progress in Photovoltaics: Research and Applications*, vol. 18, pp. 144-150, 2010.

[31] P.I. Widenborg and A.G. Aberle, "Hydrogen-induced dopant neutralisation in p-type AIC poly-Si seed layers functioning as buried emitters in ALICE thin-film solar cells on glass," *Journal of Crystal Growth*, vol. 306, pp. 177-186, 2007.

[32] Ö. Tüzün, A. Slaoui, I. Gordon, A. Focsa, D. Ballutaud, G. Beaucarne *et al.*, "N-type polycrystalline silicon films formed on alumina by aluminium induced crystallization and overdoping," *Thin Solid Films*, vol. 516, pp. 6892-6895, 2008.

[33] L. Carnel, I. Gordon, D. Van Gestel, G. Beaucarne, J. Poortmans and A. Stesmans, "High open-circuit voltage values on fine-grained thin-film polysilicon solar cells," *Journal of Applied Physics*, vol. 100, p. 063702, 2006.

[34] W. Jui-Hao, L. Shui-Yang, C. Chen, x, Fu and W. Wha-Tzong, "Large-grain polycrystalline silicon solar cell on epitaxial thickening of AIC seed layer by hot wire CVD," *Electron Device Letters, IEEE,* vol. 31, pp. 38-40, 2010.

[35] S. Gall, C. Becker, K.Y. Lee, B. Rau, F. Ruske and B. Rech, "Poly-crystalline silicon thin-film solar cells on ZnO:Al-coated glass substrates," *in 34th IEEE Photovoltaic Specialists Conference (PVSC), 2009*, pp. 000197-000201.

[36] K. Yue, L. Chi-Chou and S. Verkhoturov, "Crystallization of a-Si thin film using an ultra thin n^+ poly-Si seed layer for solar cell applications," *in 38th IEEE Photovoltaic Specialists Conference (PVSC), 2012*, pp. 000342-000345.

[37] J. Haschke, D. Amkreutz, L. Korte, F. Ruske and B. Rech, "Towards wafer quality crystalline silicon thin-film solar cells on glass," *Solar Energy Materials and Solar Cells,* vol. 128, pp. 190-197, 2014.

[38] A.G. Aberle, P. Widenborg and N. Chuangsuwanich, "Glass texturing," European patent EP1613562 B1 (granted 20 July 2011).

[39] G. Jin, "Advanced polycrystalline silicon thin film solar cells using high rate plasma enhanced chemical vapour deposited amorphous silicon on textured glass," PhD thesis, The University of New South Wales, Sydney, 2010.

[40] Y. Huang, F. Law, P.I. Widenborg and A.G. Aberle, "Crystalline silicon growth in the aluminium-induced glass texturing process," *Journal of Crystal Growth,* vol. 361, pp. 121-128, 2012.

[41] P.I. Widenborg and A.G. Aberle, "Polycrystalline silicon thin-film solar cells on AIT-textured glass superstrates," *Advances in OptoElectronics,* vol. 2007, p. 7, 2007.

[42] G. Jin, P.I. Widenborg, P. Campbell and S. Varlamov, "Lambertian matched absorption enhancement in PECVD poly-Si thin film on aluminum induced textured glass superstrates for solar cell applications," *Progress in Photovoltaics: Research and Applications,* vol. 18, pp. 582-589, 2010.

[43] R.E. Schropp and M. Zeman, *Amorphous and microcrystalline silicon solar cells: Modeling, materials and device technology*: Kluwer Academic, Boston, 1998.

[44] Y. Tao, S. Varlamov, O. Kunz, Z. Ouyang, J. Wong, T. Soderstrom, *et al.*, "Effects of annealing temperature on crystallisation kinetics, film properties and cell performance of silicon thin-film solar cells on glass," *Solar Energy Materials and Solar Cells,* vol. 101, pp. 186-192, 2012.

[45] Y. Tao, "Crystallisation studies of silicon thin films on glass for solar cell application," PhD thesis, University of New South Wales, Sydney, 2011.

[46] F. Law, H. Hidayat, A. Kumar, P. Widenborg, J. Luther and B. Hoex, "On the transient amorphous silicon structures during solid phase crystallization," *Journal of Non-Crystalline Solids,* vol. 363, pp. 172-177, 2013.

[47] H. Hidayat, "Post-crystallisation treatment and characterisation of polycrystalline silicon thin-film solar cells on glass," PhD thesis, National University of Singapore, Singapore, 2013.

[48] A. Kumar, P. Widenborg, H. Hidayat, Q. Zixuan and A.G. Aberle, "Impact of rapid thermal annealing and hydrogenation on the doping concentration and carrier mobility in solid phase crystallized poly-Si thin films," in *MRS Proceedings*, 2011.

[49] H. Hidayat, A. Kumar, F. Law, C. Ke, P.I. Widenborg and A.G. Aberle, "Impact of rapid thermal annealing temperature on non-metallised polycrystalline silicon thin-film diodes on glass," *Thin Solid Films,* vol. 534, pp. 629-635, 2013.

[50] P.J. Gress, P.I. Widenborg, S. Varlamov and A.G. Aberle, "Wire bonding as a cell interconnection technique for polycrystalline silicon thin-film solar cells on glass," *Progress in Photovoltaics,* vol. 18, pp. 221-228, May 2010.

[51] P.I. Widenborg, S.V. Chan, T. Walsh and A.G. Aberle, "Thin-film poly-Si solar cells on AIT-textured glass - Importance of the rear reflector," in *33rd IEEE Photovoltaic Specialists Conference,* 2008, pp. 1-3.

[52] L.L. Kazmerski, "Photovoltaics characterization: A survey of diagnostic measurements," *Journal of Materials Research,* vol. 13, pp. 2684-2708, 1998.

[53] P.Y. Yu and M. Cardona, *Fundamentals of semiconductors: Physics and materials properties*: Springer, Berlin, 1999.

[54] T. Kamins, *Polycrystalline silicon for integrated circuit applications*: Kluwer Academic Publishers, 1988.

[55] A. Straub, P.I. Widenborg, A. Sproul, Y. Huang, N.P. Harder and A.G. Aberle, "Fast and non-destructive assessment of epitaxial quality of polycrystalline silicon films on glass by optical measurements," *Journal of Crystal Growth,* vol. 265, pp. 168-173, 2004.

[56] R.C. Teixeira, I. Doi, M.B.P. Zakia, J.A. Diniz and J.W. Swart, "Micro-Raman stress characterization of polycrystalline silicon films grown at high temperature," *Materials Science and Engineering: B,* vol. 112, pp. 160-164, 2004.

[57] I. De Wolf, "Micro-Raman spectroscopy to study local mechanical stress in silicon integrated circuits," *Semiconductor Science and Technology*, vol. 11, pp. 139-154, 1996.

[58] A. Kumar, H. Hidayat, C. Ke, S. Chakraborty, G.K. Dalapati, P.I. Widenborg *et al.*, "Impact of the n^+ emitter layer on the structural and electrical properties of p-type polycrystalline silicon thin-film solar cells," *Journal of Applied Physics*, vol. 114, p.134505, 2013.

[59] K. Kitahara, H. Ogasawara, J. Kambara, M. Kobata and Y. Ohashi, "Characterization of defects in polycrystalline silicon thin films using chemical etching, hydrogenation, and Raman spectroscopy," *Japanese Journal of Applied Physics*, vol. 47, p. 54, 2008.

[60] K. Kitahara, T. Ishii, J. Suzuki, T. Bessyo and N. Watanabe, "Characterization of defects and stress in polycrystalline silicon thin films on glass substrates by Raman microscopy," *International Journal of Spectroscopy*, vol. 2011, p. 632139, 2011.

[61] K. Kitahara and A. Hara, "Oriented lateral growth and defects in polycrystalline-silicon thin films on glass substrates." *Crystallization - Science and Technology*, 2012, DOI: 10.5772/37040.

[62] P. Münster, M. Sarret, T. Mohammed-Brahim, N. Coulon and J.-Y. Mevellec, "Polycrystalline silicon deposited on glass by subatmospheric-pressure chemical vapour deposition at a high rate," *Philosophical Magazine Part B*, vol. 82, pp. 1695-1701, 2002.

[63] S. Nakashima and M. Hangyo, "Characterization of semiconductor-materials by Raman microprobe," *IEEE Journal of Quantum Electronics*, vol. 25, pp. 965-975, 1989.

[64] F. Law, "On the solid phase crystallization for thin film silicon solar cells on glass," PhD Thesis, National University of Singapore, Singapore 2013.

[65] F.J. Humphreys, "Review grain and subgrain characterisation by electron backscatter diffraction," *Journal of Materials Science*, vol. 36, pp. 3833-3854, 2001.

[66] L. Brewer, M. Othon, L. Young and T. Angeliu, "Misorientation mapping for visualization of plastic deformation via electron back-scattered diffraction," *Microscopy and Microanalysis*, vol. 12, pp. 85-91, 2006.

[67] F. Dunne, R. Kiwanuka and A. Wilkinson, "Crystal plasticity analysis of micro-deformation, lattice rotation and geometrically necessary dislocation density," *Proceedings of the Royal Society A: Mathematical, Physical and Engineering Science*, vol. 468, pp. 2509-2531, 2012.

[68] F. Law, Y. Yi, Hidayat, P.I. Widenborg, J. Luther and B. Hoex, "Identification of geometrically necessary dislocations in solid phase crystallized poly-Si," *Journal of Applied Physics*, vol. 114, p. 043511, 2013.

[69] L. Brewer, D. Field and C. Merriman, "Mapping and assessing plastic deformation using EBSD," in *Electron Backscatter Diffraction in Materials Science*, A. J. Schwartz, M. Kumar, B.L. Adams and D.P. Field, Eds., ed: Springer, USA, 2009, pp. 251-262.

[70] A. Wilkinson, E. Clarke, T. Britton, P. Littlewood and P. Karamched, "High-resolution electron backscatter diffraction: An emerging tool for studying local deformation," *The Journal of Strain Analysis for Engineering Design*, vol. 45, pp. 365-376, 2010.

[71] *Transmission electron microscopy*. Available: http://en.wikipedia.org/wiki/Transmission_electron_microscopy

[72] D. Williams and C.B. Carter, "The transmission electron microscope," in *Transmission Electron Microscopy*, ed: Springer, USA, 1996, pp. 3-17.

[73] R. Egerton, "The transmission electron microscope," in *Physical Principles of Electron Microscopy*, ed: Springer, USA, 2005, pp. 57-92.

[74] A. Benninghoven, F. G. Rüdenauer and H.W. Werner, *Secondary ion mass spectrometry: Basic concepts, instrumental aspects, applications, and trends*: J. Wiley, 1987.

[75] D. K. Schroder, *Semiconductor Material and Device Characterization, 3rd Edition*: Wiley-VCH, 2005.

[76] R. Sinton and A. Cuevas, "A quasi-steady-state open-circuit voltage method for solar cell characterization," in *16th European Photovoltaic Solar Energy Conference*, Glasgow, UK, 2000, pp. 1152-1155.

[77] J. Wong, J.L. Huang, O. Kunz, Z. Ouyang, S. He, P.I. Widenborg *et al.*, "Anomalous temperature dependence of diode saturation currents in polycrystalline silicon thin-film solar cells on glass," *Journal of Applied Physics*, vol. 105, p.103705, 2009.

[78] Z. Ouyang, O. Kunz, A.B. Sproul and S. Varlamov, "Influence of the absorber doping for p-type polycrystalline silicon thin-film solar cells on glass prepared by electron beam evaporation and solid-phase crystallization," *Journal of Applied Physics*, vol. 109, p. 054510, 2011.

[79] D.A. Neamen, *Semiconductor Device Physics: Basic Principles*, 3rd ed., New York, McGraw Hill, 2002.

[80] J.D. Wiley and G.L. Miller, "Series resistance effects in semiconductor C-V profiling," *IEEE Transactions on Electron Devices,* vol. 22, pp. 265-272, 1975.

[81] L. Carnel, I. Gordon, D. Van Gestel, G. Beaucarne, J. Poortmans and A. Stesmans, "High open-circuit voltage values on fine-grained thin-film poly-silicon solar cells," *Journal of Applied Physics,* vol. 100, p. 063702, 2006.

[82] T. Ambridge and M.M. Faktor, "An automatic carrier concentration profile plotter using an electrochemical technique," *Journal of Applied Electro-chemistry,* vol. 5, pp. 319-328, 1975.

[83] J.Y. Lee and S.H. Lee, "Boron back surface field using spin-on dopants by rapid thermal processing," *Journal Korean Physical Society,* vol. 44, pp. 1581-1586, 2004.

[84] I. Mayes, "Accuracy and reproducibility of the electrochemical profiler," *Materials Science and Engineering B,* vol. 80, pp. 160-163, 2001.

[85] E. Peiner, A. Schlachetzki and D. Krüger, "Doping profile analysis in Si by electrochemical capacitance voltage measurements," *Journal of the Electro-chemical Society,* vol. 142, p. 576, 1995.

[86] P. Blood, "Capacitance-voltage profiling and the characterisation of III-V semiconductors using electrolyte barriers," *Semiconductor Science and Technology,* vol. 1, p. 7, 1986.

[87] C. Honsberg and S. Bowden. *PVCDROM*. *2014*. Available: http://www.pveducation.org/pvcdrom.

Chapter 3

Chapter 3- Growth and Characterization of Large-Grained n^+ Poly-Si Thin Films

3.1. Introduction

3.2. Experimental Procedures

3.3. Results and Discussion

3.4. Conclusion

3.1 Introduction

Thin-film polycrystalline silicon (poly-Si) is a promising semiconductor material for a variety of large-area electronic applications ranging from thin-film transistors (TFTs) [1] and active matrix type liquid-crystal displays (LCDs) [2, 3] to photovoltaics (PV) [4-9]. The thin-film poly-Si solar cell technology [6, 7, 10-13] received significant attention after the promising device efficiencies reported by SANYO in the 1990s [4]. Among various poly-Si technologies [6, 7, 14], the thin-film poly-Si on glass solar cell prepared by solid-phase crystallization (SPC) is one of the most innovative technologies which combines the robustness of the c-Si wafer-based technology with the advantages of thin films [10]. In 2006, CSG Solar was the first company that attempted to commercialize this technology [15]. CSG Solar achieved an efficiency of 10.4% for a 94-cm^2 mini-module using a simple single-junction diode structure in a superstrate configuration [16]. This single-junction device is believed to have an energy conversion efficiency potential of more than 13% [17].

It has been hypothesized that an enhancement in the grain size of the poly-Si thin film could lead to further improvements in the performance of solar cells [18], and a high field effect mobility as required for TFTs [19]. However, recent reports suggest that the efficiency of hydrogen-passivated poly-Si thin-film solar cells does not only depend on the grain size, but also on the intra-grain defects and dislocations [20, 21]. Thus, in order to consider poly-Si thin films for future large-scale electronic applications, it is desirable to have a better understanding of

the effect of grain microstructures (size, orientation, boundaries and intra-grain defects) on the structural and electronic qualities of the poly-Si thin film.

Matsuyama *et al*. [4, 22] reported that *n*-type poly-Si thin films with large grains can be fabricated by controlling the phosphorus dopant density in the film, but not much information was given about the grain size distribution, orientation and the crystal quality. Recently, our group reported that large-grain *n*-type SPC poly-Si thin films can be formed by increasing the concentration of phosphorus (P) in the film [23]. This finding differs from the results previously reported by SANYO [4], where the average grain size was reported to be inversely proportional to the phosphorus concentration. Furthermore, we also observed from UV reflectance measurements that the crystal quality deteriorates with increasing grain size of the poly-Si film [23]. However, the mechanism behind the deterioration of the crystal quality of the poly-Si thin film with the increase of the grain size was still unclear and required further experimental investigation.

In this chapter, we fabricate and evaluate large-grained n^+ doped poly-Si thin films prepared by SPC of hydrogenated amorphous silicon (a-Si:H). The effect of an increasing PH_3 (2% in H_2)/SiH_4 gas flow ratio on the phosphorus (P) doping concentration and the carrier mobility of the poly-Si thin film is studied using Hall effect measurements. Furthermore, its impact on grain size, orientation and the crystal quality of the n^+ poly-Si film is investigated in detail using Raman and EBSD measurements. Finally, HRTEM and high-angle annular dark field

scanning tunnelling microscopy (HAADF-STEM) is used to investigate the intra-grain defects and reveal the dislocations in the poly-Si films.

3.2 Experimental Procedures

About 500 nm thick n^+ doped SPC poly-Si thin films with varying doping concentrations were prepared for this study. First, the a-Si:H films were deposited onto a SiN_x (~70 nm) coated planar glass sheet (Schott, Borofloat) in a PECVD (plasma-enhanced chemical vapour deposition) clustertool (MVSystems, USA). The *n*-type doping of the a-Si:H films was obtained by in-situ doping with phosphorus (P) from the PH_3 (2% in H_2) gas mixed with SiH_4 during the PECVD process. The n^+ a-Si:H thin films were deposited using different PH_3 (2% in H_2)/SiH_4 gas flow ratios, as summarized in Table 3.1. An ~100 nm thick SiO_x capping layer was then deposited onto the a-Si:H films. The SiO_x layer acts as a barrier for impurities from the ambient during the SPC process as well as the subsequent rapid thermal annealing (RTA) process.

Table 3.1: *Experimental details used for the PECVD of the n^+ a-Si:H films.*

Process condition	*n^+ a-Si layer*
SiH_4 (sccm)	40
2% PH_3:H_2 (sccm)	1-20
Substrate temperature (ºC)	410
Pressure (Pa)	106
RF power density (mW/cm^2)	34

The deposited a-Si:H films were then annealed (Nabertherm, N 120/65HAC furnace, Germany) at 610 ºC in a N_2 atmosphere for a duration of 12 hours to achieve solid phase crystallization of the film. A rapid thermal anneal (RTA, CVD Equipment, USA) for 1 minute at a peak temperature of 1000 ºC in N_2 atmosphere was then used to remove crystallographic defects from the SPC poly-Si thin films and to activate the dopants. The *n*-type poly-Si samples were then characterized for grain size and orientation maps by an EBSD system (Bruker Quantax EBSD CrystAlign, Germany) attachment onto a SEM (Carl Zeiss, Germany). The poly-Si material quality was then determined using UV reflectance measurements [24-26] (PerkinElmer, Lambda 950, UV/Vis/NIR spectrometer) and Raman spectroscopy [27, 28] measurements (Witec Alpha 300R confocal Raman microscope equipped with a 532nm Nd:YAG laser), whereby the samples were always measured from the air side. Furthermore, TEM (CM300, Philips) was used to examine the microstructure, thickness, and dislocations [21] in the poly-Si films. The defects and dislocations in the poly-Si thin films were further validated and quantified using HAADF STEM [29]. The majority carrier mobility and the doping concentration of the n^+ poly-Si films were evaluated using a Hall effect system (model HL5500 from Accent). The Hall effect measurements were conducted at a magnetic field of 0.32 T and temperature of 300 K and the system was calibrated using a c-Si reference sample at the identical magnetic field.

3.3 Results and Discussion

3.3.1 Impact of PH_3 (2% in H_2)/SiH_4 gas flow ratio on the electronic properties of the SPC poly-Si films

The effect of the PH_3 (2% in H_2)/SiH_4 gas flow on the electronic properties of the n^+ poly-Si films were evaluated using a Hall effect system. Figure 3.1 shows the carrier concentration of the n^+ poly-Si films at four different PH_3 (2% in H_2)/SiH_4 gas flow ratios (0.025, 0.125, 0.25, and 0.45). As expected, the majority carrier concentration was found to increase from 2.36×10^{19} to 3.90×10^{20} cm^{-3} when the PH_3 (2% in H_2)/SiH_4 gas flow ratio was increased from 0.025 to 0.45.

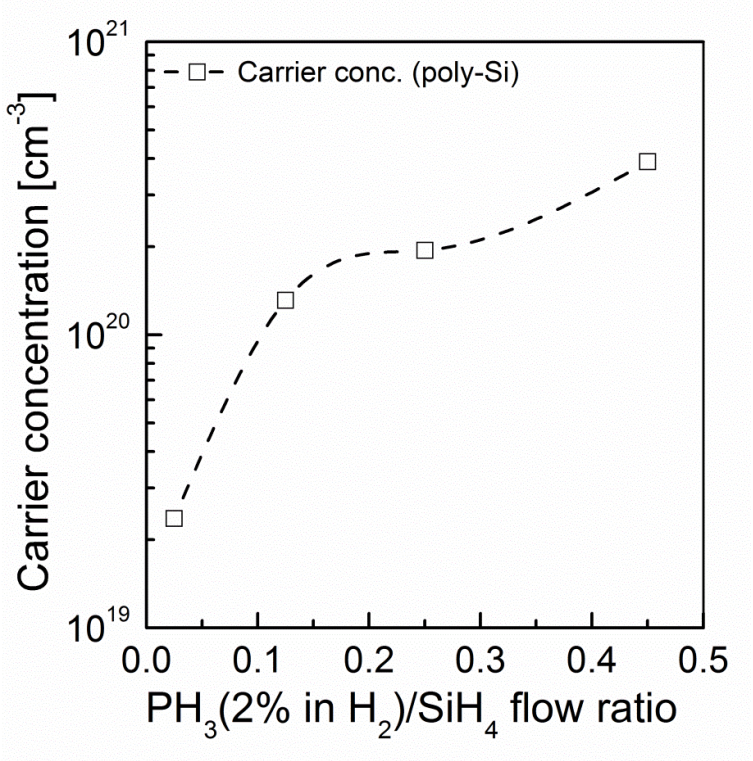

Figure 3.1: *Majority carrier concentration of n^+ poly-Si films as a function of the PH_3 (2% in H_2)/SiH_4 gas flow ratio. The dashed lines are guides to the eye.*

Furthermore, the Hall mobilities of the n^+ poly-Si films were also extracted at various doping concentrations see Fig. 3.2. Also, for comparison, the Hall mobility of phosphorus-doped single-crystal Si [30] as a function of the doping concentration (thick solid line) is presented.

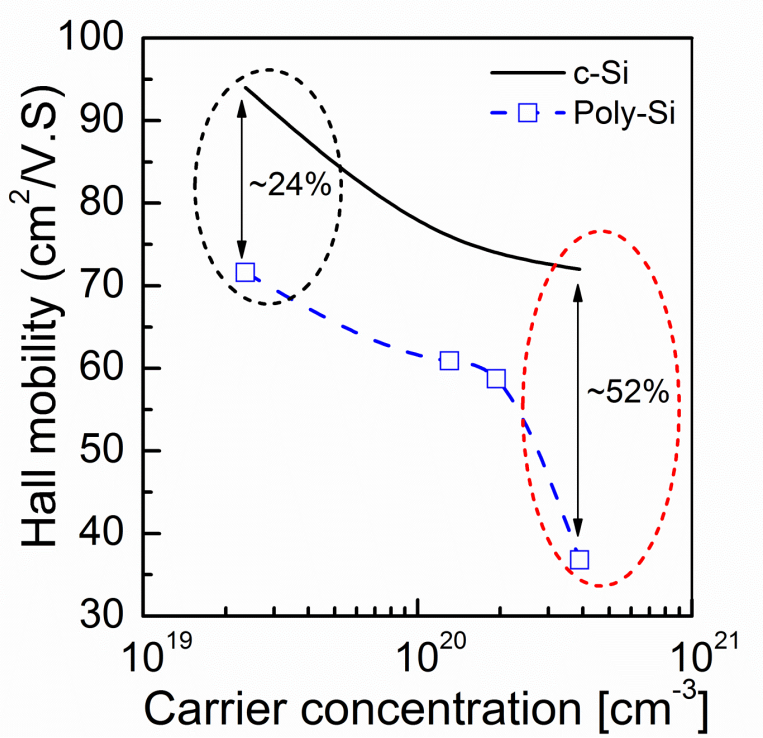

Figure 3.2: *Hall mobility of SPC n^+ poly-Si films as a function of the majority carrier concentration. The solid line indicates the Hall mobility of single-crystal n-type Si [30]. The dashed lines are guides to the eye.*

The Hall mobility of the n^+ poly-Si prepared by the SPC method decreases as the majority carrier concentration increases and follows a trend similar to that of single-crystal Si. The decrease in the Hall mobility with increasing carrier concentration is due to enhanced carrier scattering. A Hall mobility of 71.6 cm^2/Vs at a carrier concentration of 2.36×10^{19} cm^{-3} was obtained for *n*-type poly-Si fabricated with a PH_3 (2% in H_2)/SiH_4 gas flow ratio of 0.025. The Hall mobility of ~ 71.6 cm^2/Vs obtained for the poly-Si film is approximately 76% of

the Hall mobility of c-Si at the same doping concentration. The reason for this 24% drop in Hall mobility for the poly-Si film with respect to that of single-crystal Si could be due to the presence of grain boundaries, the grain orientation and the structural defects in the poly-Si. However, the mobility of the *n*-type poly-Si thin films decreased significantly to 36.8 cm^2/Vs as the carrier concentration increased to 3.9×10^{20} cm^{-3}. This is approximately 48% of the single-crystal Si Hall mobility at that same doping concentration. This sharp drop in Hall mobility of the poly-Si thin film by 52% as compared to single-crystal Si is a strong indication of the increase in defects and disorder in the poly-Si thin film with the increase in the PH_3 (2% in H_2)/SiH_4 gas flow ratio to 0.45.

3.3.2 Stress and crystal quality characteristics of the SPC poly-Si films

The n^+ poly-Si thin-film samples were further characterized using Raman spectroscopy [27] to evaluate the effect of the PH_3 (2% in H_2)/SiH_4 gas flow ratio (doping concentration) on the crystal quality of the films. Raman characterization is a powerful, non-destructive and fast technique that can be conveniently used to characterize stress and defects in polycrystalline silicon [31-33]. Figure 3.3 shows the Raman spectra acquired from the visible (532 nm) laser line for the selected poly-Si thin films fabricated with different PH_3 (2% in H_2)/SiH_4 gas flow ratios. As a reference, the Raman spectrum was also obtained for a single-crystal high-resistivity FZ silicon wafer (solid line). A strong peak at a frequency ω_0 of about 522 cm^{-1} is observed for the c-Si wafer. This peak position value of c-Si may slightly vary from experiment to experiment, depending on the calibration of the spectrometer and monochromator.

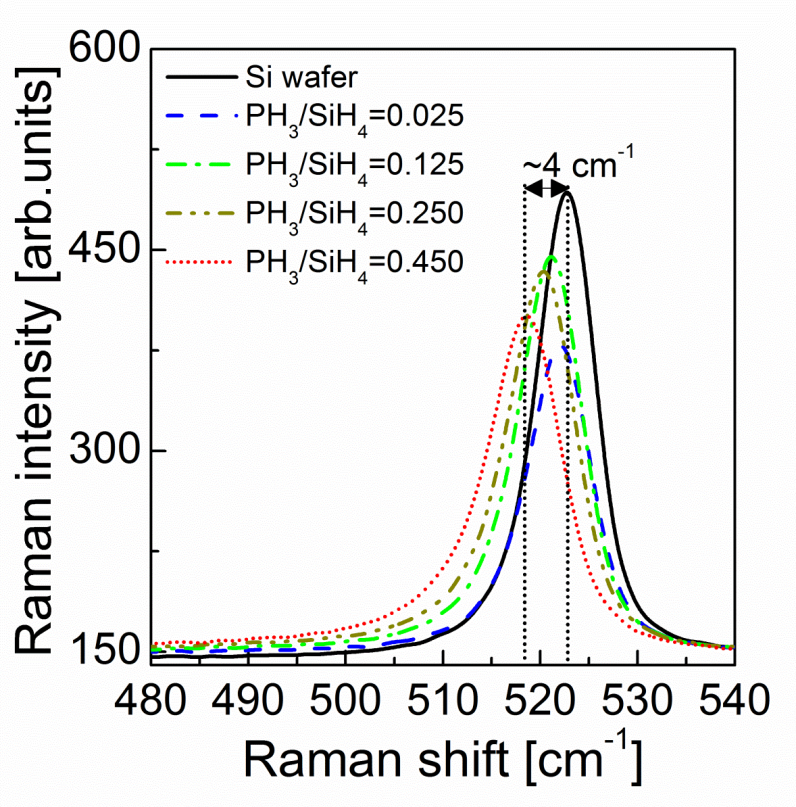

Figure 3.3: *Measured Raman spectra of n-type poly-Si thin films fabricated with four different PH_3 (2% in H_2)/SiH_4 gas flow ratios. Also shown, for comparison, is the Raman spectrum measured for a polished single-crystal Si wafer (solid black lines).*

Furthermore, the Raman spectra also reveal that there is a shift in the peak position of the poly-Si thin film towards lower wave numbers with respect to c-Si as the PH_3 (2% in H_2)/SiH_4 flow ratio is increased, indicating the presence of tensile stress in the poly-Si film [34, 35]. Stress in poly-Si thin films is of great concern, as a high stress can lead to bending, buckling, cracks and in some cases even peeling of the poly-Si films [32, 36, 37], which is detrimental for micro-electronic applications and thus needs to be controlled. The stress level in a poly-Si film can be determined from the wave number shift obtained in the Raman measurement, using the following equation [31, 32, 38]:

$$\sigma = -(250\ MPa\ cm) \times \Delta\omega \qquad 3.1$$

where σ stands for stress and Δω is the shift in the Raman peak position (wave number) of the poly-Si film compared to that of unstressed single-crystal Si.

Further, detailed analysis of the Raman spectra (see Fig. 3.3) reveals that the full width at half maximum (FWHM) of the poly-Si film increases with increasing PH_3 (2% in H_2)/SiH_4 flow ratio. The FWHM is an excellent indicator of the crystal quality of the poly-Si film. An increasing defect density and disorder in c-Si films leads to the broadening of the peak (FWHM) [27, 31, 33]. A Raman quality factor (R_Q) is defined here as the ratio between the FWHM of single-crystal Si to that of the poly-Si film ($R_Q = \frac{FWHM_{c-Si}}{FWHM_{poly-Si}}$) to quantify the defects in the poly-Si film relative to a (stress-free) single-crystalline Si wafer.

Figure 3.4 shows the calculated Raman quality factor and stress behaviour of the poly-Si thin film as a function of the PH_3 (2% in H_2)/SiH_4 flow ratio. From the trend in Figure 3.4, it is observed that the stress in the poly-Si thin film increases, while the crystal quality decreases, when the PH_3 (2% in H_2)/SiH_4 gas flow ratio increases. The increase of tensile stress in the poly-Si thin film with increasing phosphorus concentration is in good agreement with the earlier reported results by Nickel *et al.*,[39] but not much information was given about the impact of stress on the crystal quality of the poly-Si thin film. Stress in the poly-Si film could be due the combination of several factors, such as internal microstructure, different expansion coefficients of materials, and defects in the crystalline matrix during the formation of poly-Si films [31]. Raman spectroscopy confirms that the defect density in the n^+ poly-Si thin film increases with the increase of PH_3 (2% in H_2)/SiH_4 gas flow ratio or phosphorus concentration.

However, since all the parameters in this experiment except the PH_3 (2% in H_2)/SiH_4 gas flow ratio were kept constant, we suspect the internal microstructure such as crystallinity, grain size, grain orientation, and misorientation could be the major factors for stress in the poly-Si thin films. Thus, the poly-Si thin films were further analysed using the EBSD characterization technique to study the effect of the PH_3 (2% in H_2)/SiH_4 gas flow ratio (doping concentration) on the grain size, crystallographic orientation, intra- and inter-grain defects in the poly-Si thin film.

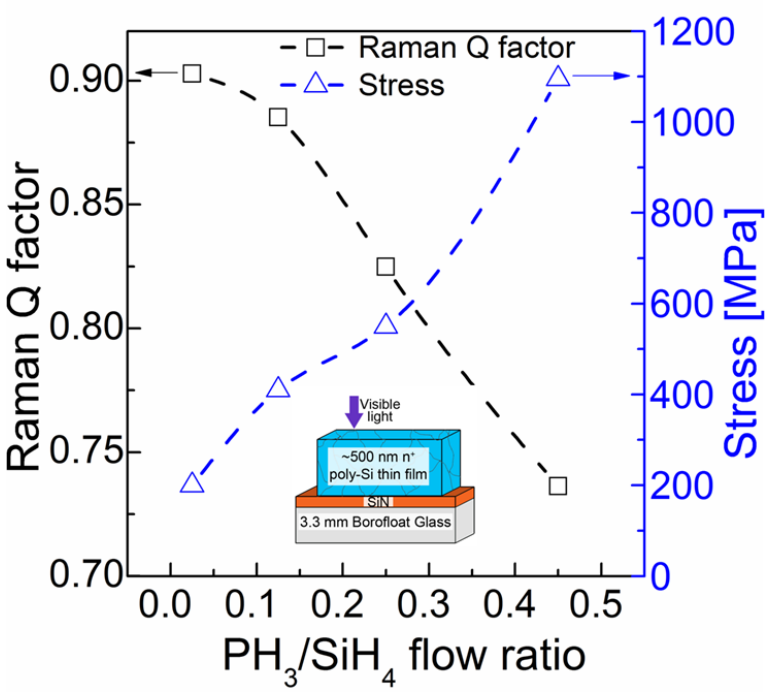

Figure 3.4: *Crystal quality factor (R_Q) and stress characteristic of the n-type poly-Si thin film as obtained from Raman spectroscopy as a function of the PH_3 (2% in H_2)/SiH_4 gas flow ratio. The dotted lines are guides to the eye. Inset: Schematic view of the poly-Si thin film under test.*

3.3.3 Grain size enlargement, crystallographic orientation and defects in the SPC poly-Si thin film

Figure 3.5 shows an EBSD grain orientation map of the poly-Si thin film for four different PH_3 (2% in H_2)/SiH_4 gas flow ratios (0.025, 0.125, 0.25, and

0.45). The grains of the *n*-type poly-Si thin films were found to be randomly oriented and the grain size increased with increasing PH_3 (2% in H_2)/SiH_4 gas flow ratio. Each colour in the orientation map represents a specific crystallographic orientation. A colour triangle representing the different crystal orientations is shown in the inset of each figure. The average grain size was found to increase from 4.3 to 18.1 µm. The increase in the grain size could be due to the enhanced growth rate from the increased phosphorus dopant concentration [40, 41]. Furthermore, detailed observation of EBSD orientation maps revealed that the number of $\sum 3$ grain boundaries in the n^+ poly-Si thin films increases with increasing PH_3 (2% in H_2)/SiH_4 gas flow ratio. An increasing number of $\sum 3$ grain boundaries in the *n*-type poly-Si are an indicator of an increasing density of crystallographic defects [14].

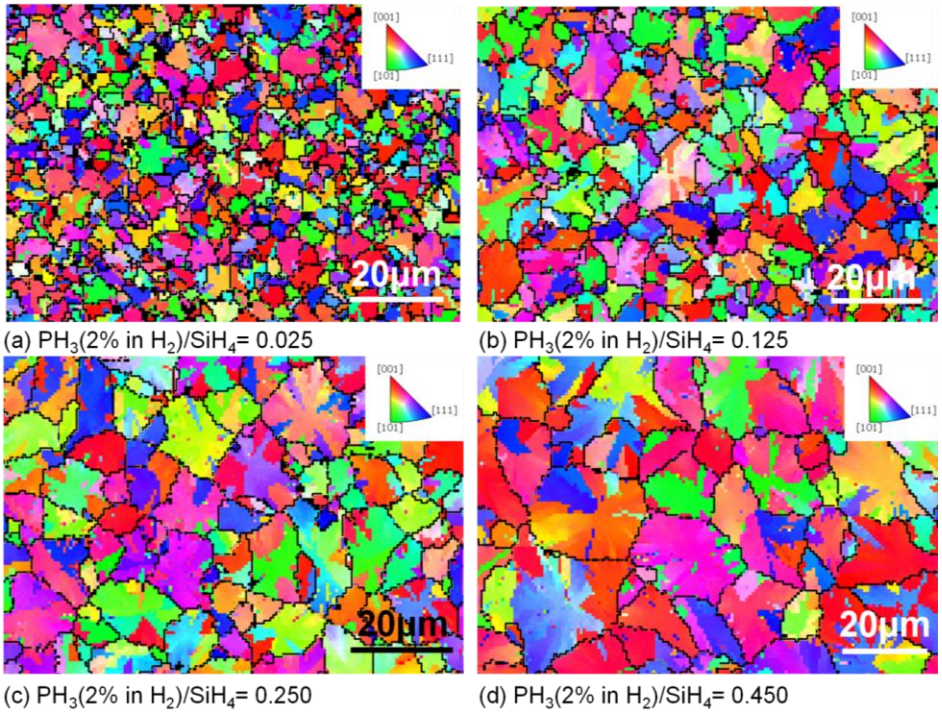

(a) PH_3(2% in H_2)/SiH_4= 0.025 (b) PH_3(2% in H_2)/SiH_4= 0.125

(c) PH_3(2% in H_2)/SiH_4= 0.250 (d) PH_3(2% in H_2)/SiH_4= 0.450

Figure 3.5: *EBSD grain size and orientation of the n-type poly-Si thin film as a function of the PH_3 (2% in H_2)/SiH_4 gas flow ratio.*

To understand the impact and mechanism behind the degradation of the poly-Si material quality with increasing grain size, a further analysis of the EBSD data was carried out to obtain qualitative and quantitative information about mis-orientation and strain present in the grain at microscopic level that could affect the poly-Si film quality. EBSD is quite sensitive and can map intra-grain mis-orientation (plastic deformation) in polycrystalline films subjected to strain gradients [42-45]. Figure 3.6 shows the grain average misorientation (GAM) map for n^+ poly-Si thin films as a function of the PH_3 (2% in H_2)/SiH_4 gas flow ratio (0.025, 0.125, 0.25, and 0.45).

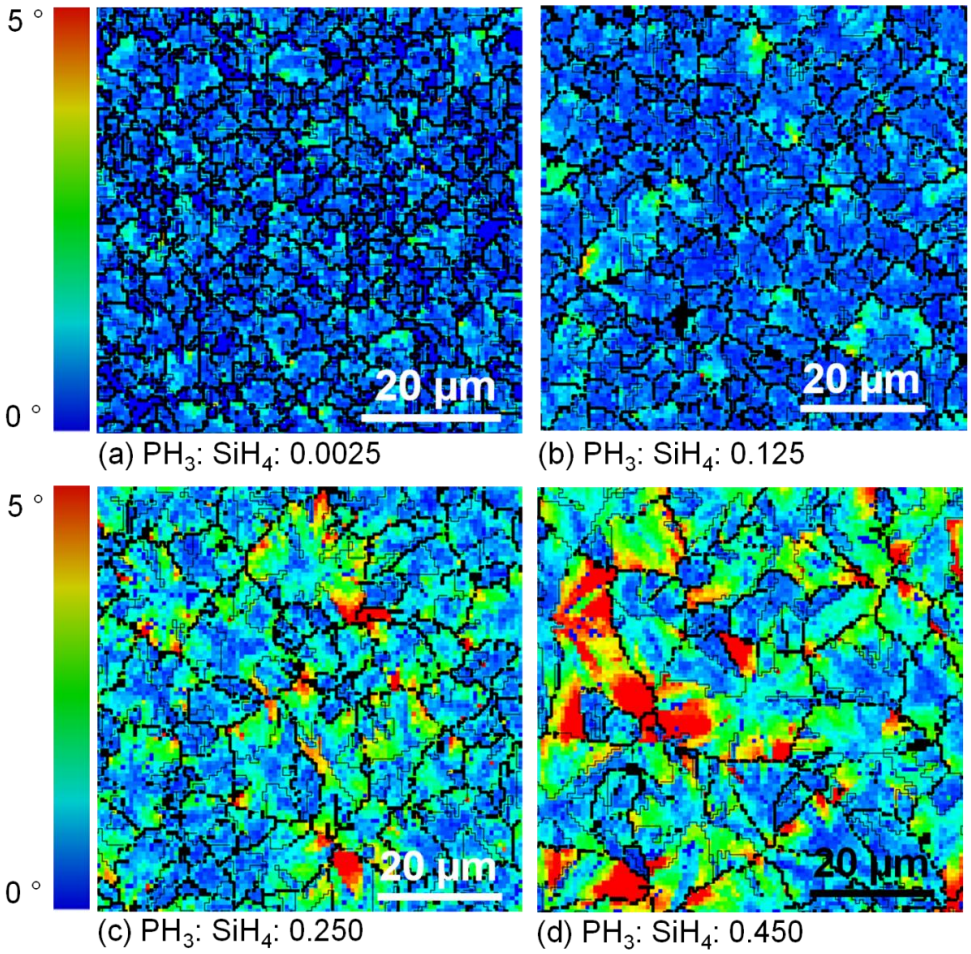

Figure 3.6: *GAM maps of the n-type poly-Si thin film as a function of the PH_3 (2% in H_2)/SiH_4 gas flow ratio (0.025, 0.125, 0.25 and 0.45).*

The accumulated orientation changes relative to the average orientation within a grain can be measured from a GAM map and thus allow the visualization of misorientation gradients within the material (plastic deformation) [42, 43, 46]. A colour map from blue (0°) to red (5°) is used to measure the misorientation between the reference pixel of a grain and every other pixel within the same grain. A small amount of misorientation (0 - 0.5°) is represented in blue colour, while a high degree of misorientation (plastic deformation) is represented by red colour (~ 4 - 5 °). It can be clearly seen that the intra-grain misorientation increases with increasing PH_3 (2% in H_2)/SiH_4 gas flow ratio. The misorientation reaches up to 5° in the film produced with a PH_3 (2% in H_2)/SiH_4 gas flow ratio of 0.45, which is nearly four times higher than for the film produced with a flow ratio of 0.025. The increase of plastic deformation (misorientation) in the poly-Si film with increasing PH_3 (2% in H_2)/SiH_4 gas flow ratio could be responsible for the increase of tensile stress in the film (see Fig. 3.4). The high degree of mis-orientation (plastic deformation) is an indication of the presence of geometrically necessary dislocations (GNDs) [46], which are detrimental for the application of the poly-Si thin films in solar cells and other devices.

EBSD is an excellent technique that provides detailed information about the grain orientation, distribution and boundary characterization of a poly-crystalline film, but is limited to the surface region of the film and hence fails to give a detailed overview of the entire film. Furthermore, to have a better under-standing for deterioration of the poly-Si thin film quality with increasing phosphorus concentration, cross-sectional TEM and HAAD-STEM studies were

performed on selected poly-Si thin-film samples. TEM was used to get detailed information about the microstructural changes in the poly-Si films as a function of the PH_3 (2% in H_2)/SiH_4 gas flow ratio, while HAAD-STEM was used to reveal the dislocations in the poly-Si films [29, 46].

Figures 3.7(a) and 3.7(b) show cross-sectional TEM images of the n^+ poly-Si thin films prepared with a PH_3 (2% in H_2)/SiH_4 flow ratio of 0.025 and 0.45, respectively. It appears from these images that there is a deterioration of the structural quality of the poly-Si film with increasing PH_3 (2% in H_2)/SiH_4 gas flow ratio. The result from TEM seems to be in good agreement with the EBSD and Raman results.

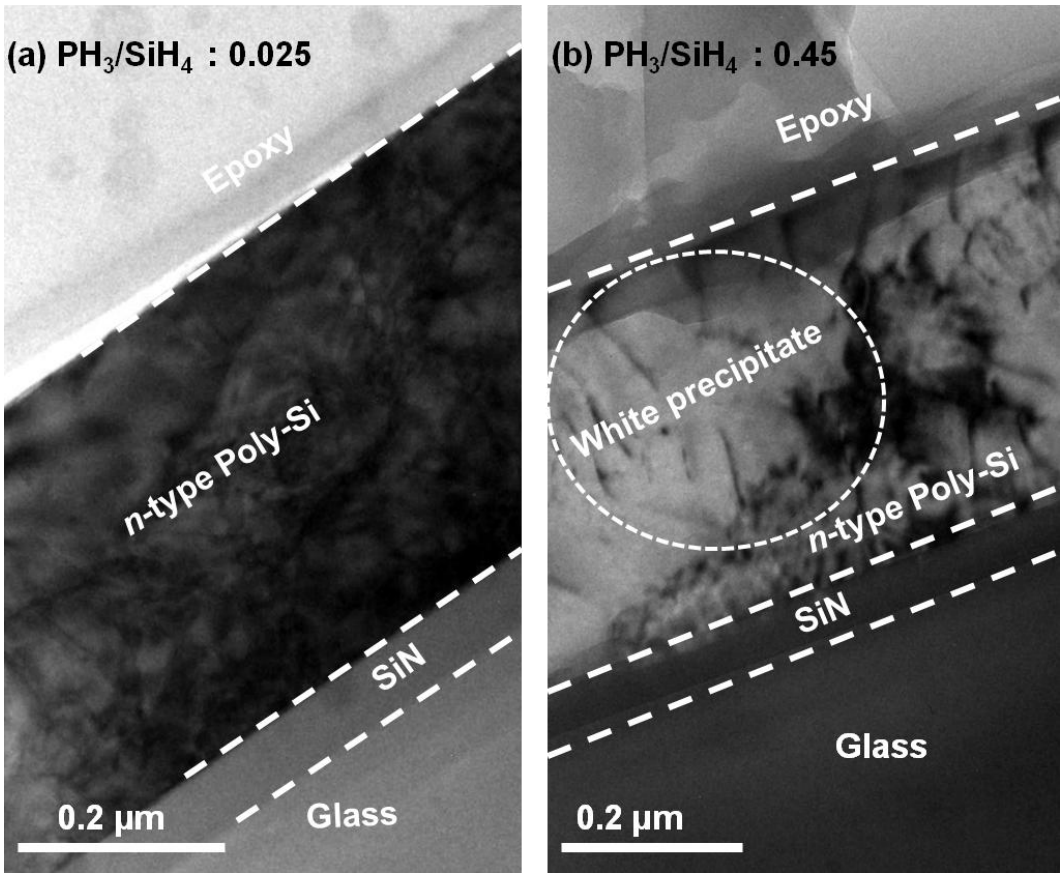

Figure 3.7: *Cross-sectional bright field TEM image of the n-type poly-Si thin film fabricated with a PH_3 (2% in H_2)/SiH_4 gas flow ratio of (a) 0.025, (b) 0.45.*

Furthermore, detailed observations of the TEM images revealed the formation of white precipitates in the heavily phosphorus doped poly-Si film. It has been reported in the literature that an excess phosphorus concentration in crystalline Si results in the formation of phosphorus-rich precipitates [47, 48] and thus the white precipitate seen in the TEM image of Fig. 3.7(b) could be due to the formation of phosphorus-rich precipitates, which in turn could produce defects in the poly-Si thin film during heat treatment [47].

Further analysis was carried out on the same specimens using weak beam dark-field (WBDF) TEM [49] to identify the nature of the defects and dislocations in the poly-Si films as a function of the phosphorus concentration. Dislocations in a poly-Si thin film can, under certain diffraction conditions, be imaged using WBDF TEM [49]. Figure 3.8 shows the cross-sectional WBDF TEM images of the n^+ poly-Si thin films prepared with a PH_3 (2% in H_2)/SiH_4 gas flow ratio of (a) 0.025 and (b) 0.45. Clear dislocations (white lines) are observed in the poly-Si film prepared with a PH_3 (2% in H_2)/SiH_4 gas flow ratio of 0.025. These dislocations could be a combination of statistically stored dislocations (SSDs) that are formed during the grain growth [46, 50], and the GNDs. The dislocation density seems to increase drastically when the PH_3 (2% in H_2)/SiH_4 gas flow ratio is increased to 0.45 (see Fig. 3.8(b)). The increase in dislocations as observed in figure 3.8(b) could be due the formation of additional GNDs. GNDs are extra defects in addition of SSDs which are formed due to the presence of strain gradient in crystalline material [50] and hence need to be minimized.

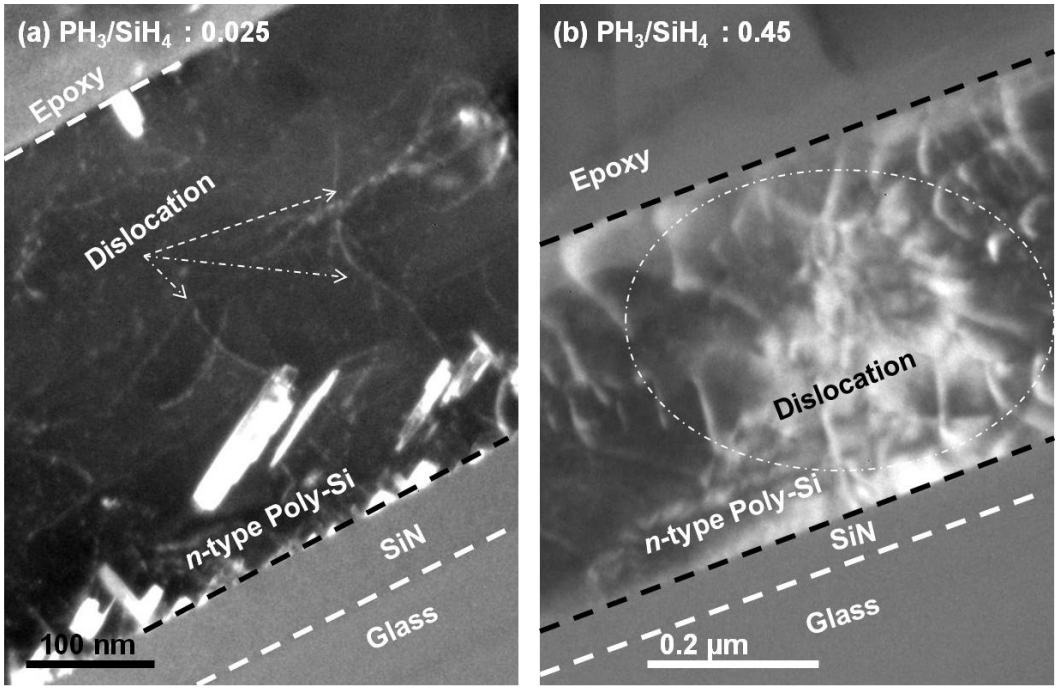

Figure 3.8: *Cross-sectional WBDF TEM image of the n-type poly-Si thin film fabricated with a PH_3 (2% in H_2)/SiH_4 gas flow ratio of (a) 0.025, (b) 0.45.*

Selected specimens were further analysed using HAADF-STEM, whereby the samples were tilted at the zone axis. In this configuration, atoms close to the core of dislocations display a high contrast in HAADF images [29]. In addition, STEM images are formed by collecting most of the scattered electrons on the annular dark-field (ADF) detector whereas only a fraction of the scattered electrons is permitted to enter the objective aperture for the formation of dark-field (DF) TEM images [49]. Thus, HAADF-STEM is more capable of providing detailed information about defects and dislocations in poly-Si thin films. Figure 3.9 shows the cross-sectional HAADF-STEM images of n^+ poly-Si thin films prepared with a PH_3 (2% in H_2)/SiH_4 gas flow ratio of (a) 0.25 and (b) 0.45. It can be seen that dislocations are present and resemble a periodic trend (white lines) in the poly-Si thin produced with a low flow ratio of 0.025. In comparison, the

dislocation density has significantly increased and is randomly distributed over the entire film for the sample prepared with a flow ratio of 0.45 (see Fig. 3.9(b)).

From HAAD-STEM, it appears that the film quality deteriorates significantly when the PH_3 (2% in H_2)/SiH_4 gas flow ratio is increased to 0.45. These additional dislocations could act as charge carrier recombination centres, which would be detrimental in solar cell applications. This interpretation of dislocations in the poly-Si films as a function of the PH_3 (2% in H_2)/SiH_4 gas flow ratio from TEM and HAAD-STEM is in good agreement with the results obtained from EBSD (see Fig. 3.6).

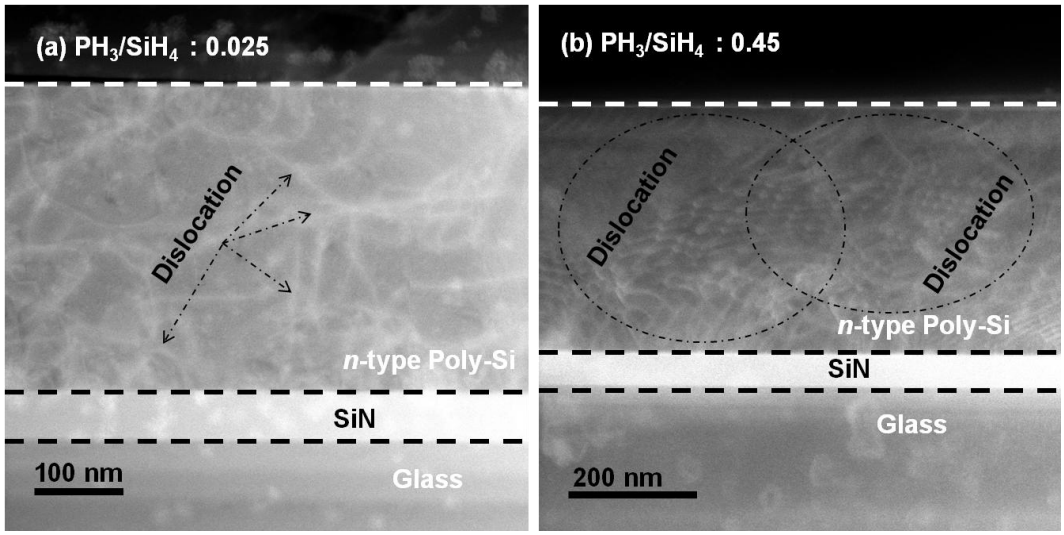

Figure 3.9: *Cross-sectional HAADF-STEM image of the n-type poly-Si thin film fabricated with a PH_3 (2% in H_2)/SiH_4 gas flow ratio of (a) 0.025, (b) 0.45.*

3.4 Conclusion

In conclusion, *n*-type poly-Si films with very large grains, exceeding 30 μm in width, were successfully fabricated. The experimental results showed that the doping concentration and the grain size of the SPC poly-Si films increased with increasing PH_3 (2% in H_2)/SiH_4 gas flow ratio, whereas the crystalline quality of the material deteriorated. The average grain size of the poly-Si films was found to increase from 4.3 to 18 μm as the PH_3 (2% in H_2)/SiH_4 gas flow ratio was increased from 0.025 to 0.45, with some grains even exceeding 30 μm in width. It was shown that the stress in the large-grained poly-Si thin films fabricated with a high PH_3 (2% in H_2)/SiH_4 gas flow ratio is the main reason for the deterioration of the material quality. The stress in the poly-Si films was found to be in excess of 1000 MPa, which leads to defects (for example dislocations) in the poly-Si films. The increased dislocation density with increasing PH_3 (2% in H_2)/SiH_4 gas flow ratio was also observed in the HAADF-STEM and EBSD studies performed in this work. With respect to device applications, it is thus desirable to control the phosphorus concentration in the poly-Si films through the control of the PH_3 (2% in H_2)/SiH_4 gas flow ratio, to strike the right balance between the grain size and the material quality of the poly-Si thin film.

References of chapter 3

[1] N. Yamauchi and R. Reif, "Polycrystalline silicon thin films processed with silicon ion implantation and subsequent solid-phase crystallization: Theory, experiments, and thin-film transistor applications," *Journal of Applied Physics,* vol. 75, pp. 3235-3257, 1994.

[2] A. Mimura, N. Konishi, K. Ono, J. I. Ohwada, Y. Hosokawa, Y. A. Ono, *et al.*, "High performance low-temperature poly-Si n-channel TFTs for LCD," *Electron Devices, IEEE Transactions on,* vol. 36, pp. 351-359, 1989.

[3] C. Spinella, S. Lombardo, and F. Priolo, "Crystal grain nucleation in amorphous silicon," *Journal of Applied Physics,* vol. 84, pp. 5383-5414, 1998.

[4] T. Matsuyama, K. Wakisaka, M. Kameda, M. Tanaka, T. Matsuoka, S. Tsuda, *et al.*, "Preparation of High-Quality *n*-Type Poly-Si Films by the Solid Phase Crystallization (SPC) Method," *Japanese Journal of Applied Physics,* vol. 29, pp. 2327-2331, 1990.

[5] R. B. Bergmann, G. Oswald, M. Albrecht, and V. Gross, "Solid-phase crystallized Si films on glass substrates for thin film solar cells," *Solar Energy Materials and Solar Cells,* vol. 46, pp. 147-155, 1997.

[6] J. Dore, R. Evans, U. Schubert, B. D. Eggleston, D. Ong, K. Kim, *et al.*, "Thin-film polycrystalline silicon solar cells formed by diode laser crystallisation," *Progress in Photovoltaics: Research and Applications,* vol. 21, pp. 1377-1383, 2013.

[7] J. Haschke, L. Jogschies, D. Amkreutz, L. Korte, and B. Rech, "Poly-crystalline silicon heterojunction thin-film solar cells on glass exhibiting 582 mV open-circuit voltage," *Solar Energy Materials and Solar Cells,* vol. 115, pp. 7-10, 2013.

[8] R. Goswami, B. Chowdhury, and S. Ray, "Solid phase crystallization of protocrystalline silicon films: Changes in structural and optical properties," *Thin Solid Films,* vol. 516, pp. 2306-2313, 2008.

[9] B. Rau, T. Weber, B. Gorka, P. Dogan, F. Fenske, K. Y. Lee, *et al.*, "Development of a rapid thermal annealing process for polycrystalline silicon thin-film solar cells on glass," *Materials Science and Engineering: B,* vol. 159–160, pp. 329-332, 2009.

[10] A. G. Aberle, "Fabrication and characterisation of crystalline silicon thin-film materials for solar cells," *Thin Solid Films,* vol. 511–512, pp. 26-34, 2006.

[11] C. Becker, D. Amkreutz, T. Sontheimer, V. Preidel, D. Lockau, J. Haschke, *et al.*, "Polycrystalline silicon thin-film solar cells: Status and perspectives," *Solar Energy Materials and Solar Cells,* pp. 112-123, 2013.

[12] T. Sontheimer, A. Schnegg, S. Steffens, F. Ruske, D. Amkreutz, K. Lips, *et al.*, "Identification of intra-grain and grain boundary defects in poly-crystalline Si thin films by electron paramagnetic resonance," *physica status solidi (RRL) – Rapid Research Letters,* vol. 7, pp. 959-962, 2013.

[13] S. Steffens, C. Becker, J. H. Zollondz, A. Chowdhury, A. Slaoui, S. Linde-kugel, *et al.*, "Defect annealing processes for polycrystalline silicon thin-film solar cells," *Materials Science and Engineering: B,* vol. 178, pp. 670-675, 2013.

[14] Ö. Tüzün, A. Slaoui, C. Maurice, and S. Vallon, "Growth kinetics and polysilicon formation by aluminium-induced crystallization on glass-ceramic substrates," *Applied Physics A,* vol. 99, pp. 53-61, 2010.

[15] P. A. Basore, "CSG-1: Manufacturing a New Polycrystalline Silicon PV Technology," *in Conference Record of the 4th IEEE World Conference on Photovoltaic Energy Conversion,* 2006, pp. 2089-2093

[16] M. A. Green, K. Emery, Y. Hishikawa, and W. Warta, "Solar cell efficiency tables (version 35)," *Progress in Photovoltaics: Research and Applications,* vol. 18, pp. 144-150, 2010.

[17] R. B. Bergmann, "Crystalline Si thin-film solar cells: a review," *Applied Physics A,* vol. 69, pp. 187-194, 1999/08/01 1999.

[18] T. Matsuyama, M. Tanaka, S. Tsuda, S. Nakano, and Y. Kuwano, "Improvement of n-type poly-Si film properties by solid phase crystalli-zation method," *Jpn. J. App. Phys. Vol,* vol. 32, pp. 3720-3728, 1993.

[19] K. Nakazawa and K. Tanaka, "Effect of substrate temperature on recrystallization of plasma chemical vapor deposition amorphous silicon films," *Journal of Applied Physics,* vol. 68, pp. 1029-1032, 1990.

[20] L. Carnel, I. Gordon, D. Van Gestel, G. Beaucarne, J. Poortmans, and A. Stesmans, "High open-circuit voltage values on fine-grained thin-film poly-silicon solar cells," *Journal of Applied Physics,* vol. 100, pp. 063702-7, 2006.

[21] D. V. Gestel, I. Gordon, H. Bender, D. Saurel, J. Vanacken, G. Beaucarne, *et al.*, "Intragrain defects in polycrystalline silicon layers grown by aluminum-induced crystallization and epitaxy for thin-film solar cells," *Journal of Applied Physics,* vol. 105, p. 114507, 2009.

[22] T. Matsuyama, N. Terada, T. Baba, T. Sawada, S. Tsuge, K. Wakisaka, *et al.*, "High-quality polycrystalline silicon thin film prepared by a solid phase crystallization method," *Journal of Non-Crystalline Solids,* vol. 198, pp. 940-944, 1996.

[23] A. Kumar, P. I. Widenborg, F. Law, H. Hidayat, G. K. Dalapati, and A. G. Aberle, "Study of large-grained *n*-type polycrystalline silicon thin films made by the solid phase crystallization method," *in 39th IEEE Photovoltaic Specialists Conference (PVSC), 2013*, pp. 0586-0588.

[24] G. Harbeke and L. Jastrzebski, "Assessment of the surface quality of simox wafers by uv reflectance," *Journal of the Electrochemical Society,* vol. 137, pp. 696-699, 1990.

[25] A. Straub, P. I. Widenborg, A. Sproul, Y. Huang, N. P. Harder, and A. G. Aberle, "Fast and non-destructive assessment of epitaxial quality of poly-crystalline silicon films on glass by optical measurements," *Journal of Crystal Growth,* vol. 265, pp. 168-173, 2004.

[26] P. I. Widenborg and A. G. Aberle, "Hydrogen-induced dopant neutralisation in p-type AIC poly-Si seed layers functioning as buried emitters in ALICE thin-film solar cells on glass," *Journal of Crystal Growth,* vol. 306, pp. 177-186, 2007.

[27] S. Nakashima and M. Hangyo, "Characterization of semiconductor-materials by Raman microprobe," *IEEE Journal of Quantum Electronics,* vol. 25, pp. 965-975, 1989.

[28] M. Holtz, W. M. Duncan, S. Zollner, and R. Liu, "Visible and ultraviolet Raman scattering studies of $Si_{1-x}Ge_x$ alloys," *Journal of Applied Physics,* vol. 88, pp. 2523-2528, 2000.

[29] J. M. Cowley and Y. Huang, "De-channelling contrast in annular dark-field STEM," *Ultramicroscopy,* vol. 40, pp. 171-180, 1992.

[30] R. Hull, *Properties of crystalline silicon*: Institution of Electrical Engineers, 1999.

[31] R. C. Teixeira, I. Doi, M. B. P. Zakia, J. A. Diniz, and J. W. Swart, "Micro-Raman stress characterization of polycrystalline silicon films grown at high temperature," *Materials Science and Engineering: B,* vol. 112, pp. 160-164, 2004.

[32] I. De Wolf, "Micro-Raman spectroscopy to study local mechanical stress in silicon integrated circuits," *Semiconductor Science and Technology,* vol. 11, pp. 139-154, 1996.

[33] A. Kumar, H. Hidayat, C. Ke, S. Chakraborty, G. K. Dalapati, P. I. Widenborg, *et al.*, "Impact of the n^+ emitter layer on the structural and electrical properties of p-type polycrystalline silicon thin-film solar cells," *Journal of Applied Physics,* vol. 114, p. 134505, 2013.

[34] K. Kitahara, H. Ogasawara, J. Kambara, M. Kobata, and Y. Ohashi, "Characterization of defects in polycrystalline silicon thin films using chemical etching, hydrogenation, and Raman spectroscopy," *Japanese Journal of Applied Physics,* vol. 47, p. 54, 2008.

[35] K. Kitahara, T. Ishii, J. Suzuki, T. Bessyo, and N. Watanabe, "Characterization of Defects and Stress in Polycrystalline Silicon Thin Films on Glass Substrates by Raman Microscopy," *International Journal of Spectroscopy,* vol. 2011, p. 632139, 2011.

[36] M. S. Benrakkad, M. A. Benitez, J. Esteve, J. M. Lopez-Villegas, J. Samitier, and J. R. Morante, "Stress measurement by microRaman spectroscopy of polycrystalline silicon structures," *Journal of Micromechanics and Microengineering,* vol. 5, p. 132, 1995.

[37] G. Kaltsas, A. G. Nassiopoulou, M. Siakavellas, and E. Anastassakis, "Stress effect on suspended polycrystalline silicon membranes fabricated by micromachining of porous silicon," *Sensors and Actuators A: Physical,* vol. 68, pp. 429-434, 1998.

[38] P. Münster, M. Sarret, T. Mohammed-Brahim, N. Coulon, and J.-Y. Mevellec, "Polycrystalline silicon deposited on glass by subatmospheric-pressure chemical vapour deposition at a high rate," *Philosophical Magazine Part B,* vol. 82, pp. 1695-1701, 2002.

[39] N. H. Nickel, P. Lengsfeld, and I. Sieber, "Raman spectroscopy of heavily doped polycrystalline silicon thin films," *Physical Review B,* vol. 61, pp. 15558-15561, 2000.

[40] Y. Wada and S. Nishimatsu, "Grain Growth Mechanism of Heavily Phosphorus-Implanted Polycrystalline Silicon," *Journal of The Electrochemical Society,* vol. 125, pp. 1499-1504, 1978.

[41] B. C. Johnson and J. C. McCallum, "Dopant-enhanced solid-phase epitaxy in buried amorphous silicon layers," *Physical Review B,* vol. 76, p. 045216, 2007.

[42] L. Brewer, M. Othon, L. Young, and T. Angeliu, "Misorientation mapping for visualization of plastic deformation via electron back-scattered diffraction," *Microscopy and Microanalysis,* vol. 12, pp. 85-91, 2006.

[43] L. Brewer, D. Field, and C. Merriman, "Mapping and Assessing Plastic Deformation Using EBSD," in *Electron Backscatter Diffraction in*

Materials Science, A. J. Schwartz, M. Kumar, B. L. Adams, and D. P. Field, Eds., ed: Springer US, 2009, pp. 251-262.

[44] A. Wilkinson, E. Clarke, T. Britton, P. Littlewood, and P. Karamched, "High-resolution electron backscatter diffraction: An emerging tool for studying local deformation," *The Journal of Strain Analysis for Engineering Design,* vol. 45, pp. 365-376, 2010.

[45] F. Dunne, R. Kiwanuka, and A. Wilkinson, "Crystal plasticity analysis of micro-deformation, lattice rotation and geometrically necessary dislocation density," *Proceedings of the Royal Society A: Mathematical, Physical and Engineering Science,* vol. 468, pp. 2509-2531, 2012.

[46] F. Law, Y. Yi, Hidayat, P. I. Widenborg, J. Luther, and B. Hoex, "Identification of geometrically necessary dislocations in solid phase crystallized poly-Si," *Journal of Applied Physics,* vol. 114, p. 043511, 2013.

[47] M. A. Green, *Solar cells: Operating principles, technology and system applications*: University of New South Wales, 1998.

[48] T. Kamins, *Polycrystalline silicon for integrated circuit applications*: Kluwer Academic Publishers, 1988.

[49] D. B. Williams and C. B. Carter, *The Transmission Electron Microscope*: Springer, 1996.

[50] A. Arsenlis and D. M. Parks, "Crystallographic aspects of geometrically-necessary and statistically-stored dislocation density," *Acta Materialia,* vol. 47, pp. 1597-1611, 1999.

Chapter 4

Chapter 4- Improved Material Quality of n^+ Poly-Si Thin Films through Stress Engineering

4.1. Introduction

4.2. Experimental Details

4.3. Results and Discussion

4.4. Conclusion

4.1 Introduction

The thin-film poly-Si on glass solar cell technology has the potential to achieve energy conversion efficiencies of more than 13% using a single-junction device [1]. However, the inter- and intra-grain defects in the poly-Si thin films presently act as a bottleneck for the technology to achieve such efficiencies. It has been hypothesised that large-grained poly-Si thin films promote better PV performance [2], and also lead to higher field effect mobility as required for TFTs [3]. Recent reports suggest that it is not the grain size, but the intra-grain defects and dislocations in the films that limit the performance of hydrogen-passivated SPC poly-Si thin-film solar cells [4, 5]. However, not much information exists in the literature that relates the material quality of the poly-Si film to its grain size, orientation and the stress within the film. Thus, it is desirable to better understand the influence of the grain microstructures (size, boundaries, orientations, inter and intra-grain defects) and stress on the structural and electrical qualities of poly-Si thin films in order to consider them for future large-scale electronic applications. The microstructure of the poly-Si films and the defects located inside the crystal grains are very important parameters that define the electronic quality of the poly-Si films [6, 7]. In the previous chapter, we presented a method to fabricate *n*-type poly-Si thin films with very large grains, exceeding 30 μm in width. However, we found that the large-grained *n*-type poly-Si films suffer from high stress and have a very high degree of intra-grain misorientation.

In this Chapter, we demonstrate the growth of high-quality *n*-type SPC poly-Si thin films on glass through stress engineering. The stress in the poly-Si films is engineered by controlling the a-Si:H deposition temperature and the gas flow ratio of PH_3 (2% in H_2)/SiH_4. We evaluate large-grained *n*-type poly-Si films prepared by SPC of a-Si:H deposited at 380 °C and 410 °C. The effects of the PH_3 (2% in H_2)/SiH_4 gas flow rate and a-Si:H deposition temperature on the stress and microstructure of the poly-Si films are investigated in detail using Raman spectroscopy and electron backscatter diffraction (EBSD). Furthermore, a detailed effort is made to understand the characteristics of the grain shape and grain boundary and intra-grain defects, which all influence the quality of the fabricated poly-Si thin films.

4.2 Experimental Details

About 500 nm thick *n*-type poly-Si films with varying doping concentrations were prepared via SPC of PECVD (plasma-enhanced chemical vapour deposition) a-Si:H films deposited at 380 °C or 410 °C. First, the n^+ a-Si:H films were deposited in a PECVD cluster tool (MVSystems, USA) onto a SiN_x (~70 nm) coated planar glass sheet (Schott, Borofloat). An ~100 nm thick SiO_x capping layer was then deposited onto the a-Si:H films. The SiO_x layer acts as a barrier for impurities from the ambient during the SPC process as well as the subsequent rapid thermal annealing (RTA) process. The n^+ a-Si:H films were obtained by in-situ doping of phosphorus (P) from the PH_3 (2% in H_2) gas mixed with SiH_4 in a PECVD chamber, using the recipe summarised in Table 4.1.

Table 4.1: *Experimental details used for the PECVD of the n^+ a-Si:H films.*

Process condition	*n^+ a-Si layer*
SiH_4 (sccm)	10
2% PH_3:H_2 (sccm)	0.2-2.5
Substrate temperature (ºC)	380-410
Pressure (Pa)	80
RF power density (mW/cm^2)	8

The deposited a-Si:H films were then annealed (Nabertherm, N 120/65HAC furnace, Germany) at 610 ºC in a N_2 atmosphere for a duration of 12 hours to achieve solid phase crystallisation of the film. A rapid thermal anneal (RTA, CVD Equipment, USA) for 1 minute at a peak temperature of 1000 ºC in N_2 atmosphere was then used to remove crystallographic defects from the SPC poly-Si thin-film diodes and to activate the dopants. The samples were then dipped into 5% diluted hydrofluoric (HF) acid solution to remove the 100 nm thick SiO_x capping layer. The material quality and stress in the poly-Si thin films were analysed using Raman spectroscopy [8, 9] measurements (Witec Alpha 300R confocal Raman microscope equipped with a 532-nm Nd:YAG laser), whereby the samples were always measured from the air side. Furthermore, the poly-Si samples were characterized for grain size, orientation and misorientation by an EBSD system (Bruker Quantax EBSD CrystAlign, Germany) attached onto a SEM (Carl Zeiss, Germany).

4.3 Results and Discussion

4.3.1 Impact of a-Si:H deposition temperature and PH_3 (2% in H_2) gas flow ratio on the stress and crystal quality of the SPC poly-Si films

Stress and defects in the poly-Si thin films can be conveniently characterised using the Raman characterisation technique [10-12]. Figure 4.1 shows the Raman spectra acquired from the visible (532 nm) laser line as a function of PH_3 (2% in H_2)/SiH_4 gas flow ratio for the *n*-type poly-Si thin films obtained from SPC of PECVD a-Si:H films deposited at (a) 380 °C and (b) 410 °C. For reference, the Raman spectrum was also obtained for a single-crystalline high-resistivity FZ silicon (c-Si) wafer (solid line).

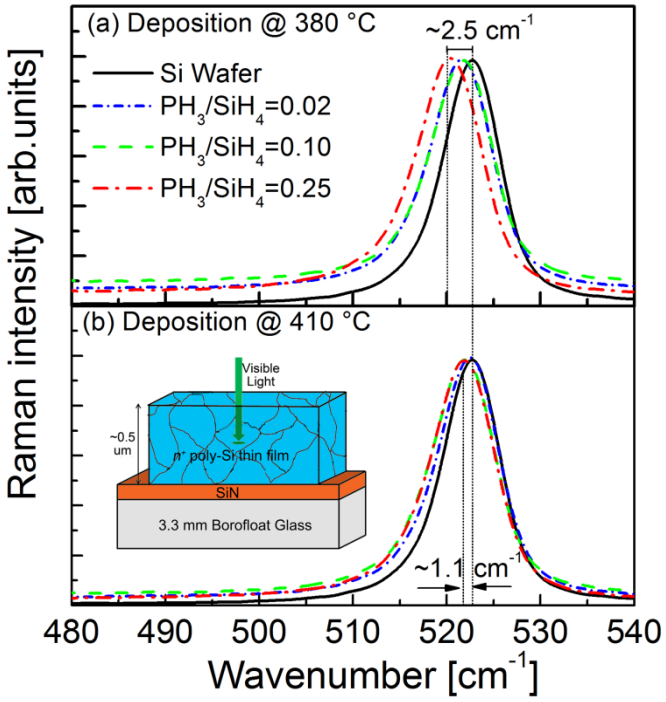

Figure 4.1: *Measured Raman spectra as function of varying PH_3 (2% in H_2)/SiH_4 gas flow ratios for the n-type poly-Si thin films obtained from SPC of PECVD a-Si:H films deposited at (a) 380°C and, (b) 410 °C. Also shown, for comparison, is the Raman spectrum measured for a polished single-crystalline Si wafer (solid black lines).*

A strong peak at a frequency of about ω_0 = 523 cm^{-1} is observed for the c-Si wafer. This peak position value of c-Si may vary slightly from experiment to experiment, depending on the calibration of the spectrometer and monochromator. From Figure 4.1(a) it can be clearly seen that, compared to c-Si, there is a significant shift in the peak position towards lower wave numbers (by up to 2.5 cm^{-1}) for poly-Si films formed via SPC of a-Si:H films deposited at 380 °C. This indicates the increase of tensile stress in the poly-Si thin film [12, 13] when the PH_3 (2% in H_2)/SiH_4 flow ratio is increased from 0.02 to 0.25. The maximum shift in the peak position is reduced to 1.1 cm^{-1} when the corresponding experiment was performed with a-Si:H films deposited at 410 °C, see Figure 4.1(b). This indicates that the stress in the poly-Si thin film can be reduced by increasing the deposition temperature of the a-Si:H films. Increase of stress in poly-Si films can lead to a deterioration of the film properties [11, 14, 15] and is detrimental for the device application. Thus, there is a need to control the stress in the poly-Si films. The stress level in poly-Si films can be conveniently determined from the wave number shift using the following equation [10, 11, 16]:

$$\sigma = -(250\ MPa\ cm) \times \Delta\omega, \qquad 4.1$$

where σ is the stress and Δω is the shift (wave number) in the Raman peak position of the poly-Si film compared to that of unstressed single-crystal Si.

Figure 4.2 shows the calculated stress behaviour as a function of the PH_3 (2% in H_2)/SiH_4 gas flow ratio for the *n*-type poly-Si films fabricated by SPC of a-Si:H films deposited at 380 °C and 410 °C, respectively.

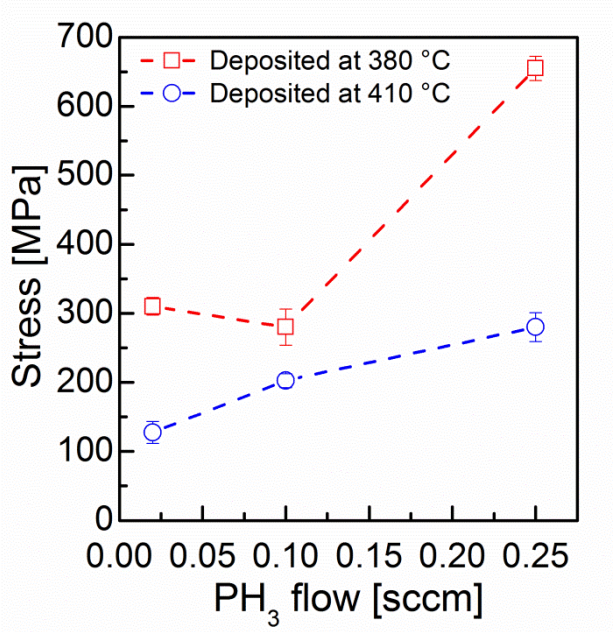

Figure 4.2: *Calculated stress behaviour as a function of PH_3 (2% in H_2)/SiH_4 flow ratio for the n-type poly-Si thin film obtained from the SPC of a-Si:H films deposited at 380 and 410 °C respectively. The dashed lines are guides to the eye.*

It is observed that the average stress in the poly-Si film fabricated by SPC of a-Si:H films deposited at 380 °C reduces slightly from 310 to 290 MPa when the PH_3 (2% in H_2)/SiH_4 flow ratio is increased from 0.025 to 0.1. However, the average stress increases drastically to 655 MPa when the gas flow ratio increases to 0.25. The *n*-type poly-Si films fabricated by SPC of a-Si:H films deposited at a slightly higher temperature of 410 °C behave differently. Here, the average stress increased marginally from 110 to 270 MPa when the PH_3 (2% in H_2)/SiH_4 flow ratio increased from 0.02 to 0.25. The average stress found in the film is much lower compared with the poly-Si film fabricated by SPC of a-Si:H films deposited at 380 °C. Further analysis of the Raman spectra of Figure 4.1 revealed that the full width at half maximum (FWHM) of the poly-Si films varies with the a-Si:H deposition conditions. The FWHM is an excellent indicator of the crystal quality of poly-Si thin films. The increase of defects and disorder in Si thin films leads to

broadening of the peak (FWHM) [8, 10, 17]. A Raman quality factor (R_Q) is defined here as the ratio between the FWHM of c-Si to that of the poly-Si film ($R_Q = \frac{FWHM_{c-Si}}{FWHM_{poly-Si}}$) to quantify the defects in the poly-Si film in relation to a stress-free c-Si wafer.

Figure 4.3 shows the calculated average Raman quality factors of the *n*-type poly-Si thin films fabricated by SPC of a-Si:H films deposited at 380 °C and 410 °C, respectively, as a function of the PH_3 (2% in H_2)/SiH_4 gas flow ratio. It is observed that the *n*-type SPC poly-Si films fabricated from a-Si:H films deposited at 410 °C have the highest average crystal quality factor of ~ 0.97 at a low PH_3 (2% in H_2)/SiH_4 gas flow ratio of 0.02. In contrast, for a-Si:H deposited at 380 °C, the average crystal quality factor peaks at an intermediate PH_3 (2% in H_2)/SiH_4 gas flow ratio.

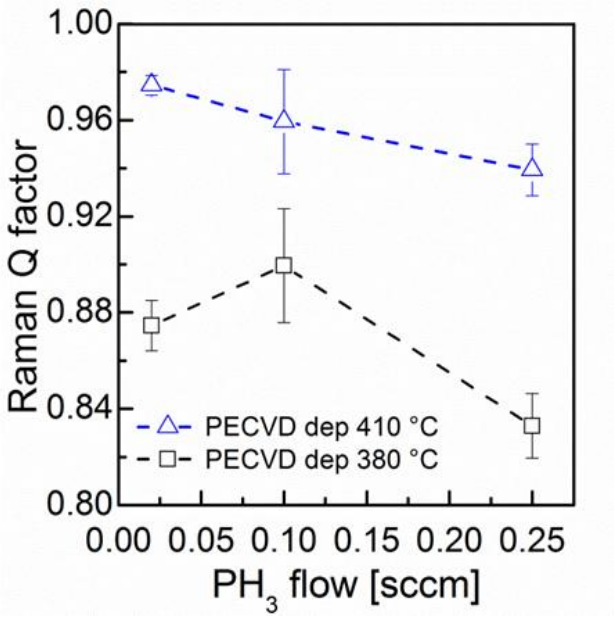

Figure 4.3: *Raman quality factor (R_Q) as function of varying PH_3 (2% in H_2)/SiH_4 gas flow ratios for the n-type poly-Si thin films obtained from SPC of PECVD a-Si:H films deposited at 380 and 410 °C respectively. The dashed lines are guides to the eye.*

It can be seen that the trend in crystal quality variation (see Figure 4.3) is similar to the trend in the tensile stress present in the poly-Si films (see Figure 4.2), establishing a relationship between the crystal quality and the stress in the film. The increasing tensile stress in the poly-Si films with increasing phosphorus (P) concentration is in good agreement with the earlier reported results by Nickel *et al*. [18], but not much information was given about the relationship between stress and the crystal quality of the poly-Si films. In addition, the effect of the a-Si:H deposition temperature on the stress in SPC poly-Si films has not yet been discussed in the literature.

There are several factors such as material geometry, different expansion coefficients of materials and defects in the crystalline matrix during the formation of SPC poly-Si films that could generate stress in the films [10]. Our Raman spectroscopy results confirm the variation of stress and crystal quality of *n*-type SPC poly-Si films with changes in the a-Si:H deposition parameters. However, the cause for this variation in crystal quality is unclear and the impact of the a-Si:H deposition temperature on the stress in the resulting SPC poly-Si films needs to be understood to grow high-quality poly-Si films. The internal micro-structure properties, such as crystallinity, grain size, grain orientation, and mis-orientation, could be the major factors for stress in poly-Si thin films. Thus, the poly-Si thin films were further analysed using the EBSD characterisation technique to study the effects of the deposition temperature of a-Si:H and the gas flow ratio of PH_3 (2% in H_2)/SiH_4 (i.e., doping concentration) on the grain size, crystallographic orientation and intra-grain defects in the SPC poly-Si films.

4.3.2 Effects of a-Si:H deposition temperature and gas flow ratio of PH_3 (2% in H_2)/SiH_4 on grain size, crystallographic orientation and defects in the SPC poly-Si films

Figure 4.4 shows the calculated average area-weighted grain size as a function of the PH_3 (2% in H_2)/SiH_4 gas flow ratio for the *n*-type SPC poly-Si films prepared from a-Si:H films deposited at 380 and 410 °C. It can be seen that, for both a-Si:H deposition temperatures, the average grain size increases with increasing PH_3 (2% in H_2)/SiH_4 gas flow ratio, which is in good agreement with our previously reported results [17, 19]. Interestingly, the rate of grain growth is significantly higher for SPC poly-Si films fabricated from a-Si:H films deposited at 380 °C instead of 410 °C.

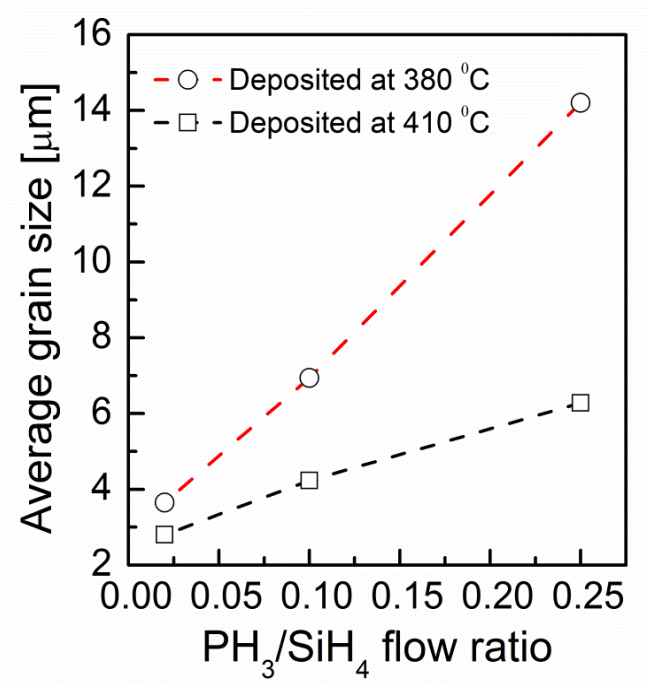

Figure 4.4: *Calculated area weighted average grain size as a function of PH_3 (2% in H_2)/SiH_4 flow ratio for the n-type poly-Si thin film obtained from the SPC of a-Si:H films deposited at 380 and 410 °C.*

It is observed that the average grain size of the SPC poly-Si films prepared from 380 °C deposited a-Si:H films increased from 3.6 to 14.2 µm when the PH_3 (2% in H_2)/SiH_4 flow ratio increased from 0.02 to 0.25, while the corresponding increase was from 2.8 to 6.2 µm for poly-Si films prepared from a-Si:H films deposited at 410 °C. The increase in the grain size of *n*-type SPC poly-Si thin films with increasing PH_3 (2% in H_2)/SiH_4 flow ratio is due to the enhanced phosphorus dopant concentration [20, 21]. The larger SPC grain size for the 380°C deposited a-Si:H films could be due to a low nucleation rate which increases with increasing a-Si:H deposition temperature [22].

Figure 4.5 shows EBSD grain orientation maps of *n*-type SPC poly-Si thin films prepared from a-Si:H films deposited at (a) 380 °C and (b) 410 °C, for a PH_3 (2% in H_2)/SiH_4 gas flow ratio of 0.25. The colour triangle in the top left corner of each graph defines the different crystal orientations.

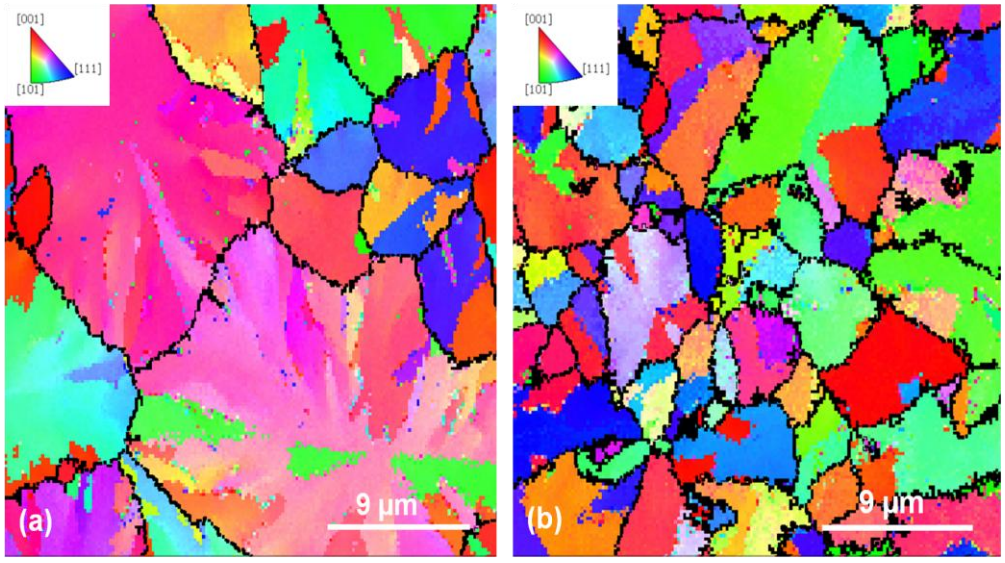

Figure 4.5: *EBSD grain size and orientation map of the n-type poly-Si thin films prepared from the SPC of a-Si:H films deposited at (a) 380 and (b) 410 °C respectively, for a PH_3 (2% in H_2)/SiH_4 gas flow ratio of 0.25.*

The individual grains of the *n*-type SPC poly-Si thin films were found to be randomly oriented. Comparison of the two images shows that, for a given PH_3 (2% in H_2)/SiH_4 gas flow ratio, the grain shape and size depend on the deposition temperature of the a-Si:H film. From Fig. 4.5(a) it can be clearly seen that the grains of the *n*-type SPC poly-Si films prepared from a-Si:H films deposited at 380°C are quite circular in shape, with an average grain size of 14.2 µm. In contrast, the grains of the *n*-type SPC poly-Si films prepared from 410°C deposited a-Si:H films (see Fig. 4.5(b)) were found to have a needle or feather-like shape, with an average grain size of 6.2 µm. Feather-like shapes of grains were also observed by Hatalis *et al.*, in poly-Si films obtained from the crystallisation of low-pressure chemical vapour deposited (LPCVD) a-Si:H films [22]. The a-Si:H films in this case were deposited at a significantly higher temperature of 545 °C [22]. The observed changes in shape and size of the *n*-type SPC poly-Si films with increasing a-Si:H deposition temperature are due to a nucleation rate that increases with the a-Si:H deposition temperature [22]. The increasing phosphorus dopant concentration enhances the grain growth rate [20, 21], while the increasing a-Si:H deposition temperature enhances the nucleation rate [22]. The combined effect could lead to the changes in grain shape and size as observed in Figs. 4.5(a) and 4.5(b).

Further analysis of the EBSD data was carried out to understand the possible mechanisms behind the improvement of the SPC poly-Si thin film material quality with increasing a-Si:H deposition temperature. EBSD can provide detailed information on the intra-grain misorientation (plastic deformation) in

polycrystalline films subjected to strain gradients [23-26]. Thus, it can be used to obtain qualitative and quantitative information on the misorientation present in the poly-Si thin film grains and on their impact on the film quality.

Figure 4.6 shows the grain average misorientation (GAM) maps as a function of the PH_3 (2% in H_2)/SiH_4 flow ratio for the *n*-type SPC poly-Si films fabricated from a-Si:H films deposited at (a) 380 °C and (b) 410 °C. GAM maps allow the visualization of misorientation gradients within the material (plastic deformation) and thus the accumulated orientation changes relative to the average orientation within a grain can be measured [23, 24, 27].

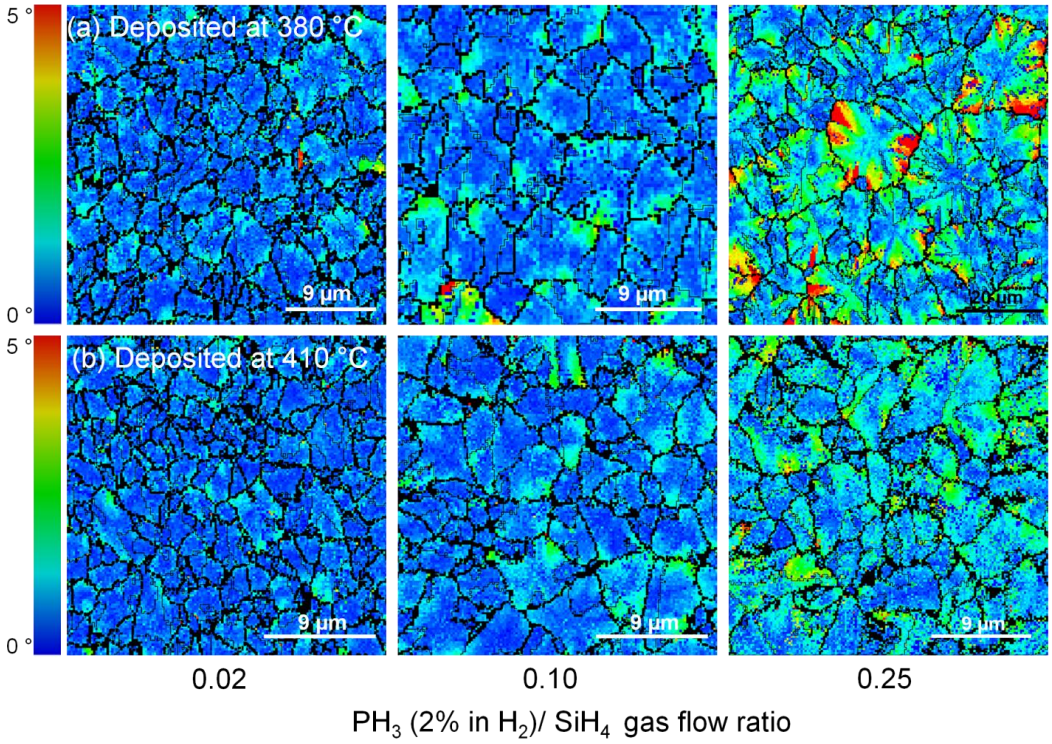

Figure 4.6: *GAM map as a function of PH_3 (2% in H_2)/SiH_4 flow ratio for the n-type poly-Si thin fabricated from the SPC of a-Si:H films deposited at (a) 380 and (b) 410 °C.*

A colour code from blue (0°) to red (5°) is used to measure the misorientation between the reference pixel and every other pixel, within each grain. Small amounts of misorientation are represented by blue colour (0-0.5°) whereas large misorientations (plastic deformations) are represented by red colour (~4-5°).

From Fig. 4.6(a), it can be clearly seen that the intra-grain misorientation increases with increasing PH_3 (2% in H_2)/SiH_4 gas flow ratio for SPC poly-Si films fabricated from a-Si:H films deposited at 380 °C. The intra-grain mis-orientation goes as high as 5°, which is nearly four times higher than in the case of SPC poly-Si films produced with a PH_3 (2% in H_2)/SiH_4 gas flow ratio of 0.02. For SPC poly-Si films obtained from a-Si:H films deposited at a slightly higher temperature of 410 °C (see Fig. 4.6(b)), the trends are the same, but the magnitude of the intra-grain misorientation is lower (up to 2.5°). The high degree of plastic deformation (misorientation) observed in the grains of SPC poly-Si films fabricated from 380°C deposited a-Si:H films (see Fig. 4.6(a)) could be the reason for the high tensile stress found in these poly-Si films (see Fig. 4.2). The trend observed here in the variation of the intra-grain misorientation (plastic deformation) among the grains of the SPC poly-Si films made with increasing a-Si:H deposition temperature and increasing PH_3 (2% in H_2)/SiH_4 gas flow ratio is in good agreement with the calculated stress from our Raman spectroscopy measurements, see Fig. 4.2. These results suggest that a small increase in the deposition temperature of the a-Si:H films can lead to a significant reduction (~50%) in the intra-grain misorientation of the poly-Si films. Large intra-grain misorientations are detrimental for the performance of SPC poly-Si thin-film solar

cells and other microelectronics applications. It is thus desirable to control the intra-grain misorientation (plastic deformation) in order to facilitate poly-Si thin films for large-scale electronic applications. From the results obtained in this work it is clear that the material quality of SPC poly-Si thin films can be improved through the control of intra-grain misorientation and stress.

4.4 Conclusion

The effects of the deposition temperature of the a-Si:H films and the PH_3 (2% in H_2)/SiH_4 gas flow ratio on the material quality of *n*-type SPC poly-Si thin films on planar glass were studied using the Raman spectroscopy and EBSD characterization techniques. It was found that the poly-Si thin films are tensile stressed. The stress was found to increase to more than 650 MPa when the PH_3 (2% in H_2)/SiH_4 gas flow ratio was increased to 0.25. The stress in the poly-Si thin films was found to affect their crystal quality. The stress was successfully engineered to values below 130 MPa through the control of the a-Si:H deposition temperature and the PH_3 (2% in H_2)/SiH_4 gas flow ratio. The best poly-Si crystal quality was obtained for a-Si:H films deposited at 410 °C, using a low PH_3 (2% in H_2)/SiH_4 gas flow ratio of 0.02. This SPC poly-Si film was found to have the least tensile stress (128 MPa) and a low intra-grain misorientation of ~1°.

References of Chapter 4

[1] R. B. Bergmann, "Crystalline Si thin-film solar cells: a review," *Applied Physics A*, vol. 69, pp. 187-194, 1999.

[2] T. Matsuyama, M. Tanaka, S. Tsuda, S. Nakano, and Y. Kuwano, "Improvement of n-type poly-Si film properties by solid phase crystallization method," *Jpn. J. Appi. Phys. Vol*, vol. 32, pp. 3720-3728, 1993.

[3] K. Nakazawa and K. Tanaka, "Effect of substrate temperature on recrystallization of plasma chemical vapor deposition amorphous silicon films," *Journal of Applied Physics*, vol. 68, pp. 1029-1032, 1990.

[4] L. Carnel, I. Gordon, D. Van Gestel, G. Beaucarne, J. Poortmans, and A. Stesmans, "High open-circuit voltage values on fine-grained thin-film polysilicon solar cells," *Journal of Applied Physics*, vol. 100, pp. 063702-063702-7, 2006.

[5] D. V. Gestel, I. Gordon, H. Bender, D. Saurel, J. Vanacken, G. Beaucarne, *et al.*, "Intragrain defects in polycrystalline silicon layers grown by aluminum-induced crystallization and epitaxy for thin-film solar cells," *Journal of Applied Physics*, vol. 105, p. 114507, 2009.

[6] N. M. Johnson, D. K. Biegelsen, and M. D. Moyer, "Deuterium passivation of grain-boundary dangling bonds in silicon thin films," *Applied Physics Letters*, vol. 40, pp. 882-884, 1982.

[7] N. H. Nickel, G. B. Anderson, and R. I. Johnson, "Grain-boundary defects in laser-crystallized polycrystalline silicon," *Physical Review B*, vol. 56, pp. 12065-12068, 1997.

[8] S. Nakashima and M. Hangyo, "Characterization of semiconductor-materials by raman microprobe," *IEEE Journal of Quantum Electronics*, vol. 25, pp. 965-975, 1989.

[9] M. Holtz, W. M. Duncan, S. Zollner, and R. Liu, "Visible and ultraviolet Raman scattering studies of $Si_{1-x}Ge_x$ alloys," *Journal of Applied Physics*, vol. 88, pp. 2523-2528, 2000.

[10] R. C. Teixeira, I. Doi, M. B. P. Zakia, J. A. Diniz, and J. W. Swart, "Micro-Raman stress characterization of polycrystalline silicon films grown at high temperature," *Materials Science and Engineering: B*, vol. 112, pp. 160-164, 2004.

[11] I. De Wolf, "Micro-Raman spectroscopy to study local mechanical stress in silicon integrated circuits," *Semiconductor Science and Technology*, vol. 11, pp. 139-154, 1996.

[12] K. Kitahara, H. Ogasawara, J. Kambara, M. Kobata, and Y. Ohashi, "Characterization of defects in polycrystalline silicon thin films using chemical etching, hydrogenation, and Raman spectroscopy," *Japanese Journal of Applied Physics*, vol. 47, p. 54, 2008.

[13] K. Kitahara, T. Ishii, J. Suzuki, T. Bessyo, and N. Watanabe, "Characterization of Defects and Stress in Polycrystalline Silicon Thin Films on Glass Substrates by Raman Microscopy," *International Journal of Spectroscopy*, vol. 2011, p. 632139, 2011.

[14] M. S. Benrakkad, M. A. Benitez, J. Esteve, J. M. Lopez-Villegas, J. Samitier, and J. R. Morante, "Stress measurement by microRaman spectroscopy of polycrystalline silicon structures," *Journal of Micromechanics and Microengineering*, vol. 5, p. 132, 1995.

[15] G. Kaltsas, A. G. Nassiopoulou, M. Siakavellas, and E. Anastassakis, "Stress effect on suspended polycrystalline silicon membranes fabricated by micromachining of porous silicon," *Sensors and Actuators A: Physical*, vol. 68, pp. 429-434, 1998.

[16] P. Münster, M. Sarret, T. Mohammed-Brahim, N. Coulon, and J.-Y. Mevellec, "Polycrystalline silicon deposited on glass by subatmospheric-pressure chemical vapour deposition at a high rate," *Philosophical Magazine Part B*, vol. 82, pp. 1695-1701, 2002.

[17] A. Kumar, H. Hidayat, C. Ke, S. Chakraborty, G. K. Dalapati, P. I. Widenborg, *et al.*, "Impact of the n^+ emitter layer on the structural and electrical properties of p-type polycrystalline silicon thin-film solar cells," *Journal of Applied Physics*, vol. 114, p. 134505, 2013.

[18] N. H. Nickel, P. Lengsfeld, and I. Sieber, "Raman spectroscopy of heavily doped polycrystalline silicon thin films," *Physical Review B*, vol. 61, pp. 15558-15561, 2000.

[19] A. Kumar, P. I. Widenborg, F. Law, H. Hidayat, G. K. Dalapati, and A. G. Aberle, "Study of large-grained n-type polycrystalline silicon thin films made by the solid phase crystallization method," in Proc. *39th IEEE Photovoltaic Specialists Conference (PVSC)*, pp. 0586-0588, 2013.

[20] Y. Wada and S. Nishimatsu, "Grain Growth Mechanism of Heavily Phosphorus-Implanted Polycrystalline Silicon," *Journal of The Electrochemical Society*, vol. 125, pp. 1499-1504, 1978.

[21] B. C. Johnson and J. C. McCallum, "Dopant-enhanced solid-phase epitaxy in buried amorphous silicon layers," *Physical Review B,* vol. 76, p. 045216, 2007.

[22] M. K. Hatalis and D. W. Greve, "Large grain polycrystalline silicon by low-temperature annealing of low-pressure chemical vapor deposited amorphous silicon films," *Journal of Applied Physics,* vol. 63, pp. 2260-2266, 1988.

[23] L. Brewer, M. Othon, L. Young, and T. Angeliu, "Misorientation mapping for visualization of plastic deformation via electron back-scattered diffraction," *Microscopy and Microanalysis,* vol. 12, pp. 85-91, 2006.

[24] L. Brewer, D. Field, and C. Merriman, "Mapping and Assessing Plastic Deformation Using EBSD," in *Electron Backscatter Diffraction in Materials Science,* A. J. Schwartz, M. Kumar, B. L. Adams, and D. P. Field, Eds., ed: Springer US, 2009, pp. 251-262.

[25] A. Wilkinson, E. Clarke, T. Britton, P. Littlewood, and P. Karamched, "High-resolution electron backscatter diffraction: An emerging tool for studying local deformation," *The Journal of Strain Analysis for Engineering Design,* vol. 45, pp. 365-376, 2010.

[26] F. Dunne, R. Kiwanuka, and A. Wilkinson, "Crystal plasticity analysis of micro-deformation, lattice rotation and geometrically necessary dislocation density," *Proceedings of the Royal Society A: Mathematical, Physical and Engineering Science,* vol. 468, pp. 2509-2531, 2012.

[27] F. Law, Y. Yi, H. Hidayat, P. I. Widenborg, J. Luther, and B. Hoex, "Identification of geometrically necessary dislocations in solid phase crystallized poly-Si," *Journal of Applied Physics,* vol. 114, p. 043511, 2013.

Chapter 5

Chapter 5- Impact of the n^+ Emitter Layer on the Structural and Electrical Properties of *p*-type Polycrystalline Silicon Thin-Film Solar Cells

5.1. Introduction

5.2. Experimental Procedures

5.3. Results and Discussion

5.4. Conclusion

5.1 Introduction

The SPC poly-Si thin-film PV technology was pioneered by the Japanese company SANYO in the 1990s, giving efficiencies of up to 9.2% for 1-cm^2 solar cells fabricated on metal substrates [1]. CSG Solar then developed SPC poly-Si on glass solar cells and in 2007 achieved a record efficiency of 10.4% for a 94-cm^2 mini-module [2, 3]. There is scope to further improve the efficiency of poly-Si PV modules by optimising (i) the doping profiles of the n^+ and p^+ poly-Si layers (thereby improving their electronic properties) and (ii) the material quality of the individual layers of the poly-Si thin film ($n^+/p^-/p^+$). Of crucial importance for obtaining higher PV efficiency is the electronic and structural quality of the n^+ emitter layer. In superstrate configuration, the n^+ emitter layer is the first semiconductor layer deposited in the case of a *p*-type poly-Si thin-film solar cell and it has been hypothesised to act as a 'nucleation layer' for the crystal growth of subsequent layers [1, 4]. The quality of this layer depends on the density of the phosphorus dopants [P] in the film, which is controlled by the PH_3 gas flow rate in the plasma-enhanced chemical vapour deposition (PECVD) reactor. Matsuyama *et al.* [1, 4] reported that it is possible to obtain large-grained SPC poly-Si thin films by controlling the phosphorus dopant density in the film, but not much information was given about the crystal quality of the film as a function of the n^+ doping concentration. Recent reports suggest that the open-circuit voltage (V_{oc}) of hydrogen-passivated poly-Si thin-film solar cells does not necessarily depend on the grain size [5], but on the intra-grain crystal quality of the film. Thus, it is important to study the effect of phosphorus atoms on the

crystal quality of SPC poly-Si thin-film solar cells.

Furthermore, the efficiency of the solar cell depends on the generation rate of electron-hole pairs and the collection probability of the generated minority carriers [6]. Thus, the cell should have its *p-n* junction close to the illuminated surface. Adjustments to the emitter, absorber and back surface field (BSF) layers are opportunities for achieving this. One way is to control the thickness and doping of the emitter region in the solar cell. Additionally, the cell's absorber layer should not be too highly doped, to ensure a good carrier collection across its entire thickness. Furthermore, a highly doped, thin BSF region would reduce surface recombination losses and ensure contactability of the rear surface. The influence of the absorber layer doping on the efficiency of SPC poly-Si thin-film solar cells has been studied in the literature [7, 8]. However, to our knowledge, there are no significant reports about the impact of the p^+ BSF and n^+ emitter layers on the efficiency of *p*-type SPC poly-Si thin-film solar cells, and in particular not where the a-Si precursor diode was deposited by PECVD.

In this chapter, we investigate the impact of the doping density and the structural quality of the n^+ emitter layer on the efficiency of an ~2.2 µm thick *p*-type SPC poly-Si on glass thin-film solar cell structure with an ~30 nm thick n^+ layer (emitter), an ~2000 nm thick p^- layer (absorber), and an ~100 nm thick p^+ layer (BSF). The structural quality of the poly-Si thin-film solar cells as a function of the PH_3 gas flow rate for n^+ layer formation is evaluated using UV reflectance and Raman spectroscopy measurements. Subsequently, the influence of the PH_3

gas flow rate on the peak n^+ emitter layer doping concentration and location of the *p-n* junction is investigated using the electrochemical capacitance-voltage (ECV) method. Finally, its impact on the electrical performance of the *p*-type poly-Si thin-film solar cell is investigated using external quantum efficiency (EQE), Suns-V_{oc} [9], and light *I-V* measurements.

5.2 Experimental Details

5.2.1 Sample preparation

SPC poly-Si thin-film solar cells with different emitter doping concentrations were prepared for this study. a-Si:H diodes with the structure ~30 nm n^+/~2 µm p^-/~100 nm p^+ were deposited in a PECVD clustertool (MVSystems, USA) onto a SiN_x (~70 nm) coated planar glass sheet (Schott, Borofloat). An ~100 nm thick SiO_x capping layer was then deposited onto the a-Si:H diodes. The SiN_x film acts as an antireflection coating and diffusion barrier to impurities from the glass substrate, while the SiO_x layer acts as a barrier for impurities from the ambient during the SPC process as well as the subsequent rapid thermal annealing (RTA) process. The n^+ emitter layers were deposited using different SiH_4/PH_3 (2% in H_2) gas flow ratios. The absorber and BSF layers were kept constant in this work. The deposition parameters of the $n^+/p^-/p^+$ a-Si precursor diode are summarised in Table 5.1.

Table 5.1: *Experimental details used for the PECVD process of the n^+, p^- and p^+ a-Si:H films.*

Process condition	*n^+ layer*	*p^- layer*	*p^+ layer*
SiH_4 (sccm)	10	40	40
2% PH_3:H_2 (sccm)	0.2 - 3	0	0
100 ppm B_2H_6:H_2 (sccm)	0	0.2	6
Substrate temperature (ºC)	380	380	380
Pressure (Pa)	80	107	107
RF power density (mW/cm^2)	8	33	33

The deposited a-Si:H films were then annealed (Nabertherm, N 120/65HAC furnace, Germany) at 610 ºC in a N2 atmosphere for a duration of 12 hours to achieve solid phase crystallisation of the film. A rapid thermal anneal (RTA, CVD Equipment, USA) for 1 minute at a peak temperature of 1000 ºC in N_2 atmosphere was then used to remove crystallographic defects from the SPC poly-Si thin-film diodes and to activate the dopants. Subsequently, the samples were hydrogenated in hydrogen plasma (AK800 system, Roth & Rau, Germany) at a substrate temperature of 475 °C to passivate the grain boundaries and defects. The diode structure in superstrate configuration is illustrated in Figure 5.1.

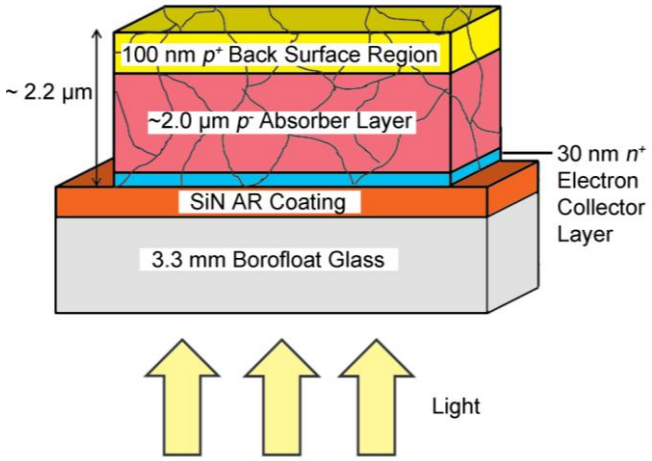

Figure 5.1: *Cross-sectional schematic of the investigated SPC poly-Si thin-film solar cell structure in superstrate configuration (not to scale).*

5.2.2 Metallization

An ~100 nm thick SiO_x film was then deposited as back surface reflector (BSR) and the cells were then metallised using an interdigitated scheme as described by Gress *et al.*, [10]. The metallisation scheme of fully metallised SPC poly-Si thin-film solar cell is illustrated in Figure 5.2.

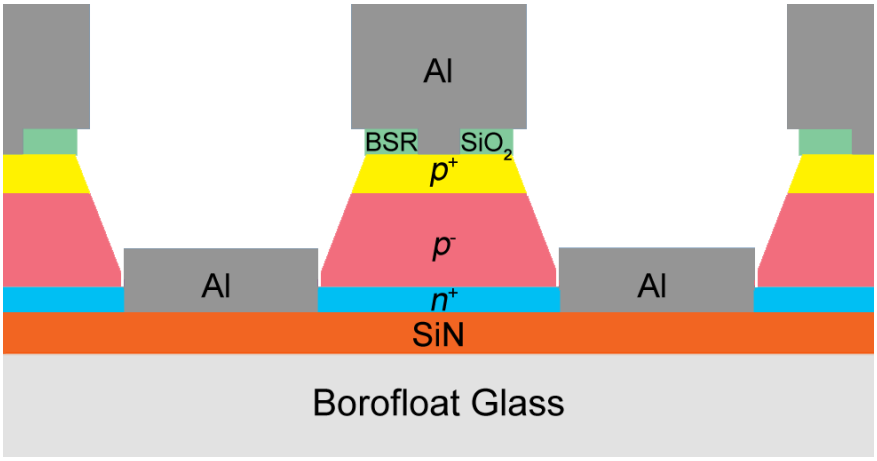

Figure 5.2: *Cross-sectional schematic of the metallisation scheme used in this work for poly-Si thin-film solar cells (not to scale).*

5.2.3 Characterization

The poly-Si material quality of the diodes was determined using UV reflectance measurements [11-13] (PerkinElmer, Lambda 950, UV/Vis/NIR spectrometer) and Raman spectroscopy [14, 15] measurements (LabRam HR system equipped with a 325 nm (UV) and 488 nm (visible) laser line), whereby the samples were always measured from the air side. Electron backscatter diffraction (EBSD) measurements (Bruker QUANTAX CrystAlign, Germany) was used to study the crystal orientation and plastic deformation of n^+ poly-Si thin-film emitter layers (specially made test samples). Furthermore, the peak

doping concentration of each layer in the poly-Si thin-film solar cell, the doping profile across the sample's thickness, and the *p-n* junction location were determined using ECV profiling [16, 17] (ECV, CVP21 doping profiler from WEP Control, Germany). Further, the V_{oc} , pseudo fill factor (*pFF*) and effective ideality factor (n_{eff}) [18] of the non-metallised solar cell test structures were extracted from Suns-V_{oc} measurements [7, 9, 16]. The J_{sc} was calculated from the EQE curve (Solar Cell Scan 100, Zolix Instruments, China). Finally, the efficiency (*Eff*) and fill factor (*FF*) were obtained from the light *I-V* measurement (Thin film I-V tester, IVT Solar, Singapore) under AM1.5 illumination.

5.3 Results and Discussion

5.3.1 Structural quality of the poly-Si thin-film solar cell

Figure 5.3 shows the UV reflectance of the poly-Si thin-film solar cells measured from the air side, for three PH_3 gas flow rates (0.2, 0.5 and 2.0 sccm). Two characteristic peaks closely related to direct optical transitions in c-Si [19] were observed in the UV reflectance spectrum at ~360 nm and ~275 nm (e1 and e2), respectively. Structural disorder and defects in the surface region of the probed poly-Si film lead to a decrease and broadening of the peaks [20]. There was a marginal improvement in the crystal quality when the PH_3 gas flow rate increased from 0.2 to 1 sccm, followed by a significant deterioration of the film quality when the PH_3 flow was increased to 2 sccm. Furthermore, the poly-Si thin film samples were characterised from the air side by Raman spectroscopy, to better understand the impact of the PH_3 gas flow rate on the structural quality.

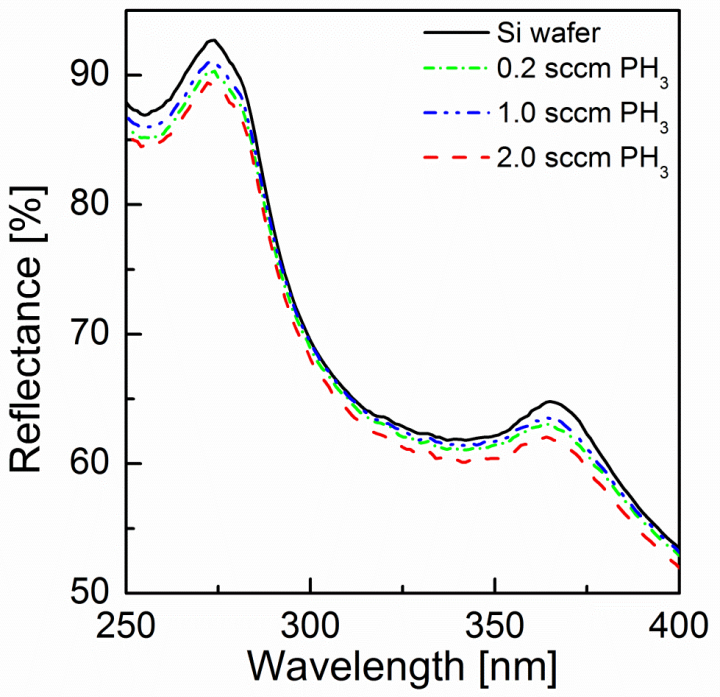

Figure 5.3: *Measured hemispherical UV reflectance of poly-Si thin-film solar cells fabricated with three different phosphine flow rates (i.e., n^+ layer concentrations). Also shown, for comparison, is the UV reflectance measured on a polished single-crystalline Si wafer (solid black line).*

Figure 5.4 shows the Raman spectra acquired from the UV (325 nm) and visible (488 nm) laser line for selected poly-Si thin-film solar cells made with different PH_3 gas flow rates. For comparison, the Raman spectrum (UV/visible) was also taken for a polished single-crystalline high-resistivity FZ silicon wafer. The Raman spectrum obtained on the c-Si wafer with the UV laser displays a sharp distinct Lorentzian peak at ~520.4 cm^{-1} with a measured full width at half maximum (FWHM) of ~5.0 cm^{-1}. Using the visible laser, the corresponding peak sits at ~521 cm^{-1} and has a FWHM value of ~3.3 cm^{-1}. Defects and disorder in crystalline Si lead to the broadening of the peak (larger FWHM) [14] and hence, is a frequently used indicator for the crystal quality of poly-Si films. The FWHM value of the poly-Si film was around ~6.5 cm^{-1} and ~5 cm^{-1} for the Raman

spectrum acquired with the UV and visible laser line, respectively, which is significantly higher than that of the c-Si wafer, indicating the presence of defects and disorder in the SPC poly-Si thin-film solar cells. However, the FWHM value of the visible-light Raman peak of the SPC poly-Si thin film is in good agreement with reported values and slightly better than earlier reported results [4, 13], indicating that our poly-Si thin films have reasonable crystal quality. The reason for the higher FWHM value for the UV laser Raman peak as compared to the visible laser Raman peak is not known as yet and needs further investigation. A shift of the peak towards the right can be observed for the poly-Si thin film as compared to c-Si in the Raman spectra (Fig. 5.4), suggesting the presence of compressive stress in the poly-Si thin-film solar cells.

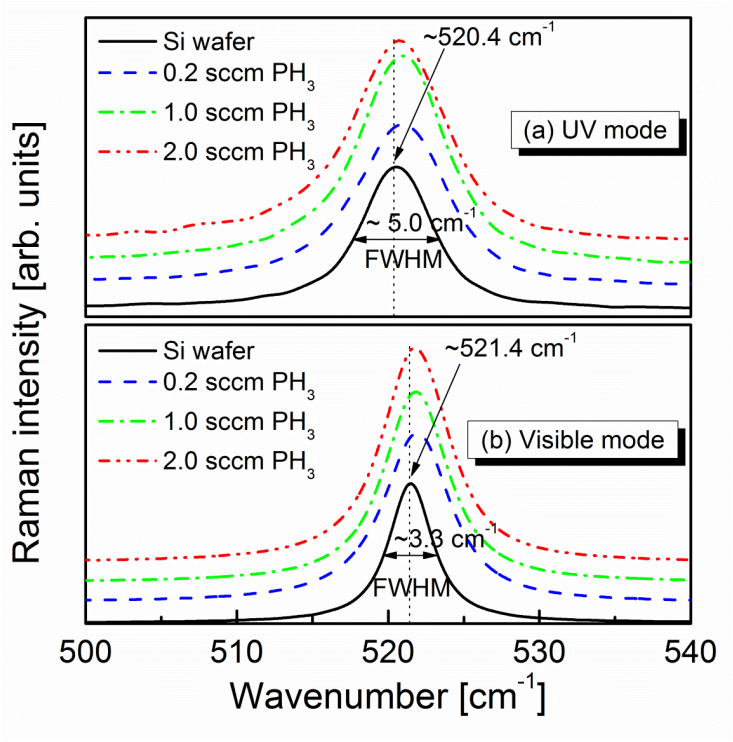

Figure 5.4: *Measured Raman intensity of poly-Si thin-film solar cells fabricated with three different phosphine flow rates, for (a) excitation with UV light ('UV mode') and (b) excitation with visible light ('visible mode'). Also shown, for comparison, is the Raman intensity measured for a polished single-crystalline Si wafer (solid black lines).*

The UV reflectance and Raman spectroscopy (UV/visible laser) results were quantified in terms of the crystal quality and Raman quality factors. A Raman quality factor (R_Q) is defined as the ratio between the FWHM of the Raman peak of the c-Si wafer and the poly-Si sample ($FWHM_{c\text{-}Si}$ / $FWHM_{poly\text{-}Si}$). The details of the UV reflectance crystal quality can be found in the literature [12, 13] and in Chapter 2.

Figure 5.5 shows the crystal quality factor obtained from the UV reflectance measurements and the R_Q factor calculated from the Raman spectra (UV and visible laser line), as a function of the PH_3 flow rate. From the trends it is observed that there is a significant improvement in the crystal quality when the PH_3 gas flow rate increases from 0.2 to 1 sccm, followed by a significant deterioration when the flow rate is increased to 2 sccm.

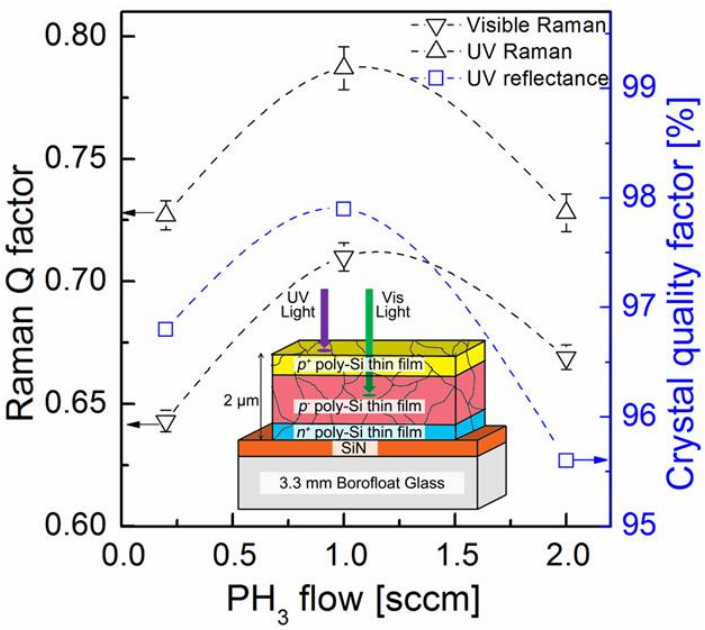

Figure 5.5: *Raman quality factor (R_Q) and crystal quality factor from UV reflectance measurements on selected poly-Si thin-film solar cells as a function of the PH_3 gas flow rate. The dotted lines are guides to the eye. Inset: Schematic view of poly-Si thin-film solar cell under test.*

The best crystal quality factor of almost 98% was obtained for the diode with an n^+ layer produced with a PH_3 flow rate of 1 sccm. The worst poly-Si thin-film diode had a crystal quality factor of around 95.5%. Hence, it can be assumed that the poly-Si diode's crystal quality is strongly influenced by the PH_3 gas flow rate. This assumption is further validated by the similarity of the trends observed for the crystal quality from the UV reflectance measurements and the R_Q factor obtained from the Raman measurements. The initial improvement in the crystal quality with increasing PH_3 flow might be due to the improvement of the nucleation layer. However, at higher phosphorus concentrations the crystal quality of the poly-Si thin-film deteriorates due to the increase of plastic deformation in the grains, as discussed in Chapter 3 [21].

5.3.2 ECV doping profiles

The doping profiles of the poly-Si thin-film solar cells were further measured using the ECV technique. This technique determines the doping concentration as a function of depth by measuring the capacitance of an electrolyte-semiconductor Schottky contact. The doping profile is then obtained by etching and subsequently measuring the capacitance across the depth of the semiconductor [16, 17, 22-27]. Figure 5.6 shows the ECV doping profiles of selected poly-Si thin-film solar cells as a function of the PH_3 gas flow rate. The air side of the poly-Si thin-film solar cells is defined as the reference point (i.e., as etch depth = 0 µm). As expected, the peak n^+ doping concentration increases with increasing PH_3 gas flow. A high n^+ peak doping concentration of 6.0×10^{19} cm^{-3} was obtained for a PH_3 gas flow of 3 sccm. A widening of the *n*-type layer

thickness was observed for an increasing peak n^+ doping concentration, resulting in (i) a shift of the *p-n* junction away from glass side (i.e., towards the centre of the diode) and (ii) a reduction of the p^- layer thickness.

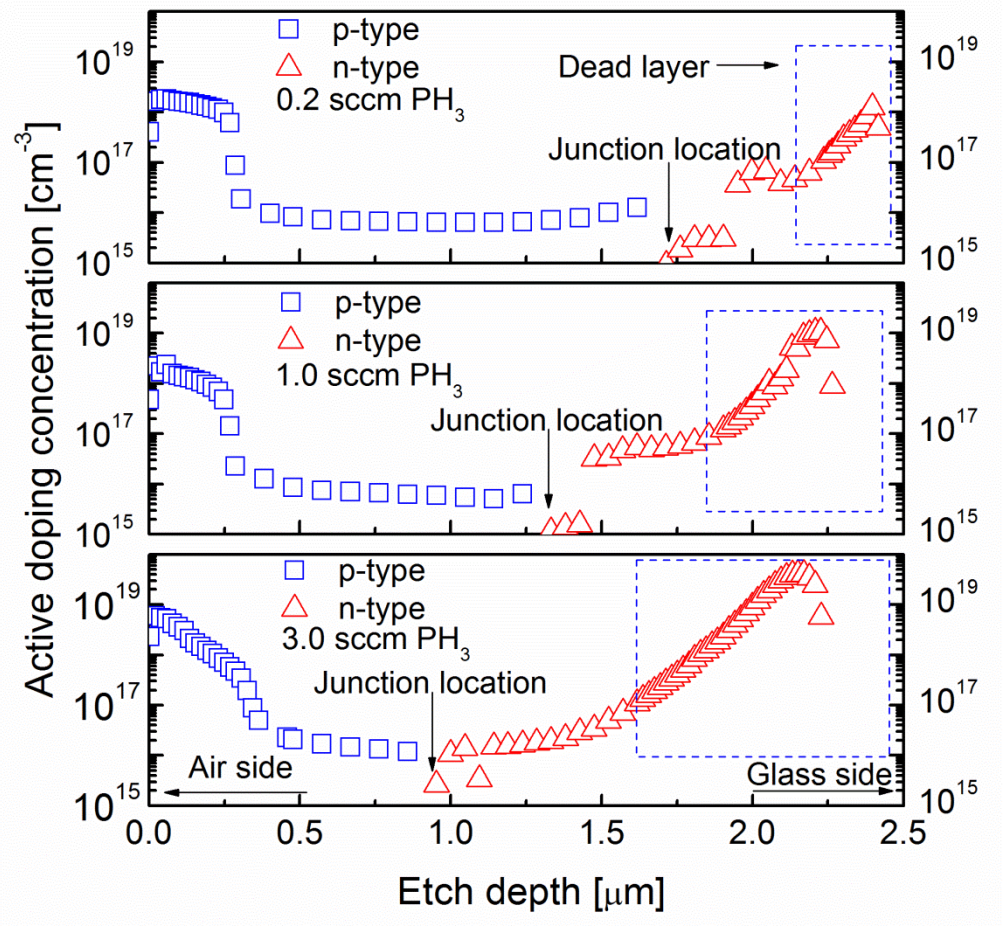

Figure 5.6: *Measured ECV doping profile of the selected poly-Si thin-film solar cells, for three different phosphine flow rates. The blue squares and red triangles indicate the p-type doping layer and n-type doping layer, respectively.*

5.3.3 Solar cell performance

The *pEff* and *pFF* approach was used to investigate the electronic quality of the poly-Si thin-film solar cells. The open-circuit voltage at 1 sun obtained from Suns-V_{oc} measurements is labelled as V_{oc}, while *pFF* was extracted from the pseudo light *I-V* curve [9] on un-metallised samples via [7]:

$$pFF = \frac{V_{OC}(MPP) \times J_{norm}(MPP)}{V_{OC}} \ , \quad (5.1)$$

where V_{oc} (MPP) and J_{norm} (MPP) denotes the open-circuit voltage and the normalized current density at the maximum power point (MPP) of the pseudolight *I-V* curve [9], respectively. The *pEff* can then be determined via:

$$pEff = V_{oc} \times J_{SC} \times pFF. \quad (5.2)$$

The J_{sc} value was calculated from the EQE curve (Zolix system) measured on metallised samples using the following relation:

$$J_{SC}(EQE) = q \int EQE(\lambda) S(\lambda) d(\lambda) \ , \quad (5.3)$$

where q is the electron charge and $S(\lambda)$ is the standard spectral photon density of sunlight at the earth's surface (AM1.5G). The variation in the cells' series resistances associated with the metallisation process for individual solar cells can be eliminated using the *pEff –pFF* approach, as the *pFF* is extracted from the pseudo light *I-V* curve which is a function of the light intensity instead of a short-circuit current [9]. Thus, the data from the solar cell can be extracted without the impact of metallisation-induced factors such as the series and shunt resistances [9]. For comparison, the efficiency (*Eff*) and fill factor (*FF*) were determined from standard 1-Sun *I-V* measurements.

To evaluate the diode quality and understand the recombination mechanism in the solar cell, another very useful parameter called n_{eff} [18, 28] was calculated from the slope of the suns-V_{oc} curve using [28]:

$$n_{eff} = \frac{V_{OC}(MPP) - V_{OC}(1\ Sun)}{V_T \times \ln(Suns(MPP))}, \quad 5.4$$

where V_{oc} (*MPP*) and V_{oc} (1 *Sun*) denotes the open-circuit voltage at *MPP* and 1

Sun illumination, respectively. V_T is the thermal voltage (0.0257 V at 25 °C) and Suns (*MPP*) is the illumination level at *MPP* of the pseudolight *I-V* curve [9]. An effective ideality factor close to 1 is an indication that the solar cell is dominated by bulk recombination, whereas an n_{eff} higher than 1 indicates that recombination in the diode's space charge regions (such as the *p-n* junction and extended defects along grain boundaries, grains and dislocations) plays an important role [18]. The space charge recombination impacts the fill factor of the device. In addition, Shockley Read Hall (SRH) recombination with ideality factor higher than 1 is dominated in the space charge region which is especially detrimental for the performance of the solar cell.

Figure 5.7 shows the measured EQE curves of three poly-Si thin-film solar cells made with different PH_3 gas flow rates (0.2, 0.5 and 1.5 sccm). The blue response decreased with increasing PH_3 gas flow rate (i.e., increasing n^+ doping concentration). At 300 nm, the EQE is approximately 20% and 5% for PH_3 gas flows of 0.2 and 1.5 sccm, respectively. This could be due to the formation of a very heavily doped emitter, forming a so-called "dead layer". Light-generated minority carriers within a dead layer have a very low chance of being collected by the *p-n* junction [6]. Furthermore, compared to the 0.2 sccm PH_3 sample, a slight "red shift" of the EQE peak can be observed for the samples with higher PH_3 gas flow rates (and thus higher n^+ doping concentrations). This could be a consequence of the shift in the junction depth away from surface, as is evident in Figure 5.6.

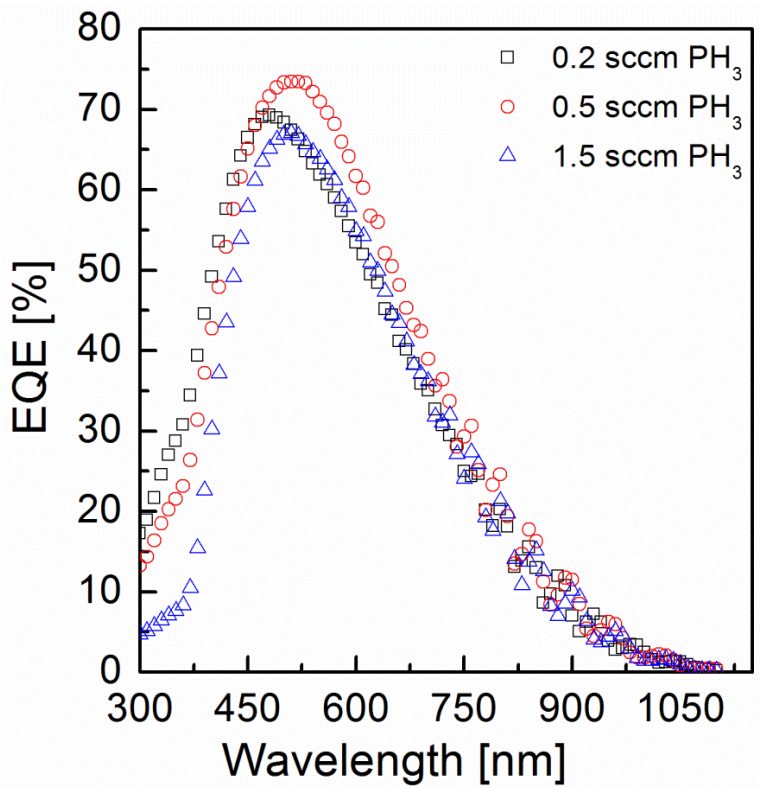

Figure 5.7: *Measured external quantum efficiency curves of the three selected poly-Si thin-film solar cells. The phosphine flow rate was 0.2, 0.5 and 1.5 sccm, respectively.*

Measured solar cell parameters and doping densities of selected poly-Si thin-film solar cells are summarised in Table 5.2. It is evident that the n^+ emitter layer doping influences the efficiency of the solar cells. In addition, the calculated n_{eff} value of ~1.33 ± 0.05 for the SPC poly-Si thin-film diodes is a strong indication that space charge recombination has a significant influence on the properties of the poly-Si thin-film diodes, which is in good agreement with the earlier reported results on SPC poly-Si thin-film solar cells prepared by electron beam evaporation (EVA) [7, 28].

Table 5.2: *Experimental parameters of the poly-Si thin-film solar cells obtained by (i) suns-V_{oc}, (V_{oc} and pFF), (ii) integration of the EQE curves over the AM1.5G solar spectrum (J_{sc}), (iii) 1-sun I-V measurements on the IVT system, (iv) ECV (doping concentration of n^+ layer). All cells have an area of 2.0 cm^2.*

Solar Cell ID	PH_3 gas flow [sccm]	n^+ doping concentration [cm^{-3}]	J_{sc} [mA/ cm^2]	V_{oc} [mV]	*pFF* [%]	n_{eff}	*pEff* [%]	Eff [%]	*FF* [%]
SPC A	0.2	~2.0×10^{18}	13.84	425	73.7	1.35	4.3	2.8	48
SPC B	0.5	~8.0×10^{18}	15.04	434	74.1	1.36	4.8	3.5	64
SPC C	1.0	~1.0×10^{19}	14.98	443	75.6	1.33	5.0	4.1	64
SPC D	1.5	~1.9×10^{19}	13.00	456	76.4	1.32	4.6	3.6	62
SPC E	2.0	~2.5×10^{19}	-	445	77.2	1.23	-	-	-
SPC F	3.0	~4.0×10^{19}	-	445	74.3	1.39	-	-	-

Figure 5.8 shows the impact of the PH_3 flow rate on the V_{oc} and J_{sc}. There was a 30 mV increase in the V_{oc} (from 425 to 456 mV) with increase of the PH_3 gas flow from 0.2 to 1.5 sccm. The V_{oc} saturated at a marginally lower value of ~445 mV when the PH_3 gas flow was further increased to 3 sccm. In comparison, there was an increase in the J_{sc} with the increase in PH_3 flow rate from 0.2 to 0.5 sccm (n^+ doping concentration: 2×10^{18} to $8\text{x}10^{18}$ cm^{-3}) and thereafter, a decreasing trend was observed (Fig. 5.8). The increase in V_{oc} with increasing n^+ doping concentration can be attributed to the decrease in diode saturation current [6]. A contributing factor for the lower V_{oc} at high PH_3 flows could be a poorer material quality, as is evident from the Raman and UV measurements (Fig. 5.5). In addition, increased defects and dislocation at grain boundaries and with grain at higher PH_3 flow could well be another reason for the decrease in the V_{oc} [29].

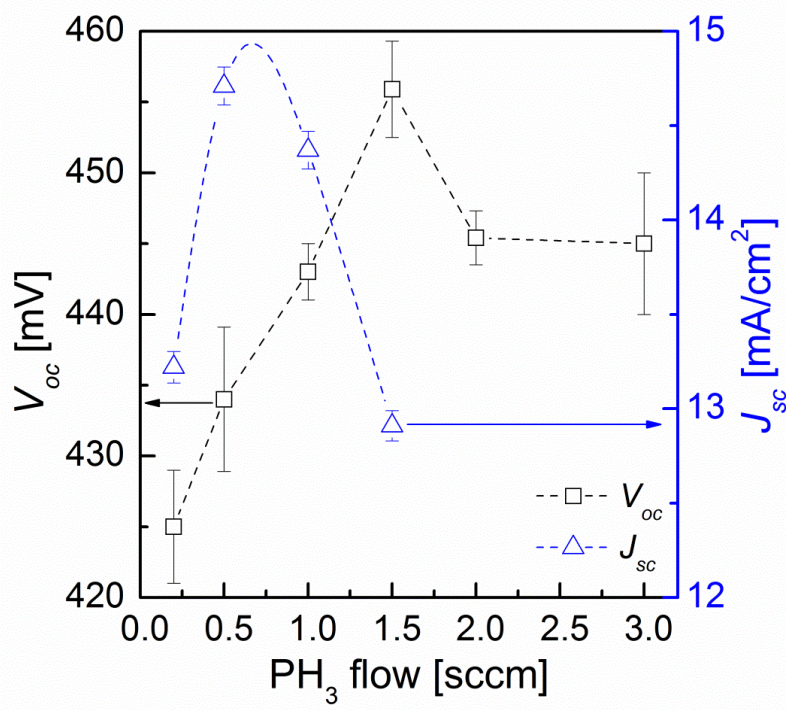

Figure 5.8: *Measured V_{oc} and J_{sc} of poly-Si thin-film solar cells vs. PH_3 gas flow rate. The dotted lines are guides to the eye.*

The low J_{sc} at 0.2 sccm of PH_3 gas flow rate could be due to several factors. One is a poorer material quality of the poly-Si thin film, as is evident from the Raman and UV measurements (Fig. 5.5). Another is a higher series resistance caused by the lower emitter doping concentration, which is further evident from the low *FF* at 0.2 sccm of PH_3 gas flow rate (Table 5.2). The effects of doping and sheet resistance on the emitter contact of the poly-Si thin-film solar cell are discussed in detail by L. Shi [29]. An increasing PH_3 gas flow rate increases the doping concentration of the n^+ emitter layer thereby, improving its sheet resistance. This in turn improves the *FF* of the device and the crystal quality of the poly-Si thin film. The latter may have led to the initial improvement in the J_{sc} observed in Fig. 5.8. However, with further increasing n^+ emitter layer doping, the *p-n* junction shifts further away from the glass interface (Fig. 5.6), reducing

the collection probability of the minority carrier holes generated in the n^+ emitter layer. In addition, the crystal quality of the thin-film poly-Si solar cells decreases when the PH_3 gas flow is increased beyond 1 sccm (Fig. 5.5), which will also negatively impact the J_{sc}.

Figure 5.9 shows the measured *Eff*, *FF* and the calculated *pEff* of the selected poly-Si thin-film solar cells as a function of the PH_3 gas flow. A significant increase in the *Eff* from 2.8 to 4.1% can be observed as the PH_3 gas flow increased from 0.2 to 1 sccm , corresponding to a change in the n^+ peak emitter layer doping concentration from 2.0×10^{18} to 1.0×10^{19} cm^{-3}. Thereafter, the *Eff* decreased with further increase in the PH_3 gas flow rate (n^+ peak doping concentration).

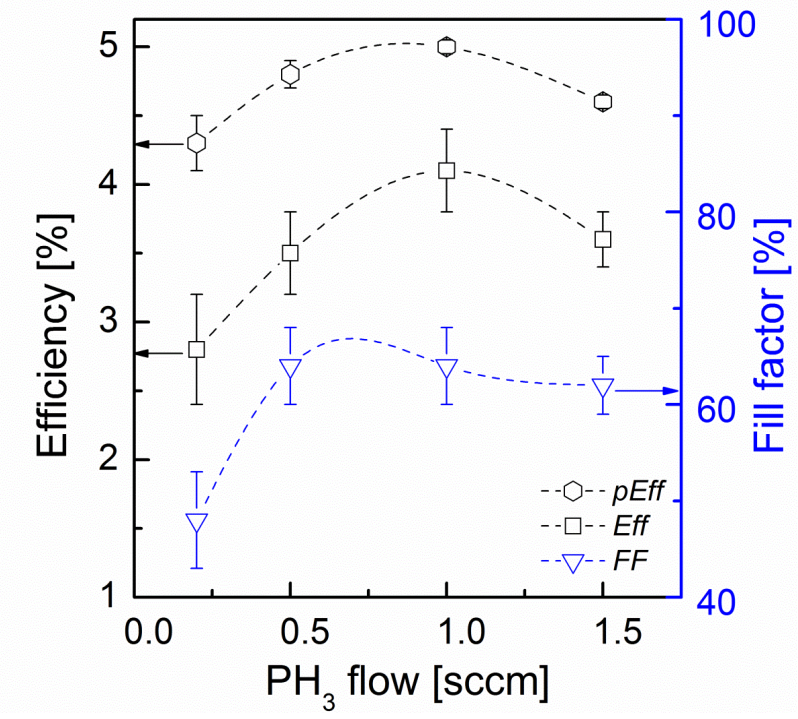

Figure 5.9: *Measured efficiency, pseudo efficiency and fill factor (FF) of poly-Si thin-film solar cells vs. PH_3 gas flow rate. The dotted lines are guides to the eye.*

The increase in the *Eff* towards the peak value can most likely be explained by an improvement in the *FF*, J_{sc} and the material quality of the investigated poly-Si thin film solar cell (Fig. 5.5). The decrease of the *Eff* with further increase of the PH_3 gas flow rate (n^+ peak doping concentration) is due to the decreasing J_{sc}. As expected, the calculated *pEff* values are higher than the measured *Eff* values. A significant improvement in the *FF* from 48% to 64% can be observed when the PH_3 gas flow increases from 0.2 to 0.5 sccm, whereas, it remains nearly constant thereafter for the selected poly-Si thin-film solar cells. The improvement in the *FF* is very likely due to a series resistance that initially improves strongly with increasing PH_3 flow, however, effects from the metallization process cannot be ruled out. It is also worth to note that the poly-Si thin film solar cells are fabricated on planar glass samples. The planar poly-Si samples suffer from poor light absorption, which results in significantly lower short-circuit currents. Therefore, it is possible to enhance the absorption via light trapping mechanisms, for example by using aluminium-induced texture (AIT) glass [30, 31], to fabricate more efficient poly-Si thin-film solar cells. The absorption in SPC poly-Si thin-film solar cell can be further enhanced by using one of several possible light trapping mechanisms at the rear surface [32]. In addition, the V_{oc} of the devices can be improved by optimising the doping concentrations in the three layers ($n^+/p^-/p^+$), by improving the material quality, and by controlling the density of geometrically necessary dislocations (GNDs) [33]. Therefore, even though the highest efficiency reported here is only ~4.1 %, it is possible to significantly improve the efficiency of the SPC based poly-Si thin-film solar cell by employing

an advanced light trapping scheme along with an improved material quality.

5.4 Conclusion

The influence of the PH_3 gas flow rate on the peak n^+ emitter layer doping concentration and the efficiency of solid phase crystallised poly-Si thin-film solar cells on glass was studied. The best crystal quality of the poly-Si thin-film diode was obtained with a PH_3 flow of 1.0 sccm. The location of the *p-n* junction in the poly-Si thin-film solar cells was determined by ECV measurements. We found that, with increasing PH_3 gas flow rate, the *p-n* junction moves deeper into the device. The experimental results showed that the best V_{oc} (~456 mV) was obtained for a relatively high PH_3 gas flow rate of 1.5 sccm. In contrast, due to better J_{sc} for low PH_3 flows, the best device efficiency was obtained for an intermediate PH_3 flow rate of about 1 sccm. The best poly-Si thin-film solar cells also had the best crystal quality factors, as obtained from Raman (UV and visible) and UV reflectance measurements.

References of Chapter 5

[1] T. Matsuyama, N. Terada, T. Baba, T. Sawada, S. Tsuge, K. Wakisaka, *et al.*, "High-quality polycrystalline silicon thin film prepared by a solid phase crystallization method," *Journal of Non-Crystalline Solids*, vol. 198–200, Part 2, pp. 940-944, 1996.

[2] M. J. Keevers, T. L. Young, U. Schubert, and M. A. Green, "10% efficient CSG minimodules," in *Proceedings of the 22nd European Photovoltaic Solar Energy Conference, Milan, Italy, September 2007*, pp. 1783-1790.

[3] M. A. Green, K. Emery, Y. Hishikawa, and W. Warta, "Solar cell efficiency tables (version 35)," *Progress in Photovoltaics: Research and Applications*, vol. 18, pp. 144-150, 2010.

[4] T. Matsuyama, K. Wakisaka, M. Kameda, M. Tanaka, T. Matsuoka, S. Tsuda, *et al.*, "Preparation of High-Quality n-Type Poly-Si Films by the Solid Phase Crystallization (SPC) Method," *Japanese Journal of Applied Physics*, vol. 29, pp. 2327-2331, 1990.

[5] L. Carnel, I. Gordon, D. Van Gestel, G. Beaucarne, J. Poortmans, and A. Stesmans, "High open-circuit voltage values on fine-grained thin-film polysilicon solar cells," *Journal of Applied Physics*, vol. 100, pp. 063702-063702-7, 2006.

[6] M. A. Green, *Solar cells: Operating principles, technology and system applications*: University of New South Wales, 1998.

[7] Z. Ouyang, O. Kunz, A. B. Sproul, and S. Varlamov, "Influence of the absorber doping for *p*-type polycrystalline silicon thin-film solar cells on glass prepared by electron beam evaporation and solid-phase crystallization," *Journal of Applied Physics*, vol. 109, pp. 054510-7, 2011.

[8] B. Ba, M. Kane, and J. Sarr, "Modelling recombination current in polysilicon solar cell grain boundaries," *Solar Energy Materials and Solar Cells*, vol. 80, pp. 143-154, 2003.

[9] R. Sinton and A. Cuevas, "A quasi-steady-state open-circuit voltage method for solar cell characterization," in *16th European Photovoltaic Solar Energy Conference*, Glasgow, UK, 2000, pp. 1152-1155.

[10] P. J. Gress, P. I. Widenborg, S. Varlamov, and A. G. Aberle, "Wire bonding as a cell interconnection technique for polycrystalline silicon thin-film solar cells on glass," *Progress in Photovoltaics*, vol. 18, pp. 221-228, 2010.

[11] G. Harbeke and L. Jastrzebski, "Assessment of the surface quality of simox wafers by UV reflectance," *Journal of the Electrochemical Society*, vol. 137, pp. 696-699, 1990.

[12] A. Straub, P. I. Widenborg, A. Sproul, Y. Huang, N. P. Harder, and A. G. Aberle, "Fast and non-destructive assessment of epitaxial quality of polycrystalline silicon films on glass by optical measurements," *Journal of Crystal Growth*, vol. 265, pp. 168-173, 2004.

[13] P. I. Widenborg and A. G. Aberle, "Hydrogen-induced dopant neutralisation in p-type AIC poly-Si seed layers functioning as buried emitters in ALICE thin-film solar cells on glass," *Journal of Crystal Growth*, vol. 306, pp. 177-186, 2007.

[14] S. Nakashima and M. Hangyo, "Characterization of semiconductor-materials by raman microprobe," *IEEE Journal of Quantum Electronics*, vol. 25, pp. 965-975, 1989.

[15] M. Holtz, W. M. Duncan, S. Zollner, and R. Liu, "Visible and ultraviolet Raman scattering studies of Si1-xGex alloys," *Journal of Applied Physics*, vol. 88, pp. 2523-2528, Sep 2000.

[16] H. Hidayat, A. Kumar, F. Law, C. Ke, P. I. Widenborg, and A. G. Aberle, "Impact of rapid thermal annealing temperature on non-metallised polycrystalline silicon thin-film diodes on glass," *Thin Solid Films*, vol. 534, pp. 629-635, 2013.

[17] H. Hidayat, A. Kumar, F. Law, P.I. Widenborg, and A. G. Aberle, "Electro-chemical capacitance voltage measurements as a novel doping profiling method for polycrystalline silicon thin-film solar cells on glass," in *Proc. 27th European Photovoltaic Solar Energy Conference*, Frankfurt, Germany, 2012, pp. 2434-2437.

[18] O. Kunz, "Evaporated solid-phase crystallised poly-silicon thin-film solar cell on glass," PhD thesis, The University of New South Wales,Sydney, 2009.

[19] P. Y. Yu and M. Cardona, *Fundamentals of semiconductors: physics and materials properties*: Springer Berlin etc, 1999.

[20] T. Kamins, *Polycrystalline silicon for integrated circuit applications*: Kluwer Academic Publishers, 1988.

[21] A. Kumar, H. Hidayat, C. Ke, S. Chakraborty, G. K. Dalapati, P. I. Widenborg, *et al.*, "Impact of the n^+ emitter layer on the structural and electrical properties of p-type polycrystalline silicon thin-film solar cells," *Journal of Applied Physics*, vol. 114, p. 134505, 2013.

[22] T. Ambridge and M. Faktor, "An automatic carrier concentration profile plotter using an electrochemical technique," *Journal of Applied Electrochemistry,* vol. 5, pp. 319-328, 1975.

[23] J. Y. Lee and S. H. Lee, "Boron back surface field using spin-on dopants by rapid thermal processing," *Journal-Korean Physical Society,* vol. 44, pp. 1581-1586, 2004.

[24] I. Mayes, "Accuracy and reproducibility of the electrochemical profiler," *Materials Science and Engineering B-Solid State Materials for Advanced Technology,* vol. 80, pp. 160-163, 2001.

[25] E. Peiner, A. Schlachetzki, and D. Krüger, "Doping Profile Analysis in Si by Electrochemical Capacitance-Voltage Measurements," *Journal of the Electrochemical Society,* vol. 142, pp. 576-580, 1995.

[26] P. Blood, "Capacitance-voltage profiling and the characterisation of III-V semiconductors using electrolyte barriers," *Semiconductor science and technology,* vol. 1, p. 7, 1986.

[27] D. A. Neamen, "Semiconductor Device Physics: Basic Principles," ed: Tata McGraw Hill, 2002.

[28] O. Kunz, Z. Ouyang, J. Wong, and A. G. Aberle, "Advances in Evaporated Solid-Phase-Crystallized Poly-Si Thin-Film Solar Cells on Glass (EVA)," *Advances in OptoElectronics,* vol. 2008, p. 10, 2008.

[29] L. Shi, "Contact Resistance Study on Polycrystalline Silicon Thin-Film Solar Cells on Glass," Master thesis, The University of New South Wales,Sydney, 2008.

[30] P. I. Widenborg and A. G. Aberle, "Polycrystalline Silicon Thin-Film Solar Cells on AIT-Textured Glass Superstrates," *Advances in OptoElectronics,* vol. 2007, 2007.

[31] G. Jin, P. I. Widenborg, P. Campbell, and S. Varlamov, "Lambertian matched absorption enhancement in PECVD poly-Si thin film on aluminum induced textured glass superstrates for solar cell applications," *Progress in Photovoltaics: Research and Applications,* vol. 18, pp. 582-589, 2010.

[32] Z. Ouyang, S. Pillai, F. Beck, O. Kunz, S. Varlamov, K. R. Catchpole, *et al.*, "Effective light trapping in polycrystalline silicon thin-film solar cells by means of rear localized surface plasmons," *Applied Physics Letters,* vol. 96, p. 261109, 2010.

[33] F. Law, Y. Yi, Hidayat, P. I. Widenborg, J. Luther, and B. Hoex, "Identification of geometrically necessary dislocations in solid phase crystallized poly-Si," *Journal of Applied Physics*, vol. 114, p. 043511, 2013.

Chapter 6

Chapter 6- SPC Poly-Si Absorber Layers from High-Rate Deposited a-Si:H Films

6.1 Introduction

SPC poly-Si thin-film material is a promising semiconductor for the PV industry, combining the robustness of c-Si with the advantages of the thin-film approach [1]. SPC poly-Si thin films are obtained from the annealing of a-Si:H films in a N_2 atmosphere for 12 hours at 610 °C [2]. Plasma-enhanced chemical vapour deposition (PECVD) is widely used in industry for large-area deposition of a-Si:H films. However, the low deposition rate of a-Si:H films (25-35 nm/min) in traditional PECVD processes significantly adds to the cost of poly-Si thin-film solar cells [3]. There are other deposition techniques such as e-beam evaporation and hot wire chemical vapour deposition (HWCVD) which are capable of a-Si:H film depositions at a very high rate (>> 100 nm/min). However, the electronic properties of SPC poly-Si films obtained by these deposition techniques are inferior to those obtained from PECVD, which makes them difficult to commercialise. The a-Si:H films deposited by the e-beam evaporation technique have a high degree of thickness non-uniformity over large areas, which leads to problems at the device level (such as laterally non-uniform short-circuit current densities of solar cells, or pinholes and cracks that are detrimental to the solar cell performance [4]). On the other hand, a-Si:H films deposited by HWCVD have a very high nucleation rate, leading to SPC poly-Si films with much smaller grains compared with films deposited by PECVD [5].

Some results on a-Si:H films deposited with the high-rate PECVD technique can be found in the literature [6-11]. However, most of these deposited

films suffered from internal stress, large microvoids and high dangling bond densities. The possible reason for this could be the fact that the substrate temperature (T_s) used for these a-Si:H depositions was restricted to below 250 °C. Recently, G. Jin demonstrated in his doctoral thesis that an increase in the substrate temperature to 400 °C yields a high-quality poly-Si film prepared from the SPC of an a-Si:H film deposited at significantly higher rate using PECVD [12]. The performance of the poly-Si thin-film solar cell obtained from the SPC of a-Si:H films deposited at high rate was also found to be comparable to that of the standard low-rate deposited cells [12]. In addition, it was shown that there was a decrease in the contamination level in the absorber layer when the a-Si:H film deposition rate was increased [12]. In a traditional PECVD, contaminants such as carbon (C), Nitrogen (N) and Oxygen (O) are controlled in the a-Si:H films by keeping the base deposition pressure extremely low in the rate of 10^{-8} Torr. This is generally achieved by the use of expensive turbo pumps. Thus, by controlling the contaminants, high-rate PECVD provides the flexibility to deposit at higher base pressure. This makes high-rate PECVD very interesting for large-scale industrial applications where the use of expensive turbo pumps is often not economical. In addition, a much thicker absorber layer is possible through the use of high-rate deposition, which otherwise is virtually impossible with a low deposition rate (< 35nm/min). A thicker absorber layer is required to enhance the current of poly-Si thin-film solar cells, and hence their PV efficiency. Furthermore, the electronic properties of a SPC poly-Si thin film largely depend on the post-deposition treatments, which gives us the possibility to extensively

explore the process parameter space of a-Si:H deposition for SPC poly-Si thin-film solar cell applications far beyond of what has been investigated for the a-Si:H solar cell field.

This chapter investigates the effects of the main deposition parameters (RF power density (mW/cm^2), SiH_4 gas flow (sccm), process pressure, etc) on the deposition rate and thickness uniformity of a-Si:H films deposited on 30 × 40 cm^2 large-area glass substrates. Furthermore, the chapter presents a detailed study of the impact of the deposition parameters of the a-Si:H films on the structural quality of the resulting SPC poly-Si films. A high deposition rate for the a-Si:H films of up to 146 nm/min at 13.56 MHz is achieved and is investigated as an absorber layer formation for SPC poly-Si thin-film solar cells.

6.2 Experimental Details

An ~70 nm thick SiN_x barrier coating was deposited onto 300 x 400 x 3.3 mm^3 planar glass sheets (Schott, Borofloat) in a PECVD chamber (MVSystems, USA) at a temperature ~ 460 ºC. The SiN_x film acts as an antireflection coating as well as a diffusion barrier for impurities in the glass substrate. The SiN_x coated glass was then loaded into a special PECVD chamber with an electrode spacing of 23 mm. The a-Si:H films were then deposited using different combinations of SiH_4 gas flow rate and RF power density, at the conventional plasma generation frequency of 13.56 MHz. The complete recipe used to achieve a high-rate deposition of a-Si:H films is summarised in Table 6.1.

***Table 6.1**: Experimental details used for the PECVD of the p^- a-Si:H films.*

Process condition	*p^- a-Si layer*
SiH_4 (sccm)	60-400
100 ppm B_2H_6:H_2 (sccm)	0.2
Substrate temperature (ºC)	380
Pressure (Pa)	107
Time (min)	5-20
RF power density (mW/cm^2)	67-167

The deposited a-Si:H films were then annealed (Nabertherm, N 120/ 65HAC furnace, Germany) at 610 ºC in a N_2 atmosphere for a duration of 12 hours to achieve solid phase crystallisation of the film. A rapid thermal anneal (RTA, CVD Equipment, USA) for 1 minute at a peak temperature of 1000 ºC in N_2 atmosphere was then used to remove crystallographic defects from the SPC poly-Si thin-film diodes and to activate the dopants. Each 30 × 40 cm^2 poly-Si coated glass sheet was then cut into 12 equal small pieces of size 10×10 cm^2 in a configuration as shown in Figure 6.1.

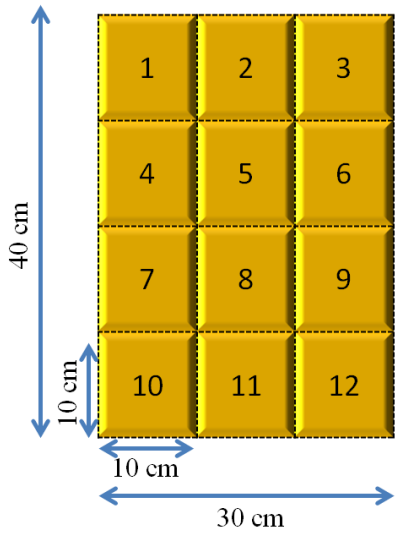

***Figure 6.1:** Schematic of configuration used to cut the 30 ×40 cm^2 poly-Si coated glass sheet into 12 equal 10×10 cm^2 glass pieces.*

Optical reflectance measurements in the 250-1500 nm wavelength range were performed on each of the 12 pieces of the poly-Si film using an UV-VIS-NIR spectrophotometer (PerkinElmer, Lambda 950, UV/VIS Spectrometer).The thickness of the poly-Si thin film was then calculated by curve fitting of the reflectance data with an optical simulation programme (WVASE). The thickness uniformity of the poly-Si thin film over the 30 × 40 cm^2 glass sheet was determined by calculating the thickness of each of the 12 pieces of the poly-Si film obtained from the glass sheet. The thicknesses of selected a-Si:H samples were also determined by ellipsometry and were found to be in good agreement with the thickness data of the poly-Si films obtained from WVASE. The deposition rate was then obtained by dividing the average thickness of the poly-Si film by the deposition time. Finally, the material quality of the poly-Si thin film was determined using UV reflectance measurements [13-15] and Raman spectroscopy [16, 17] measurements (Witec Alpha 300R confocal Raman microscope equipped with a 532nm Nd:YAG laser), whereby the samples were always measured from the air side.

6.3 Results and Discussion

6.3.1 Effect of SiH_4 gas flow rate on the deposition rate of a-Si:H films

Figure 6.2 shows the deposition rate of a-Si:H films as a function of the SiH_4 gas flow rate. The plasma power density, process pressure and the substrate temperature were kept constant at 67 mW/cm^2, 107 Pa and ~ 360 ºC, respectively, while the SiH_4 gas flow rate was systematically increased as described in Table

6.2. It is found that the deposition rate of the a-Si:H films increases from 17 to 75 nm/min when the SiH_4 gas flow rate is increased from 60 to 225 sccm.

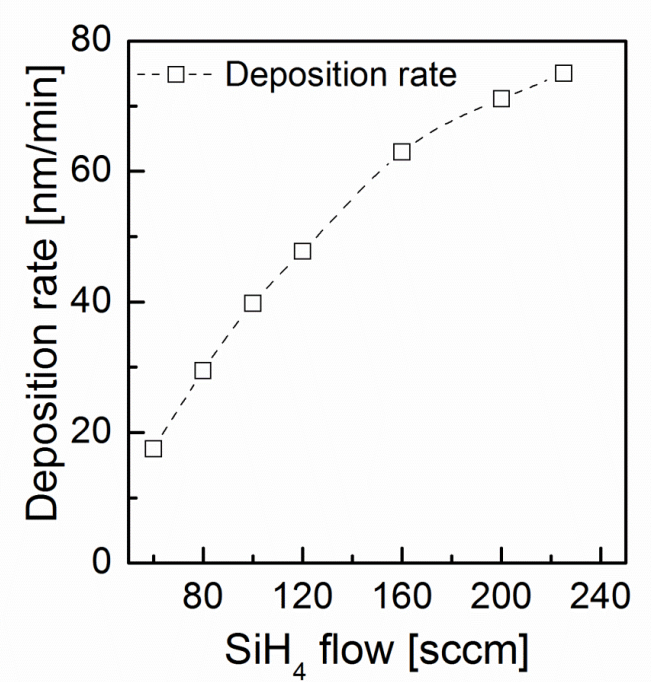

Figure 6.2: *Deposition rate of a-Si:H films as a function of SiH_4 flow.*

Table 6.2: *Recipe for high-rate deposition of a-Si:H films as a function of the SiH_4 gas flow rate.*

Sample no	*SiH_4 flow (sccm)*	*RF power density (mW/cm^2)*	*Deposition rate (nm/min)*
HRD 1.1	60	67	18
HRD 1.2	80	67	29
HRD 1.3	100	67	40
HRD 1.4	120	67	48
HRD 1.5	160	67	63
HRD 1.6	200	67	71
HRD 1.7	225	67	75

As can be seen from Figure 6.2, the deposition rate approaches a saturation value when the SiH_4 gas flow rate is increased beyond about 200 sccm.

A parameter (R_D) can be defined here that quantifies the change in deposition rate with respect to the increase in the SiH_4 gas flow:

$$R_D = \frac{\Delta d_r}{\Delta \text{gas flow}} = \frac{\text{deposition rate}_{final} - \text{deposition rate}_{initial}}{\text{gas flow}_{final} - \text{gas flow}_{initial}} \left[\frac{nm}{min.sccm}\right] \qquad 6.1$$

Figure 6.3 shows R_D as a function of the SiH_4 gas flow rate. R_D is found to be ~ 0.55 nm/(min.sccm) up to a SiH_4 gas flow rate of about 100 sccm. R_D then drops to approximately 0.15 nm/(min.sccm) when the SiH_4 gas flow is increased to 225 sccm. The significantly reduced R_D at high SiH_4 gas flows could be from the limitation of plasma power density to ionize the gas present in the chamber. Thus, further studies were carried out to understand the effect of the plasma power density on the deposition rate of a-Si:H films at high SiH_4 gas flow rate.

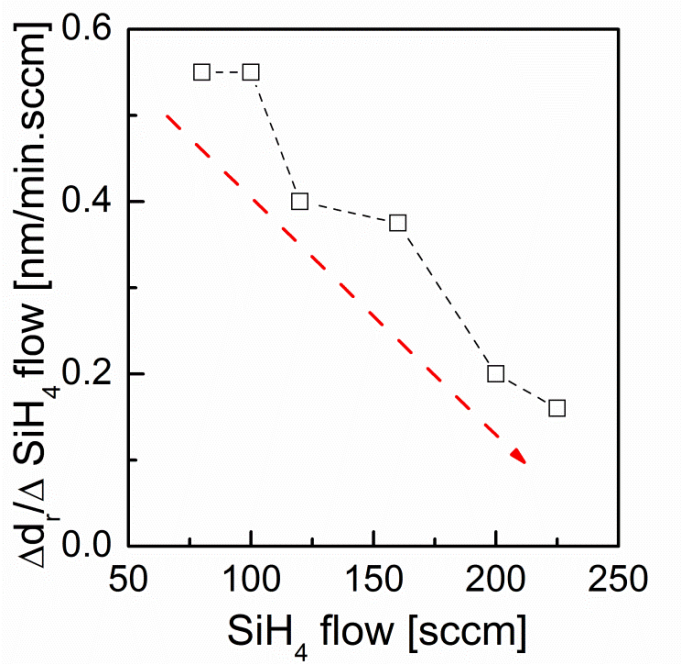

Figure 6.3: *Change in deposition rate of a-Si:H films with respect to the change in the gas flow(i.e., R_D) as a function of the SiH_4 gas flow. The dotted lines are guides to the eye.*

6.3.2 Effect of RF power density on the deposition rate of a-Si:H films.

Figure 6.4 shows the deposition rate of a-Si:H films as a function of the RF plasma power density. The SiH_4 gas flow rate, process pressure and the substrate temperature were kept constant at 200 sccm, 107 Pa and ~ 360 ºC, respectively, while the plasma power density was systematically increased. The deposition parameters and the calculated deposition rates of the a-Si:H films are presented in Table 6.3.

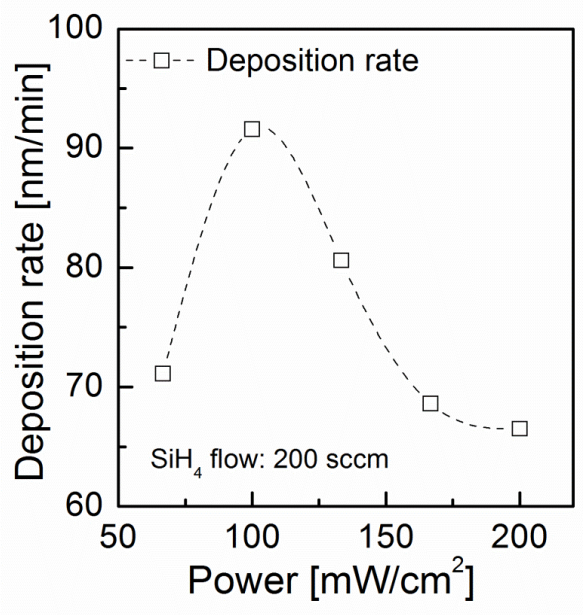

Figure 6.4: *Deposition rate of a-Si:H films as a function of the RF power density. The dotted lines are guides to the eye.*

Table 6.3: *Recipe for the deposition of a-Si:H films as function of plasma power density.*

Sample	*SiH_4 flow (sccm)*	*RF power density (mW/cm^2)*	*Deposition rate (nm/min)*
HRD 1.8	200	67	71
HRD 1.9	200	100	92
HRD 1.10	200	133	81
HRD 1.11	200	167	69
HRD 1.12	200	200	67

At 200 sccm of SiH_4 gas flow, there is a significant increase in the a-Si:H deposition rate from 71 to 93 nm/min when the plasma power density is increased from 67 to 100 mW/cm^2. The a-Si:H deposition rate then decreases with a further increase of the plasma power density. It seems that the further increase of the plasma power density led to the saturation of the active species (responsible for the deposition rate) present in the plasma region at 200 sccm of SiH_4 gas flow rate [18]. In addition, the increase in the plasma power density also results in the formation of dust or small particles [18]. The combined effects of dust generation and saturation of the active species (positive ions) might be responsible for the decrease in the a-Si:H deposition rate. Furthermore, the dust particles generated at high power density plasma get accumulated and form a sheath near the throttle valve connected to the pump, as can be seen in Figure 6.5. This accumulated layer of dust particles impacts the flow of gas in the chamber, which also causes a laterally more non-uniform deposition (discussed in detail in Section 6.3.4). From sections 6.3.1 and 6.3.2, it follows that the increase in the deposition rate cannot be sustained by adjusting the power and gas flow rate individually. It is desired to establish a relationship between the RF power density and the SiH_4 gas flow rate to have a sustained growth rate of the a-Si:H films. Thus, the next section presents a study on the combined effect of the plasma power density and the SiH_4 gas flow rate on the deposition rate of the a-Si:H films.

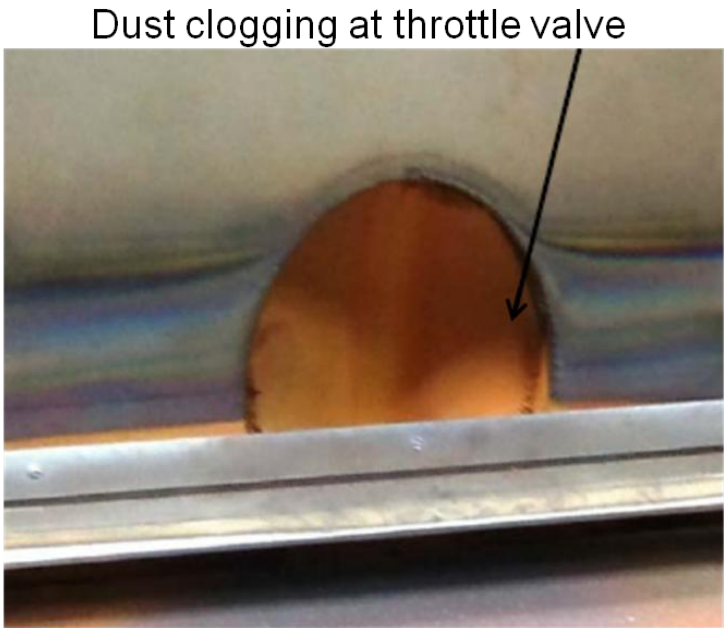

Figure 6.5: *Dust formation near the throttle valve at high plasma power density.*

6.3.3 Effect of SiH_4 gas flow rate and RF power density on the a-Si:H deposition rate

From the discussions in sections 6.3.1 and 6.3.2, it follows that the a-Si:H deposition rate is not just an independent function of the SiH_4 gas flow rate or the RF power density, but seems to be a combined function of flow rate and power density. Figure 6.6 shows the a-Si:H deposition rate as a combined function of the SiH_4 gas flow rate and the RF plasma power density. It can be clearly seen from Figure 6.6, that at a RF power density of 67 mW/cm^2, the a-Si:H deposition rate starts to saturate with a significant decrease in R_D (see section 6.3.2) when the SiH_4 gas flow rate increases beyond 200 sccm. A very different trend in the deposition rate is observed when the RF power density was varied. There is a drastic increase in the a-Si:H deposition rate from 71 to 91 nm/min when the power density is increased from 67 to 100 mW/cm^2. The deposition rate then

decreased with the further increase in the RF power density until it saturated at a significantly lower value of 67 nm/min. Furthermore, a detailed analysis of Fig. 6.6 reveals that a sustainable increase in the a-Si:H deposition rate can be achieved through the *simultaneous* control of the SiH_4 gas flow and the power density. In this work, we found that a SiH_4 gas flow to RF power density ratio of around 2.4 sccm/mWcm^{-2} gives a sustainable increase in the a-Si:H deposition rate. A high deposition rate of 146 nm/min was obtained through the control of the SiH_4 gas flow to RF power density ratio. The deposition parameters, along with the sample names and their calculated a-Si:H deposition rates as a function of the SiH_4 flow and the RF power are summarised in Table 6.4.

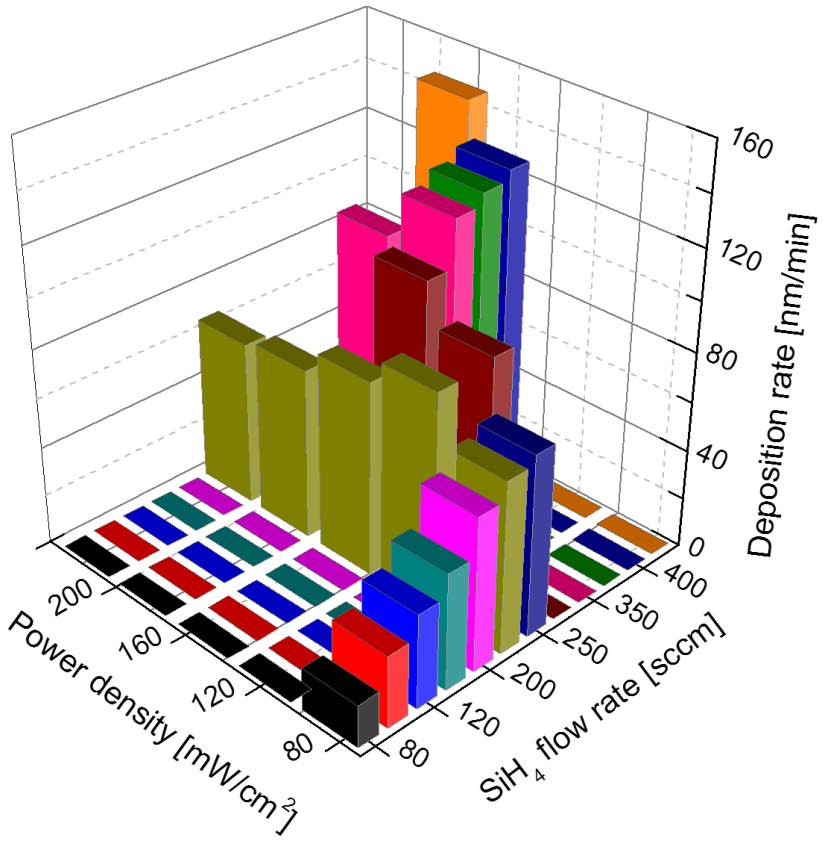

Figure 6.6: *Deposition rate of the a-Si:H films as a combined function of the plasma power and the SiH_4 flow rate.*

Table 6.4: *Recipe for high rate deposition of a-Si:H films as function of SiH_4 gas flow rate and RF power density.*

Sample	*SiH_4 flow (sccm)*	*RF power density (mW/cm^2)*	*Deposition rate (nm/min)*	*Flow/RF power density*
HRD 1.13	250	100	91	2.5
HRD 1.14	250	133	107	1.9
HRD 1.15	300	133	125	2.3
HRD 1.16	300	167	107	1.8
HRD 1.17	350	130	130	2.7
HRD 1.18	400	167	146	2.4
HRD 1.19	400	133	135	3.0

6.3.4 Impact of deposition rate on thickness uniformity of the a-Si:H films over the 30 × 40 cm^2 glass sheet

Thickness uniformity over large areas is one of the key issues for any film deposition technique and is very critical for many semiconductor applications. The PECVD technique is renowned for its conformal deposition over large areas at low deposition rates. However, very few results are available in the literature for high-rate conformal PECVD deposition over large area. This section investigates the thickness uniformity of high-rate deposited a-Si:H films over the large-area (30 × 40 cm^2) glass sheet. The thickness non-uniformity is quantified using the following relation:

$$non-uniformity\ \% = \left[\frac{max_{thickness} - min_{thickness}}{max_{thickness} + min_{thickness}}\right] \times 100. \qquad (6.2)$$

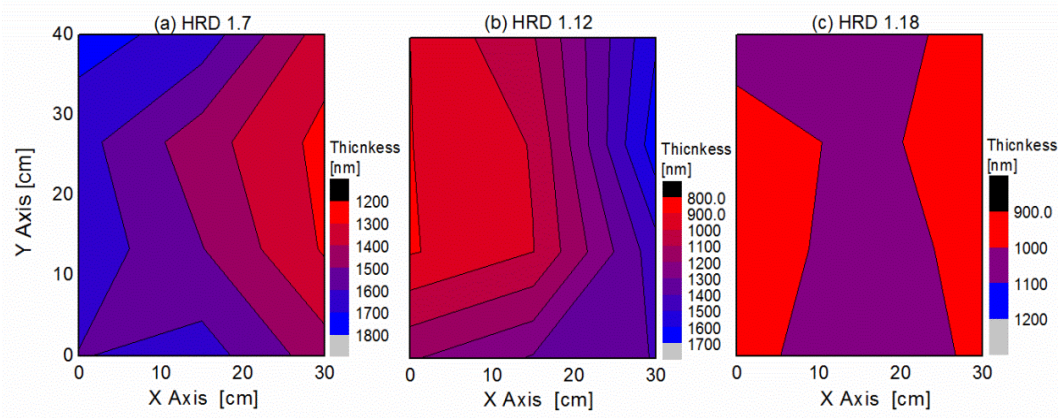

Figure 6.7: *Contour maps for a-Si:H thickness non-uniformity over the 30 × 40 cm^2 glass sheet at a deposition rate of (a) 75 nm/min, (b) 67 nm/min and (c) 146 nm/min.*

Figure 6.7 shows the contour maps for the a-Si:H thickness non-uniformity over the 30 × 40 cm^2 glass sheet at an a-Si:H deposition rate of (a) 75 nm/min, (b) 67 nm/min and (c) 146 nm/min. It is found that the a-Si:H films deposited at 75 nm/min have a thickness non-uniformity of ± 16% over the 30 × 40 cm^2 glass sheet, whereas the a-Si:H films deposited at a slightly lower deposition rate of 67 nm/min are found to be highly non-uniform (thickness non-uniformity of ± 30%). However, the a-Si:H films deposited at a very high deposition rate of 146 nm/min are found to be highly uniform over the 30 × 40 cm^2 glass sheet, with a thickness non-uniformity value of less than ± 6% (see Figure 6.7(c)). A detailed analysis of the thickness non-uniformity contour maps and the deposition parameters reveals that a highly uniform a-Si:H deposition is possible at high deposition rate, provided that the ratio of SiH_4 gas flow rate to RF power density is kept at around 2.4 sccm/mWcm^{-2}. We also observed that SiH_4 gas flow to RF power density ratios of below 1.6 sccm/mWcm^{-2} or above 3 sccm/mWcm^{-2} lead to a very high lateral thickness variation of the a-Si:H film on the 30 × 40 cm^2 glass sheet. The samples HRD 1.7 and HRD 1.12 (see Figure 6.7)

were obtained with a SiH_4 gas flow to RF power density ratio of 3.3 sccm/mWcm^{-2} and 1.0 sccm/mWcm^{-2}, respectively. These samples were found to have a thickness non-uniformity of ± 16% and ± 30%, respectively, over the 30 × 40 cm^2 glass sheet. In contrast, the sample HRD 1.18 which was produced using a SiH_4 gas flow to RF power density ratio of 2.4 sccm/mWcm^{-2} is found to have a very low thickness non-uniformity of ± 6% over the 30 × 40 cm^2 glass sheet. A high thickness non-uniformity of the a-Si:H film on the large-area (30 × 40 cm^2) glass sheet leads to the formation of cracks during the SPC process. The cracks are mainly formed by the stress produced in the film during the heat treatment process. The large thickness variation in the a-Si:H film on the 30 × 40 cm^2 glass sheet area is one of the main causes for the stress generation. The cracks formed during the SPC process open up during the RTA process and cover the entire film, as can be seen in Figure 6.8.

Figure 6.8 shows photographs of selected poly-Si thin-film samples obtained from SPC of a-Si:H films deposited using a SiH_4 gas flow to RF power density ratio of (a) 3.3 sccm/mWcm^{-2} and (b) 2.4 sccm/mWcm^{-2}. The photos shown here were taken after the RTA process and depict a small sample area of 10×10 cm^2 from the centre of 30 × 40 cm^2 glass sheet. It can be clearly seen that the poly-Si film prepared from SPC of laterally highly non-uniform a-Si:H films (HRD 1.7) has cracks all over the surface (see Fig. 6.8(a)). In contrast, no cracks are observed after the RTA process for the poly-Si film obtained from SPC of a highly uniform a-Si:H film (see Fig. 6.8(b)). The high density of cracks makes the poly-Si film unsuitable for solar cell applications and thus needs to be avoided.

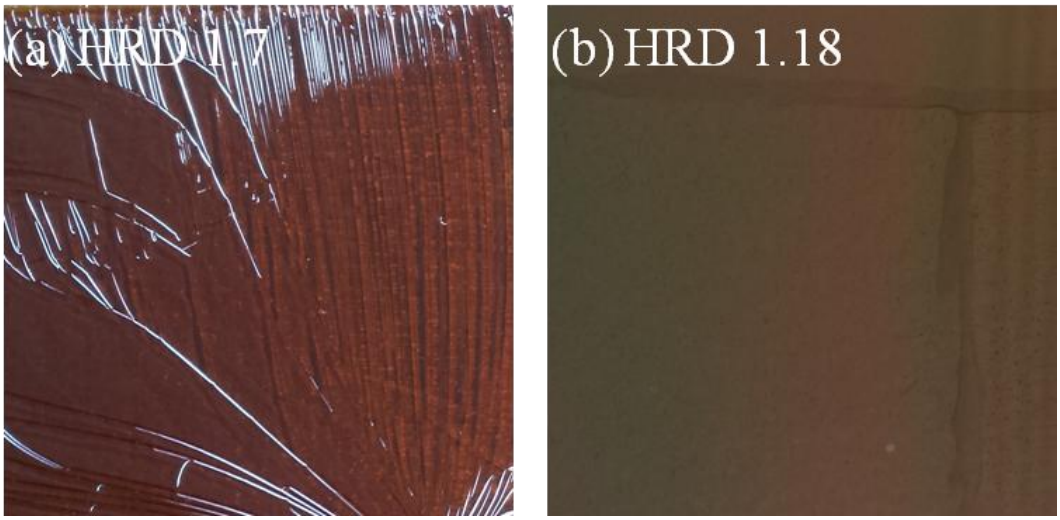

Figure 6.8: *Photograph of a poly-Si film obtained from SPC of a-Si:H films deposited with a SiH_4 gas flow to RF power density ratio of (a) 3.3 sccm/mWcm^{-2} and (b) 2.4 sccm/mWcm^{-2}.*

6.3.5 Effect of deposition rate on the crystal quality of the poly-Si thin film

The material quality of the poly-Si thin film is one of the key parameters for its electrical quality. Thus, it is desirable to obtain a high crystal quality of the poly-Si film while trying to achieve a high-rate deposition. This section investigates the effect of a high deposition rate on the crystal quality, using the UV reflectance and Raman characterization techniques.

Figure 6.9 shows the total hemispherical reflectance at short wavelengths (UV region, 250-400 nm) measured on two different poly-Si thin films prepared by SPC of high-rate deposited a-Si:H films, as well as on a polished c-Si wafer. Two characteristic peaks resulting from direct optical transitions in c-Si [19] were observed in the UV reflectance spectrum at ~360 nm and ~275 nm (*Re1* and *Re2*), respectively. Structural disorder and defects in the surface region of the probed poly-Si film lead to a decrease and broadening of the peaks [20].

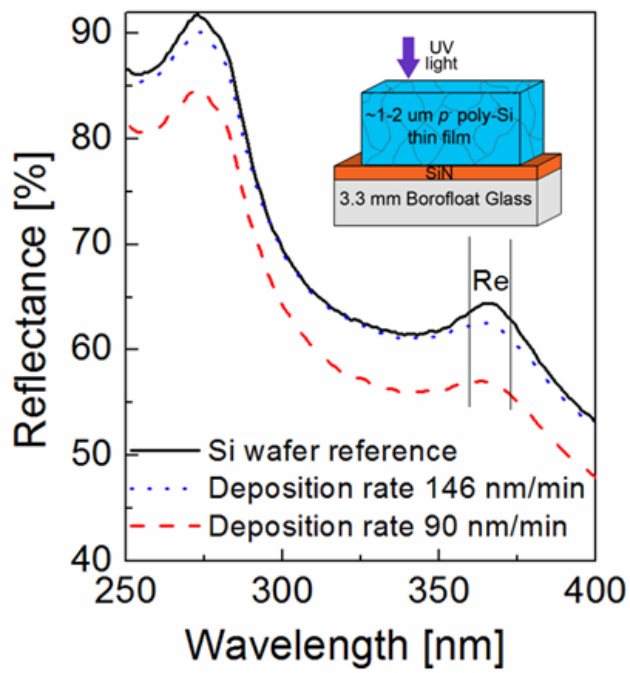

Figure 6.9: *Hemispherical UV reflectance measured on two poly-Si films obtained by SPC of a-Si:H films deposited at 90 and 146 nm/min, respectively. Also shown (solid line) is the UV reflectance measured on a polished single-crystalline Si wafer.*

It can be clearly seen that the poly-Si thin film fabricated by SPC of an a-Si:H film deposited at 146 nm/min has fewer defects than the poly-Si film fabricated by SPC of an a-Si:H film deposited at 90 nm/min. In addition, the reflectance spectrum obtained for the poly-Si film is quite close to that of a single-crystal Si wafer. The UV reflectance spectra obtained for the c-Si wafer and the poly-Si thin films were quantified in terms of the crystal quality using the relationship given in the literature [14, 15] and in Chapter 2 (see Eq. 2.2).

Figure 6.10 shows the calculated crystal quality factor for selected poly-Si thin films obtained from a-Si:H films deposited at various deposition rates. It can be clearly seen that the poly-Si films fabricated by SPC of a-Si:H films deposited at high rate have a better UV crystal quality than those obtained from a-Si:H

deposited at lower rate. Detailed analysis of the graph (see Figure 6.10) and the experimental data revealed that the SPC poly-Si films with the best crystal quality were fabricated from a-Si:H films deposited using a SiH_4 flow to RF power density ratio of about 2.4 sccm/mWcm^{-2}. In contrast, the SPC poly-Si films with poor crystal quality were found to be fabricated from a-Si:H films using a SiH_4 gas flow to RF power density ratio of less than 1.6 sccm/mWcm^{-2}. The further increase of the RF power density was found to significantly affect the crystal quality of the poly-Si film. It was also observed that some of the poly-Si thin films with low UV crystal quality had an extremely high number of cracks (see Figure 6.10). These cracks might have been generated during the SPC and RTA processes due to the large a-Si:H thickness variation across the large area of 30 × 40 cm^2, as discussed earlier (see section 6.3.4). The UV reflectance merely probes the surface region (~5 nm thickness) of the poly-Si film and thus the obtained UV crystal quality could just be a representation of the surface quality of the poly-Si film. The poor UV crystal quality observed in some of the poly-Si films with an extreme number of cracks could well be due to the effects of the cracks and thus does not represent the true effect of the a-Si:H deposition rate on the crystal quality of the SPC poly-Si film. Hence, selected poly-Si thin film samples were further characterised from the air side by Raman spectroscopy [16] (scanning depth ~400 nm), to better understand the effect of the a-Si:H deposition rate on the structural quality of the SPC poly-Si film.

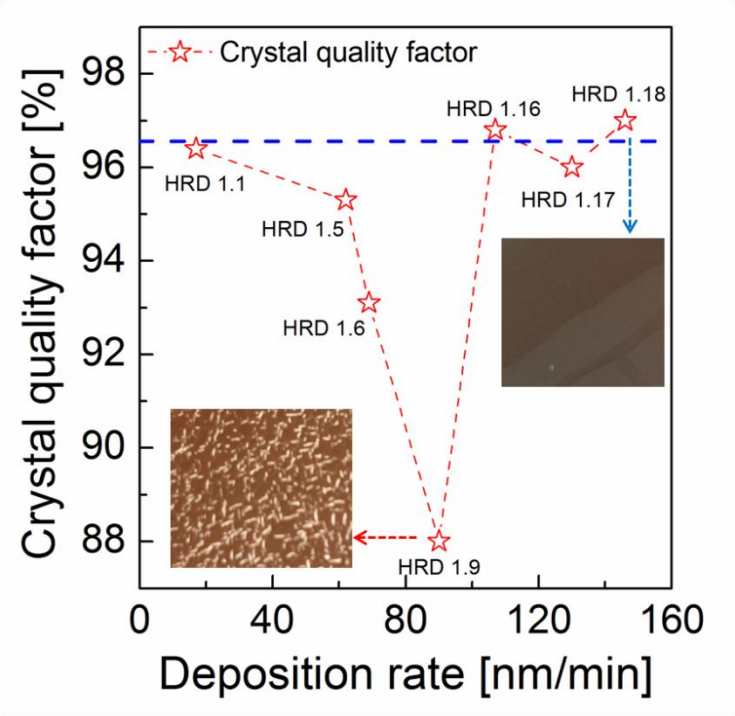

Figure 6.10: *Crystal quality of the SPC poly-Si thin films calculated from UV reflectance as a function of the a-Si:H deposition rate. The dotted lines are guides to the eye.*

Figure 6.11 shows Raman spectra acquired from the visible (532 nm) laser line for selected poly-Si thin films fabricated by SPC of a-Si:H films deposited at different deposition rates. As a reference, the Raman spectrum was also obtained for a single-crystalline high-resistivity FZ-grown silicon wafer (solid line). A strong peak at a frequency ω_0 of about 522 cm^{-1} is observed for the c-Si wafer. This peak position value of c-Si may slightly vary from experiment to experiment, depending on the calibration of the spectrometer and monochromator. Furthermore, the Raman spectra for some poly-Si films reveal that there is a shift in the peak position towards higher wave numbers with respect to c-Si, indicating the presence of compressive stress in the poly-Si film [21]. However, it is worth to note that the poly-Si film fabricated by SPC of a-Si:H deposited at a high deposition rate of 146 nm/min is found to have no stress in the film.

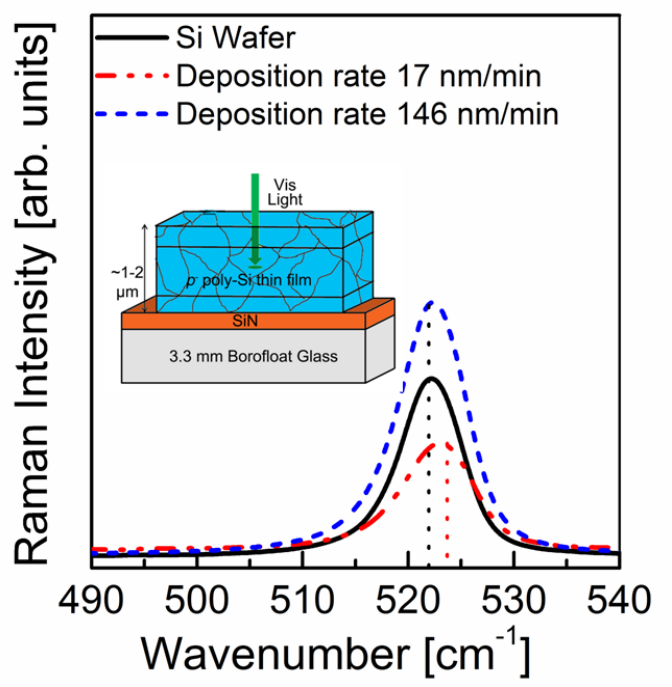

Figure 6.11: *Raman spectra of poly-Si films deposited at two different deposition rates of 17 and 146 nm/min, respectively. Also shown (solid line) for comparison is the Raman spectrum measured on a polished single-crystalline Si wafer.*

A detailed analysis of the Raman spectra and the process parameters revealed that stress in the SPC poly-Si film can be reduced by the control of the SiH4 gas flow to RF power density ratio. Further, detailed analysis of the Raman spectra (see Fig. 6.11) reveals that the full width at half maximum (FWHM) of the poly-Si film varies with the deposition rate of the a-Si:H film. The FWHM is an excellent indicator of the crystal quality of the poly-Si film. An increase in the defect density and disorder in Si thin films leads to a broadening of the peak (FWHM) [16, 22, 23]. A Raman quality factor (R_Q) (described in Chapter 2) is used to quantify the defects in the poly-Si film relative to a (stress-free) single-crystal Si wafer.

Figure 6.12 shows the calculated Raman quality factor of the poly-Si thin

film obtained by SPC of a-Si:H films as a function of the deposition rate. It can be clearly seen that few poly-Si films obtained by SPC of a-Si:H films deposited at higher rate had better crystal quality than those obtained from a-Si:H deposited at low deposition rate. The interpretation of poly-Si thin film crystal quality obtained from Raman measurements is in good agreement with the result obtained from UV reflectance measurements.

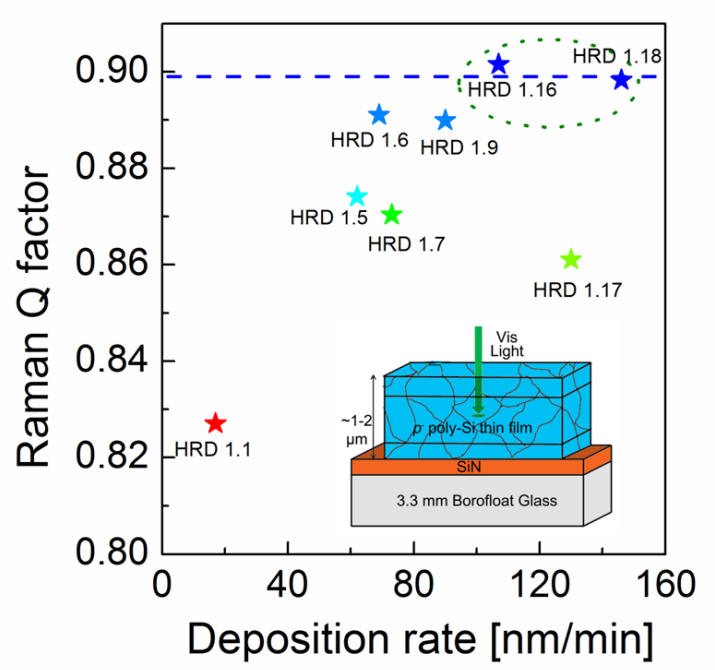

Figure 6.12: *Raman quality factor (R_Q) of SPC poly-Si thin films as a function of the a-Si:H deposition rate.*

6.4 Conclusion

In conclusion, a high deposition rate of 146 nm/min was achieved through the control of the SiH_4 gas flow and the RF power density. A laterally highly uniform deposition of a-Si:H over the large glass sheet area of 1200 cm^2 using high-rate PECVD was achieved. A relationship between the SiH_4 gas flow and the

RF power density was established. A linear increase in the deposition rate up to 146 nm/min was achieved by keeping the SiH_4 gas flow to RF power density ratio constant at about 2.4 sccm/mWcm^{-2}. The SiH_4 gas flow to RF power density ratio was also found to effect the thickness uniformity of a-Si:H films and the material quality of the SPC poly-Si films obtained from the a-Si:H films. A very high SPC poly-Si crystal quality with a thickness non-uniformity of less than ± 6% over 30×40 cm^2 was obtained. A further increase in the deposition rate to about 250 nm/min seems possible through the control of the SiH_4 gas flow and the RF power density, while maintaining good thickness uniformity and a high crystal quality.

References of Chapter 6

[1] A. G. Aberle, "Thin-film solar cells," *Thin Solid Films*, vol. 517, pp. 4706-4710, 2009.

[2] A. Kumar, P. I. Widenborg, H. Hidayat, Q. Zixuan, and A. G. Aberle, "Impact of rapid thermal annealing and hydrogenation on the doping concentration and carrier mobility in solid phase crystallized poly-Si thin films," *MRS Online Proceedings Library*, vol. 1321, 2011.

[3] P. A. Basore, "CSG-1 Manufacturing a new polycrystalline silicon PV technology", *Proc. 4th World Conference on Photovoltaic Energy Conversion, Hawaii*, 2006, pp. 874-876.

[4] Z. Ouyang, O. Kunz, M. Wolf, P. Widenborg, G. Jin, and S. Varlamov, "Challenges of evaporated solid-phase-crystallised poly-Si thin-film solar cells on textured glass," *18th International Photovoltaic Science and Engineering Conference*, Kolkata, 2009.

[5] D. L. Young, P. Stradins, Y. Xu, L. Gedvilas, B. Reedy, A. H. Mahan, et al., "Rapid solid-phase crystallization of high-rate, hot-wire chemical-vapor-deposited hydrogenated amorphous silicon," *Applied Physics Letters*, vol. 89, p. 161910, 2006.

[6] T. Takagi, K. Takechi, Y. Nakagawa, Y. Watabe, and S. Nishida, "High rate deposition of a-Si:H and a-SiN_x:H by VHF PECVD," *Vacuum*, vol. 51, pp. 751-755, 1998.

[7] T. Takagi, R. Hayashi, G. Ganguly, M. Kondo, and A. Matsuda, "Gas-phase diagnosis and high-rate growth of stable a-Si:H," *Thin Solid Films*, vol. 345, pp. 75-79, 1999.

[8] V. Kirbs, T. Drusedau, and H. Fiedler, "The temperature-dependent defect density of a-Si:H calculated from thermally activated conductivity," *Journal of Physics: Condensed Matter*, vol. 4, p. 10433, 1992.

[9] M. Estrada, A. Cerdeira, I. Pereyra, and S. Soto, "High deposition rate a-Si:H layers from pure SiH_4 and from a 10% dilution of SiH_4 in H_2," *Thin Solid Films*, vol. 373, pp. 176-179, 2000.

[10] B. A. Korevaar, G. J. Adriaenssens, A. H. M. Smets, W. M. M. Kessels, H. Z. Song, M. C. M. van de Sanden, et al., "High hole drift mobility in a-Si:H deposited at high growth rates for solar cell application," *Journal of Non-Crystalline Solids*, vol. 266–269, Part 1, pp. 380-384, 2000.

[11] J. Hautala, Z. Saleh, J. F. M. Westendorp, H. Meiling, S. Sherman, and S. Wagner, "High Deposition Rate a-Si:H for the Flat Panel Display Industry," *MRS Online Proceedings Library*, vol. 420, 1996.

[12] G. Jin, "Advanced polycrystalline silicon thin film solar cells using high rate plasma enhanced chemical vapour deposited amorphous silicon on textured glass," PhD thesis, The University of New South Wales, Sydney, 2010.

[13] G. Harbeke and L. Jastrzebski, "Assessment of the surface quality of simox wafers by UV reflectance," J*ournal of the Electrochemical Society*, vol. 137, pp. 696-699, 1990.

[14] A. Straub, P. I. Widenborg, A. Sproul, Y. Huang, N. P. Harder, and A. G. Aberle, "Fast and non-destructive assessment of epitaxial quality of poly-crystalline silicon films on glass by optical measurements," *Journal of Crystal Growth*, vol. 265, pp. 168-173, 2004.

[15] P. I. Widenborg and A. G. Aberle, "Hydrogen-induced dopant neutralisation in p-type AIC poly-Si seed layers functioning as buried emitters in ALICE thin-film solar cells on glass," *Journal of Crystal Growth*, vol. 306, pp. 177-186, 2007.

[16] S. Nakashima and M. Hangyo, "Characterization of semiconductor-materials by Raman microprobe," *IEEE Journal of Quantum Electronics*, vol. 25, pp. 965-975, 1989.

[17] M. Holtz, W. M. Duncan, S. Zollner, and R. Liu, "Visible and ultraviolet Raman scattering studies of $Si_{1-x}Ge_x$ alloys," *Journal of Applied Physics*, vol. 88, pp. 2523-2528, 2000.

[18] G. Bruno, P. Capezzuto, and G. Cicala, "*1 - Chemistry of Amorphous Silicon Deposition Processes: Fundamentals and Controversial Aspects," in Plasma Deposition of Amorphous Silicon-Based Materials*, G. Bruno, P. Capezzuto, and A. Madan, Eds., ed San Diego: Academic Press, 1995, pp. 1-62.

[19] P. Y. Yu and M. Cardona, F*undamentals of semiconductors: physics and materials properties*: Springer, Berlin, 1999.

[20] T. Kamins, *Polycrystalline silicon for integrated circuit applications*: Kluwer Academic Publishers, 1988.

[21] K. Kitahara and A. Hara, "Oriented Lateral Growth and Defects in Poly-crystalline-Silicon Thin Films on Glass Substrates." *Crystallization - Science and Technology*, 2012, DOI: 10.5772/37040.

[22] A. Kumar, H. Hidayat, C. Ke, S. Chakraborty, G. K. Dalapati, P. I. Widenborg, et al., "Impact of the n^+ emitter layer on the structural and electrical properties of p-type polycrystalline silicon thin-film solar cells," *Journal of Applied Physics*, vol. 114, p. 134505, 2013.

[23] R. C. Teixeira, I. Doi, M. B. P. Zakia, J. A. Diniz, and J. W. Swart, "Micro-Raman stress characterization of polycrystalline silicon films grown at high temperature," *Materials Science and Engineering: B*, vol. 112, pp. 160-164, 2004.

Chapter 7

Chapter 7- Integration of β-$FeSi_2$ with SPC Poly-Si Thin Films on Glass for PV Applications

7.1. Introduction

7.2. Experimental Procedures

7.3. Results and Discussion

7.4. Conclusion

7.1 Introduction

Semiconducting beta-phase iron disilicide, β-$FeSi_2$, has recently attracted interest in the photovoltaic (PV) community owing to its relatively large optical absorption coefficient (> 10^5 cm^{-1} at 1 eV) and its relatively narrow direct bandgap of 0.85 eV [1-5]. In addition, its ability to be chemically stable at temperatures of up to 937 °C [6], high resistance against environmental attacks (humidity, oxidization, cosmic rays), non-toxicity, and abundance in nature make it a promising semiconductor material for PV applications [2, 4-11]. It has been shown theoretically that β-$FeSi_2$ solar cells have the potential of obtaining energy conversion efficiencies of up to 23% [6, 12]. However, only a limited amount of experimental results on β-$FeSi_2$ solar cells exist to date [7-11, 13, 14]. Most of these are dealing with β-$FeSi_2$ thin-films grown on monocrystalline silicon (c-Si) wafers. The highest efficiency reported to date is only 3.7% for epitaxially grown β-$FeSi_2$/c-Si heterojunction solar cells prepared by phase target sputtering [8]. For cost reasons, it is desirable to deposit β-$FeSi_2$ films on inexpensive substrates. However, to our knowledge, there are no reports to date of β-$FeSi_2$ solar cells fabricated on glass or other low-cost foreign substrates, with the exception of the study by Momose *et al.*[10], where a β-$FeSi_2$ *p-n* homojunction was fabricated on a $MoSi_2$ coated glass substrate. Although the structure contained a *p-n* junction, the short-circuit current was found to be very small (order of nA). Unfortunately, other important solar cell parameters such as the open-circuit voltage, fill factor and efficiency were not reported. A possible reason for the low current is the low lateral conductance of the film and the absence of a high-quality crystalline

template for the β-$FeSi_2$ film. In the present work, given the lack of data on β-$FeSi_2$ solar cells on foreign substrates, we investigate the integration of β-$FeSi_2$ with poly-Si on glass for thin-film photovoltaic applications.

Solid phase crystallized (SPC) poly-Si on glass is a promising semi-conductor material for thin-film PV applications, as it has the potential for low fabrication costs due to reasons such as the use of relatively inexpensive large-area glass substrates, monolithic series interconnection of the solar cells to form PV modules, and the elimination of transparent conductive oxides (TCOs) from the manufacturing process due to the high lateral conductance of doped c-Si films. The highest efficiency achieved so far for a SPC poly-Si on glass thin-film PV module is 10.4% [15]. Poly-Si on glass is an interesting low-cost crystalline template for forming high-quality β-$FeSi_2$ films, given the fact that both are crystalline in nature and β-$FeSi_2$ is lattice-matched to silicon. A promising β-$FeSi_2$ based solar cell would be one with a thin poly-Si emitter layer and β-$FeSi_2$ as the absorber layer. The high optical absorption coefficient of β-$FeSi_2$ allows reducing the thickness of the photoactive layer without significantly reducing the cell's efficiency.

In this chapter, we report on the integration of β-$FeSi_2$ with SPC poly-Si on glass for thin-film solar cell applications. The interface quality between the poly-Si and the p-β-$FeSi_2$(Al) is studied using high-resolution transmission electron microscopy (HRTEM) and secondary ion mass spectroscopy (SIMS). The structural properties of the samples are investigated using X-ray diffraction

(XRD) and Raman analysis. Solar cell test structures of Al-doped β-$FeSi_2$ films with thicknesses of 49, 90 and 145 nm were fabricated on poly-Si/glass substrates and characterized using Suns-V_{oc} measurements.

7.2 Experimental Procedures

7.2.1 Sample preparation

To form the poly-Si film, an ~70 nm SiN_x:H/30 nm n^+ a-Si:H/2 µm n^- a-Si:H/100 nm SiO_x structure was deposited by plasma-enhanced chemical vapour deposition (PECVD, MV Systems, USA) onto a 400 mm × 300 mm Borofloat glass sheet with a thickness of 3.3 mm. The silicon nitride film acts both as an antireflection coating as well as a diffusion barrier for impurities from the glass sheet. The SiO_x layer acts as a barrier for impurities from the ambient during the SPC process and the subsequent rapid thermal anneal (RTA). After the deposition of the above structure in the PECVD reactor, the samples were annealed at 610 °C in a N_2 atmosphere (Nabertherm, N 120/65HAC furnace) for 12 hours to achieve SPC of the silicon film. The removal of crystallographic defects and dopant activation in the SPC polysilicon was achieved by annealing the poly-Si sample briefly for 1 min at 1000 °C using a rapid thermal anneal (RTA, CVD Equipment, USA) process. Subsequently, the samples were cleaned in a diluted (5%) HF solution to remove the capping SiO_x layer, rinsed in DI water, dried with a nitrogen gun and then immediately loaded into a magnetron sputtering chamber with a base pressure of ~10^{-7} Torr. Prior to the deposition of the $FeSi_2$ film, a thin (10 nm) Al film was sputter deposited onto the poly-Si layer to improve the interface quality [16].

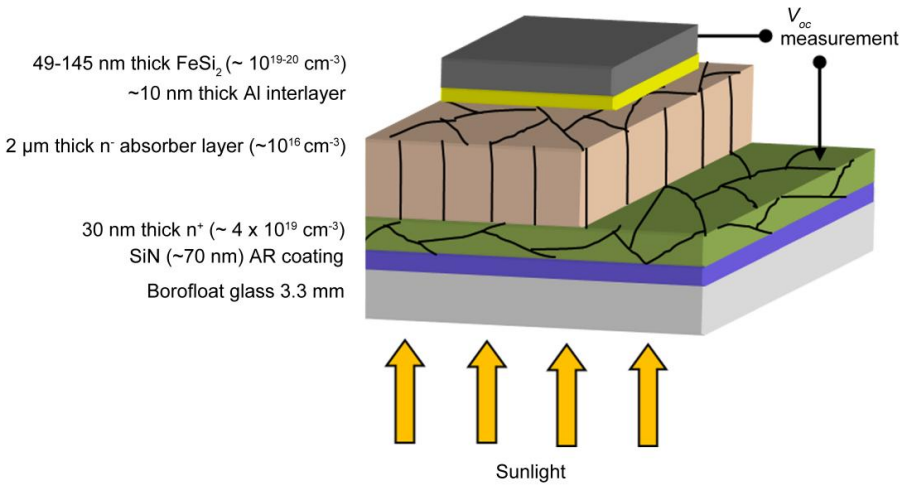

Figure 7.1: *Schematic of the thin-film solar cell test structure before annealing used in this study.*

Subsequently, an Al containing amorphous $FeSi_2$ film was deposited at room temperature by co-sputtering of stoichiometric $FeSi_2$ and Al in an Ar ambient at a working pressure of 3 mTorr. Samples with 49, 90 and 145 nm thick $FeSi_2$ films were prepared in this work. Figure 7.1 shows a cross-sectional schematic diagram of the $FeSi_2$/poly-Si heterostructure solar cell sample before annealing. After deposition of the Al-doped $FeSi_2$ films, the samples were subjected to a 60-s RTA process in N_2 ambient at temperatures of 600-700 °C. This annealing step is required for the formation of a crystalline interfacial layer between the Al-doped $FeSi_2$ film and the poly-Si thin film, as shown in Fig. 7.2.

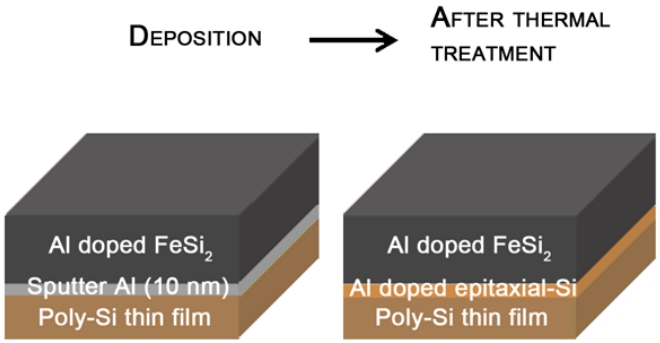

Figure 7.2: *Schematic diagram of crystalline interfacial layer formation between the Al-doped $FeSi_2$ film and the poly-Si thin film.*

One of the corners of each sample was then chemically etched using a $H_2O/HF/HNO_3$ solution to create a sloped profile and thereby exposing the buried n^+ poly-Si layer that needs to be contacted during the Suns-V_{oc} measurements. Subsequently, the samples were dipped in a 1% HF solution to remove the native oxide from the surface of the $FeSi_2$ film. The samples were then exposed to a H_2 plasma in a lab-type PECVD system (AK800, Roth & Rau, Germany) at a sample temperature of 450 °C. This hydrogenation process is required to passivate dangling bonds, point defects in poly-Si and iron vacancies in β-$FeSi_2$.

7.2.2 Characterisation of β-$FeSi_2$/poly-Si heterostructure

The crystal properties of the β-$FeSi_2$ films were studied using X-ray diffraction (XRD, D8, Bruker) in a general area detector diffraction system (GADDS) and Raman spectroscopy (Lab Ram HR system). Transmission electron microscopy (TEM, CM300, Philips) was used to examine the interface properties, thickness and microstructure of the poly-Si and β-$FeSi_2$ films. Time of flight (ToF) secondary ion mass spectroscopy (SIMS) was used to study the chemical composition and Al dopant profile in the β-$FeSi_2$ films. The doping concentration of the n^+/n^- poly-Si structure was determined by electrochemical capacitance voltage (ECV) profiling (Wafer profiler CVP 21, WEP), while the doping concentration and polarity of the β-$FeSi_2$ films were determined using Hall effect measurements.

The PV properties of the solar cell test structures were determined by Suns-V_{oc} measurements [17]. The Suns-V_{oc} technique does not require metallized

samples and thus can be used for process control by measuring the solar cell performance at various stages of the fabrication process [17-19]. The open-circuit voltage (V_{oc}) and pseudo fill factor (*pFF*) of the solar cell test structure were extracted from Suns-V_{oc} measurements. The *pFF* is a useful performance parameter as it represents the fill factor of the solar cell's current-voltage curve without the effect of series resistances.

7.3 Results and Discussion

7.3.1 Phase transformation study in $FeSi_2$ films by XRD

Figure 7.3 shows the XRD spectrum of as-deposited and RTA annealed samples. The XRD spectrum in Fig. 7.3(a) is composed of background signals of glass and a high intensity peak at 28.5° from Si (111) for all the samples. According to the XRD analysis, the as-deposited sample is amorphous in nature, however, samples annealed above 600 °C show the formation of beta-phase $FeSi_2$. For the annealed samples there is a broadening of the peak at 28.5° and appearance of other peaks due to the formation of β-$FeSi_2$. The peak intensity of β-$FeSi_2$ was overshadowed by the relatively high intensity signal from the poly-Si and the glass substrate. Further analysis of the XRD spectra [Fig. 7.3(b)] reveals three distinct peaks with a major peak indexed to (202)/(220) indicating the formation of the β-phase in $FeSi_2$. The other two peaks were attributed to a few possible (hkl) orientations, as indicated in the figure, confirming the formation of polycrystalline orthorhombic β-$FeSi_2$ [20] for the samples annealed at $\geq$ 600 °C. The samples were further analysed using Raman spectroscopy to understand and confirm the impact of the annealing temperature on the crystal quality of $FeSi_2$.

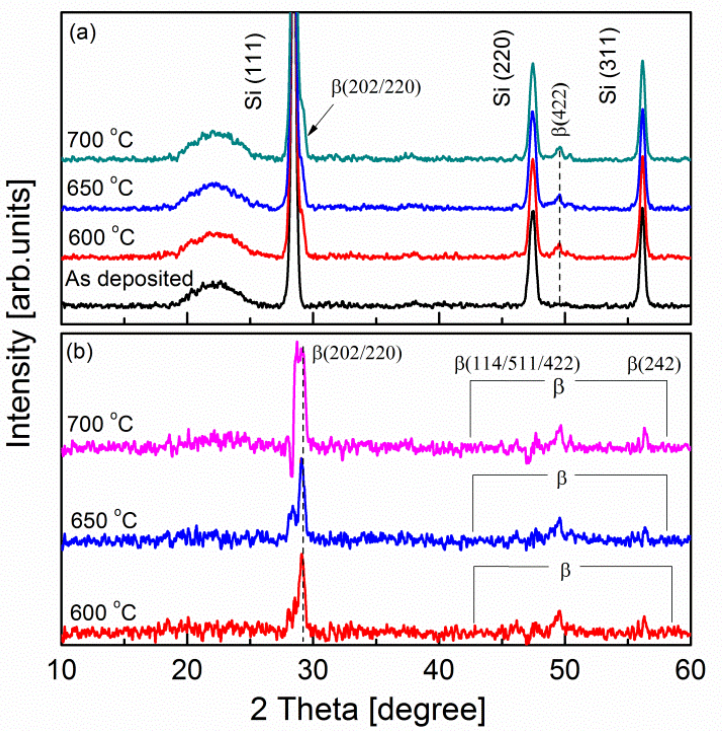

Figure 7.3: *(a) XRD spectra of as-deposited and annealed $FeSi_2$ (Al) films on poly-Si on glass under glancing angle incidence configuration (Ω = 2°). (b) XRD spectra of annealed $FeSi_2$(Al) on poly-Si on glass after noise reduction. The annealing temperature is indicated in the figure.*

7.3.2 Crystal quality characteristics study of *β*-$FeSi_2$ films by Raman

Figure 7.4 shows the Raman spectra for the as-deposited and RTA annealed samples. No clear Raman lines relating to the crystalline phase of Fe-Si can be seen for the as deposited samples, thus indicating the amorphous nature of $FeSi_2$. In contrast, two distinct peaks centred at ~192 and ~244 cm^{-1} appear for samples annealed at $\geq$ 600 °C, confirming the formation of the *β*-phase in $FeSi_2$ [20, 21]. The observation of the *β*-phase for the samples annealed at $\geq$ 600 °C is in good agreement with the results reported by other groups [16, 20, 21]. The samples annealed at 650 °C showed a slight shift towards lower wave number with respect to the samples annealed at 600 °C, indicating the improvement in the crystal quality of the *β*-$FeSi_2$ films [22].

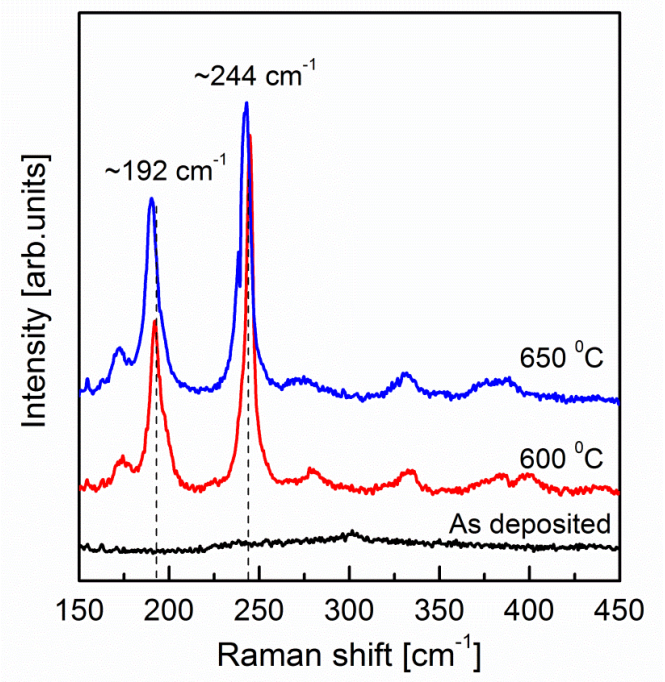

Figure 7.4: *Raman spectra of as-deposited (black) and annealed $FeSi_2$ (Al) (red, blue) films on poly-Si/SiN/glass.*

Furthermore, the crystal quality of β-$FeSi_2$ films deposited on poly-Si thin films was compared with that of β-$FeSi_2$ films deposited on single-crystalline FZ-grown silicon wafer (c-Si). Figure 7.5 shows the Raman spectra of β-$FeSi_2$/poly-Si and β-$FeSi_2$/c-Si samples annealed at 650 °C. It can be clearly seen from Figure 7.5 that the β-$FeSi_2$ film deposited on poly-Si/glass has the same crystal quality as the β-$FeSi_2$ film deposited on the c-Si wafer and annealed at 650 °C.

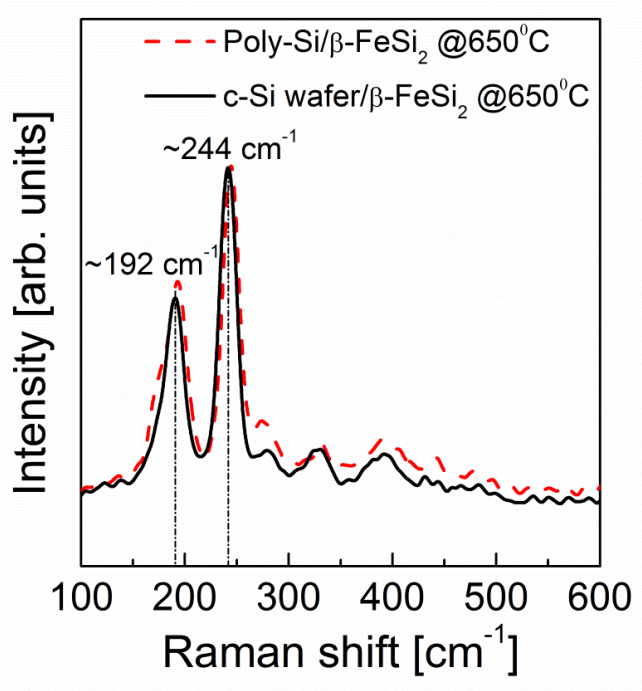

Figure 7.5: *Raman spectra of $FeSi_2$/poly-Si and $FeSi_2$/c-Si samples annealed at 650 °C.*

7.3.3 Interface study by HRTEM and SIMS

Figure 7.6(a) shows a cross-sectional TEM image of a 49 nm thick *β*-$FeSi_2$ film grown on *n*-type poly-Si/SiN/glass. The HRTEM image reveals that, as expected, there is a sharp interface formed between the SiN and the poly-Si. In addition, a high-quality crystalline interface can be detected between the *β*-$FeSi_2$ film and the *n*-type poly-Si film through the formation of a ~7 nm thick highly Al-doped epitaxial Si (p^+ Si) interfacial layer. This layer was most likely formed during the thermal treatment of the sample after the deposition of the $FeSi_2$ layer [16]. The formation of a highly Al-doped thin Si layer was also confirmed by SIMS analysis [Fig. 7.8(a)]. Further detailed analysis using HRTEM was performed on a *β*-$FeSi_2$/n-Si(100) structure to investigate and ascertain our interpretation about the nature of *β*-$FeSi_2$-Si interface. Figure 7.6(b) shows a

cross-sectional and HRTEM image of an ~50 nm thick β-$FeSi_2$ film grown on *n*-Si(100). The HRTEM image reveals a very clear lattice image and a sharp high-quality interface can be observed between β-$FeSi_2$ and the *n*-Si(100) through the formation of a p^+ Si layer, which further supports our interpretation for the interface quality of the β-$FeSi_2$ film grown on *n*-type poly-Si/SiN/glass samples.

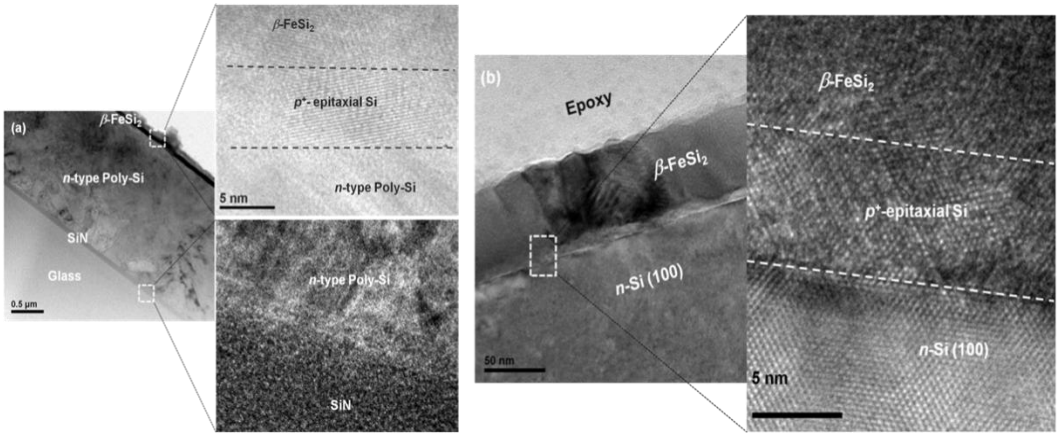

Figure 7.6: *(a) Cross-sectional TEM image of 49 nm thick β-$FeSi_2$ film grown on n-type poly-Si/SiN/glass and the HRTEM image of β-$FeSi_2$/poly-Si and poly-Si/glass interface after RTA at 600 °C.(b) Cross-sectional TEM image of ~50 nm thick β-$FeSi_2$ film grown on n-Si(100) and the HRTEM image of β-$FeSi_2$/n-Si(100) interface after RTA at 600 °C.*

Figure 7.7(a) shows a cross-sectional TEM image of a 90 nm thick β-$FeSi_2$ film grown on *n*-type poly-Si/SiN/glass and the HRTEM image of β-$FeSi_2$/poly-Si interface. It is observed that the interface is distorted and there is a reduction in the thickness of the epitaxial p^+ Si layer to ~5 nm. For the sample with the thickest β-$FeSi_2$ film of 145 nm, the interface quality is further degraded, as shown in Figure 7.7(b). A relatively thick amorphous layer is visible at the β-$FeSi_2$(Al)/p^+ epitaxial Si interface. This amorphous layer could be a complex oxide of $SiAl_xFe_yO_z$ [16].

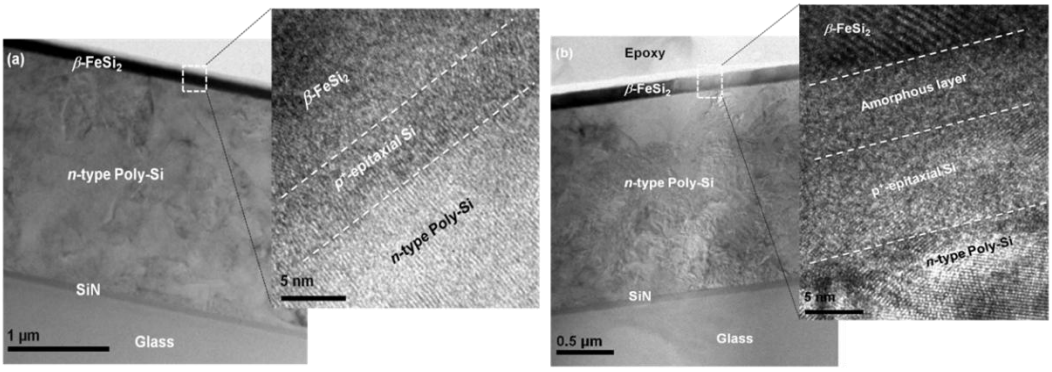

Figure 7.7: *(a) Cross-sectional TEM image of 90 nm thick β-$FeSi_2$ grown on n-type poly-Si/SiN/glass and the HRTEM image of β-$FeSi_2$/poly-Si interface after RTA at 600 °C. (b) Cross-sectional TEM image of 145 nm thick β-$FeSi_2$ grown on n-type poly-Si/SiN/glass and the HRTEM image of β-$FeSi_2$/poly-Si interface after RTA at 600 °C.*

To investigate the interface quality in more detail, we performed SIMS measurements on selected samples. Figure 7.8(a) shows the SIMS depth profile of Al, Fe, Si for the annealed sample with a 90 nm thick β-$FeSi_2$(Al) film. From these results it is clear that, as expected, the Fe and Si were distributed uniformly in the $FeSi_2$ layer and there was a highly Al doped Si interlayer between the poly-silicon and the $FeSi_2$ film. This is in agreement with the results published by Dalapati *et al*. [16], where β-$FeSi_2$ was formed on crystalline Si wafers. In Figure 7.8(b), it can be seen that the relative concentration of Al in β-$FeSi_2$ decreases with increasing $FeSi_2$ film thickness, even though the Al sputtering conditions were identical for all the cases. A possible explanation for this observation is an increasing out-diffusion of Al from the interface into the β-$FeSi_2$ layer when the $FeSi_2$ becomes thicker. This is consistent with the observation in Figure 7.7 that the interface quality degrades with increasing β-$FeSi_2$ thickness. This suggests that both the β-$FeSi_2$ and Al thickness should be considered in order to achieve a high-quality interface between the poly-Si film and the β-$FeSi_2$ film.

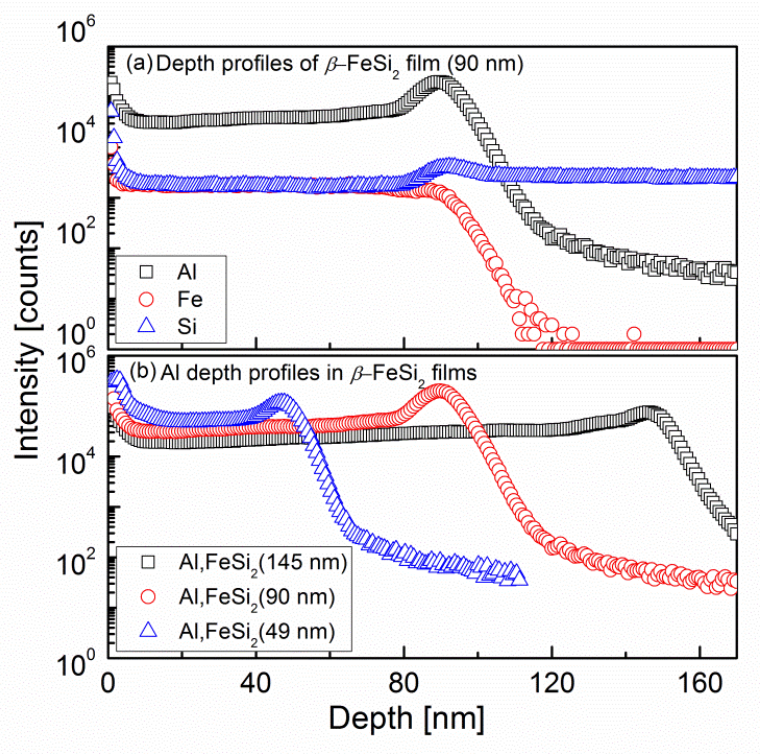

Figure 7.8: *(a) SIMS depth profile for Al, Fe, and Si measured on a sample with an 84 nm β-$FeSi_2$ (Al) film. (b) SIMS depth profile for Al for samples with a β-$FeSi_2$ (Al) film thickness of 49 nm, 90 nm, and 145 nm.*

7.3.4 Performance of β-$FeSi_2$/poly-Si heterostructure diodes

Figure 7.9 shows the V_{oc} and *pFF* of the solar cell test structure as a function of the β-$FeSi_2$ film thickness. From Fig. 7.9(a) it can be seen that a V_{oc} of 217 mV was obtained for the test structure with a 49 nm β-$FeSi_2$ film after annealing at 650 °C, which is significantly higher than previously reported results on an *n*-type β-$FeSi_2$/*p*-type c-Si heterostructure fabricated by Shaban *et al.*,[9]. The V_{oc} further increased to 320 mV due to hydrogenation. A similar trend can be observed for the *pFF* which had an initial value of 52% and increased to 67% for the test structure with a 49 nm β-$FeSi_2$ film after annealing at 650 °C. The V_{oc} and *pFF* values decreased with increasing β-$FeSi_2$ film thickness, for all investigated annealing temperatures.

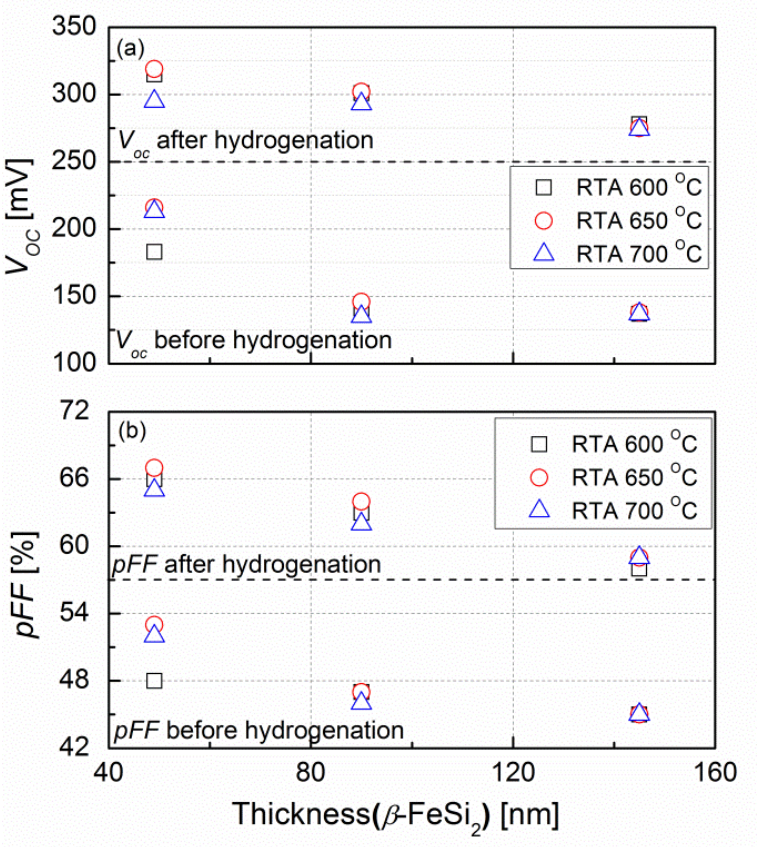

Figure 7.9: *(a) Measured Voc of the solar cell test structure as a function of β-$FeSi_2$ film thickness. (b) Measured pFF as a function of β-$FeSi_2$ film thickness.*

The best-performing test structures were annealed at 650 °C, which is again in good agreement with the results reported by Dalapati *et al.*, [16]. The performance of the test structures deteriorated for annealing temperatures of above 650 °C. The increase of V_{oc} and *pFF* due to hydrogenation for all investigated samples can most likely be explained by an improvement in the material quality of the test structure due to passivation of defects in the bulk of the poly-Si film and compensation of Fe vacancies in the β-$FeSi_2$ film. The decrease in the V_{oc} with increasing β-$FeSi_2$ film thickness can most likely be related to the interface quality between the poly-Si and the β-$FeSi_2$(Al), as observed from TEM and SIMS analysis. From the XRD and Raman analysis it was confirmed that an

annealing temperature of 600 °C is sufficient to transform amorphous $FeSi_2$ into polycrystalline β-phase material. However, the quality of the β-$FeSi_2$ film can be improved with a slight increase in annealing temperature [9]. This is consistent with Raman analysis and the slightly higher V_{oc} for the samples annealed at 650 °C instead of 600 °C. However an annealing temperature of 700 °C reduces both V_{oc} and *pFF*, especially for thinner $FeSi_2$ films, possibly due to the formation of pinholes in the β-$FeSi_2$ film [23]. The V_{oc} value of 320 mV reported here is, to our knowledge, the best value to date for a poly-Si/$FeSi_2$ thin-film structure.

From all the results presented in this chapter, it is clear that the re-grown epi-Si layer plays a key role for integrating the β-phase $FeSi_2$ with Si. The re-grown epitaxial p^+ Si layer improves the interface quality between the poly-Si and β-$FeSi_2$ films, resulting in higher V_{oc} values of the test structure through the formation of a p^+ Si/n^- Si homojunction [16]. However, it should be noted that after selective removal of the $FeSi_2$ film from the solar cell test structure, Suns-V_{oc} curves could no longer be measured on our samples, indicating the importance of the $FeSi_2$ film. The PV performance of the test structure can be improved further by optimization of the process parameters [9], such as the thickness of the poly-Si and/or $FeSi_2$ films and the annealing temperature. Further improvement can possibly be obtained by incorporation of an electron blocking layer between the metal contact and the *p*-type β-$FeSi_2$ (Al) [16].

7.3.5 Optical characteristics of β-$FeSi_2$/poly-Si thin-film heterostructure using UV-Vis-NIR spectrophotometer

Figure 7.10 shows the reflectance scan of a 60 nm thick β-$FeSi_2$ film deposited on a c-Si wafer (1 mm) and poly-Si (~2 µm)/Si/glass structure, respectively. The reflectance measurement for the β-$FeSi_2$/c-Si structure was performed in the substrate configuration, while the superstrate configuration was used for the β-$FeSi_2$/poly-Si/SiN/glass structure. It can be clearly observed that there is a reduction in reflectance by ~25% within the wavelength range of 300 nm to 800 nm for β-$FeSi_2$/poly-Si/SiN/glass structure as compared to the β-$FeSi_2$/c-Si structure. Reduction in reflectance means more light will enter the semiconductor and thus might end up producing more current, resulting in significantly higher efficiencies. The highest reported energy conversation efficiency for β-$FeSi_2$ based thin-film solar cells is 3.7% for 16-mm^2 n-type β-$FeSi_2$/*p*-type c-Si heterojunction diodes [8]. The *n*-type β-$FeSi_2$/*p*-type c-Si heterostructure was used in the substrate configuration and yielded a short-circuit current (J_{sc}) of 14.8 mA/cm^2. Thus, Figure 7.10 suggests that the proposed β-$FeSi_2$/poly-Si/SiN/glass structure for PV applications might yield significantly higher current. However, reflectance is not the true indicator for the amount of light entering the semiconductor. It just indicates that if the reflectance is lower, the chances of absorption in the semiconductor are higher. To further validate this assumption, the absorption (A) spectrum for the β-$FeSi_2$/poly-Si/SiN/glass structure was calculated using the following equation:

$$A = 100\% - R - T \tag{7.1}$$

R is the measured reflectance and T is the measured transmittance.

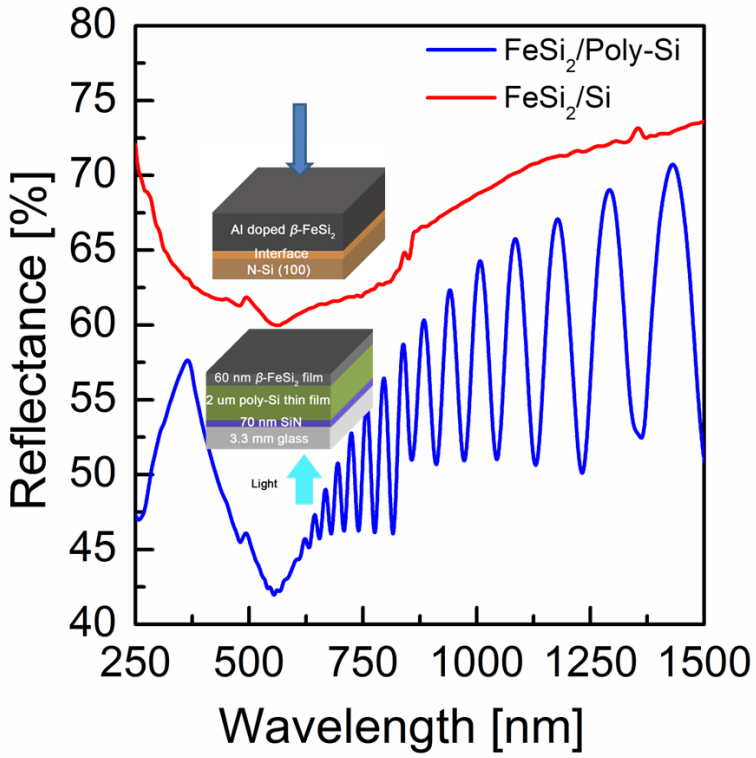

Figure 7.10: *Reflectance spectra of β-FeSi2/c-Si and β-FeSi2/Poly-Si heterostructure.*

Figure 7.11 shows the absorption spectra for the poly-Si/SiN/glass and β-$FeSi_2$/poly-Si/SiN/glass structures. It can be clearly seen from Fig. 7.11 that the absorption in the poly-Si/SiN/glass structure can be increased drastically through the addition of a thin (60 nm) β-$FeSi_2$ layer. This is a strong indication that the proposed β-$FeSi_2$/poly-Si/SiN/glass structure might lead to higher current and thus higher PV efficiencies.

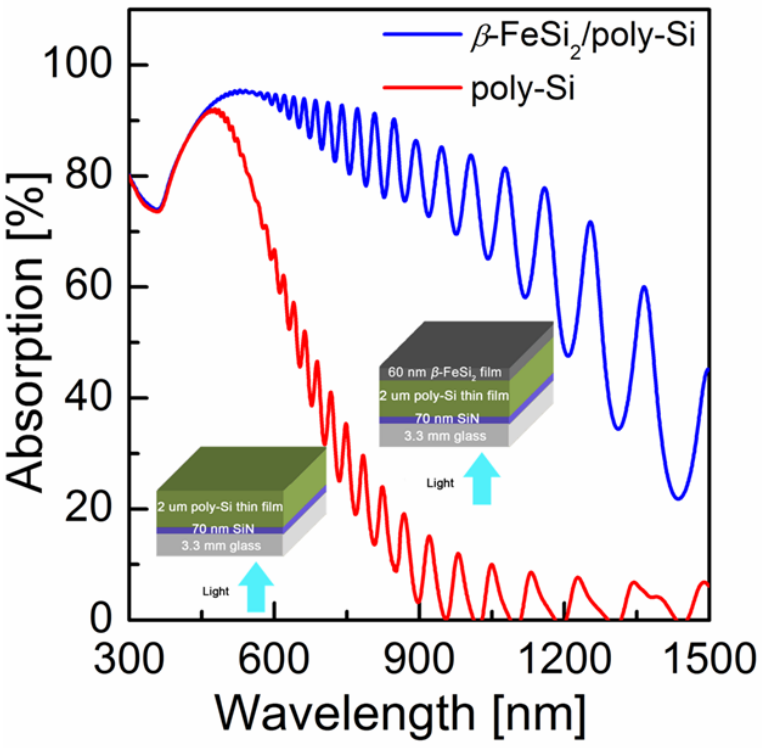

Figure 7.11: *Absorption spectra of poly-Si/SiN/glass and β-FeSi2/poly-Si/SiN/glass heterostructure.*

7.4 Conclusion

In conclusion, *p*-*β*-FeSi$_2$(Al) was successfully integrated with *n*-type poly-Si on glass and its material and photovoltaic properties were studied. The formed Al-doped p^+ Si layer was shown to play a key role for the quality of the interface between the *β*-FeSi$_2$ film and the poly-Si film. A high-quality interface between *β*-FeSi$_2$(Al)/n-poly-Si was observed through the formation of a thin epitaxial p^+ Si layer on poly-Si during thermal treatment of the FeSi$_2$ layer. The interface quality was found to degrade for thicker *β*-FeSi$_2$ films. *p*-type *β*-FeSi$_2$/ p^+ Si/n^- Si/n^+ Si/SiN/glass heterostructure thin-film solar cell test structures showed promising photovoltaic characteristics with V_{oc} and *pFF* values of 320 mV and 67%, respectively.

References of Chapter 7

[1] D. Leong, M. Harry, K. Reeson, and K. Homewood, "A silicon/iron-disilicide light-emitting diode operating at a wavelength of 1.5 μm," *Nature*, vol. 387, pp. 686-688, 1997.

[2] K. Yamaguchi and K. Mizushima, "Luminescent $FeSi_2$ crystal structures induced by heteroepitaxial stress on Si (111)," *Physical Review Letters*, vol. 86, p. 6006, 2001.

[3] H. Fujimoto, K. Ogawa, K. Takarabe, H. Udono, H. Sugiyama, J. Azuma, *et al.*, "Photoemission study on the valence band of a β-$FeSi_2$ thin film using synchrotron radiation," *Dalton Transactions*, vol. 40, pp. 6023-6027, 2011.

[4] K. Noda, Y. Terai, S. Hashimoto, K. Yoneda, and Y. Fujiwara, "Modifications of direct transition energies in β-$FeSi_2$ epitaxial films grown by molecular beam epitaxy," *Applied Physics Letters*, vol. 94, p. 241907, 2009.

[5] J. Y. He, X. Wang, X. L. Wu, and P. K. Chu, "Anisotropic etching of microscale β-$FeSi_2$ particles: Formation, mechanism, and quantum confinement of β-$FeSi_2$ nanowhiskers," *RSC Advances*, vol. 2, pp. 3254-3256, 2012.

[6] Y. Makita, T. Ootsuka, Y. Fukuzawa, N. Otogawa, H. Abe, Z. Liu, *et al.*, "β-$FeSi_2$ as a Kankyo (environmentally friendly) semiconductor for solar cells in the space application," *in Proc. SPIE 6197, Photonics for Solar Energy Systems*, 2006, p. 61970.

[7] T. Suemasu, K. Takakura, C. Li, Y. Ozawa, Y. Kumagai, and F. Hasegawa, "Epitaxial growth of semiconducting β-$FeSi_2$ and its application to light-emitting diodes," *Thin Solid Films*, vol. 461, pp. 209-218, 2004.

[8] Z. Liu, S. Wang, N. Otogawa, Y. Suzuki, M. Osamura, Y. Fukuzawa, *et al.*, "A thin-film solar cell of high-quality β-$FeSi_2$/Si heterojunction prepared by sputtering," *Solar Energy Materials and Solar Cells*, vol. 90, pp. 276-282, 2006.

[9] M. Shaban, K. Nakashima, W. Yokoyama, and T. Yoshitake, "Photovoltaic Properties of *n*-type β-$FeSi_2$/*p*-type Si Heterojunctions," *Japanese Journal of Applied Physics*, vol. 46, p. L667, 2007.

[10] N. Momose, J. Shirai, H. Tahara, Y. Todoroki, T. Hara, and Y. Hashimoto, "Toward the β-$FeSi_2$ p-n homo-junction structure," *Thin Solid Films*, vol. 515, pp. 8210-8215, 2007.

[11] Z. Liu, M. Watanabe, and M. Hanabusa, "Electrical and photovoltaic properties of iron-silicide/silicon heterostructures formed by pulsed laser deposition," *Thin Solid Films,* vol. 381, pp. 262-266, 2001.

[12] M. Libezny, J. Poortmans, T. Vermeulen, P. H. Amesz, K. Herz, M. Povalla, *et al.*, *β*-FeSi$_2$/Heterojunction properties and their depedence on the *β*-FeSi$_2$ preparation method, in *Proc. 13th European Photovoltaic Solar Energy Conference and Exhibition*, 1995, pp. 1326-9.

[13] J. Xu, R. Yao, and R. Liao, "Improved photovoltaic properties of a-Si/*β*-FeSi$_2$/c-Si double heterojunction by Al-doping," *Physica B: Condensed Matter,* vol. 407, pp. 756-758, 2012.

[14] J. Xu, R. Yao, and K. Geng, "Photovoltaic characteristics of a-Si/*β*-FeSi$_2$/c-Si double heterojunction fabricated by magnetron sputtering," *Journal of Vacuum Science & Technology A,* vol. 29, p. 051202, 2011.

[15] M. J. Keevers, T. L. Young, U. Schubert, and M. A. Green, "10% efficient CSG minimodules," in *Proceedings of the 22nd European Photovoltaic Solar Energy Conference, Milan, Italy, September 2007*, pp. 1783–1790.

[16] G. K. Dalapati, S. L. Liew, A. S. W. Wong, Y. Chai, S. Y. Chiam, and D. Z. Chi, "Photovoltaic characteristics of p-*β*-FeSi$_2$(Al)/n-Si(100) heterojunction solar cells and the effects of interfacial engineering," *Applied Physics Letters,* vol. 98, p. 013507, 2011.

[17] R. Sinton and A. Cuevas, "A quasi-steady-state open-circuit voltage method for solar cell characterization," in *16th European Photovoltaic Solar Energy Conference*, Glasgow, UK, 2000, pp. 1152-1155.

[18] J. Wong, J. L. Huang, O. Kunz, Z. Ouyang, S. He, P. I. Widenborg, *et al.*, "Anomalous temperature dependence of diode saturation currents in polycrystalline silicon thin-film solar cells on glass," *Journal of Applied Physics,* vol. 105, p.103705, 2009.

[19] Z. Ouyang, O. Kunz, A. B. Sproul, and S. Varlamov, "Influence of the absorber doping for p-type polycrystalline silicon thin-film solar cells on glass prepared by electron beam evaporation and solid-phase crystallization," *Journal of Applied Physics*, vol. 109, pp. 054510-7, 2011.

[20] S. L. Liew, Y. Chai, H. R. Tan, H. K. Hui, A. S. W. Wong, G. K. Dalapati, *et al.*, "Improvement in Photovoltaic Performance of Thin Film *β*-FeSi$_2$/Si Heterojunction Solar Cells with Al Interlayer," *Journal of The Electro-chemical Society,* vol. 159, pp. H52-H56, 2011.

[21] A. S. W. Wong, G. W. Ho, S. L. Liew, K. C. Chua, and D. Z. Chi, "Probing the growth of *β*-FeSi$_2$ nanoparticles for photovoltaic applications: a combined imaging and spectroscopy study using transmission electron

microscopy," *Progress in Photovoltaics: Research and Applications*, vol. 19, pp. 464-472, 2011.

[22] Y. Maeda, K. Umezawa, Y. Hayashi, and K. Miyake, "Raman spectroscopic study of ion-beam synthesized polycrystalline β-$FeSi_2$ on Si(100)," *Thin Solid Films,* vol. 381, pp. 219-224, 2001.

[23] R. Kuroda, Z. Liu, Y. Fukuzawa, Y. Suzuki, M. Osamura, S. Wang, *et al.*, "Formation of thin β-$FeSi_2$ template layer for the epitaxial growth of thick film on Si (111) substrate," *Thin Solid Films,* vol. 461, pp. 34-39, 2004.

Chapter 8

Chapter 8- Conclusion

8.1. Summary

8.2. Original contributions

8.3. Future work

8.1 Summary

This thesis investigates the properties of poly-Si films prepared by solid phase crystallisation (SPC) of PECVD a-Si:H films. In particular, the thesis focuses on the material quality of SPC poly-Si thin films, which acts as a bottleneck to achieve higher solar cell efficiency. It also explores the relatively low deposition rate of standard PECVD (around 30 nm/min), which significantly adds to the cost of SPC poly-Si thin-film solar cells. These are two major factors that prevent the commercialization of this PV technology. A detailed experimental investigation was carried out to study the impact of the material quality on the performance of poly-Si thin-film solar cells. Furthermore, the thesis explores the compatibility of a highly photosensitive material - β-$FeSi_2$ - with SPC poly-Si thin-films, leading to the realisation of the first such solar cells.

In this work, large-grained (> 10 μm) n^+ SPC poly-Si thin films with high Hall mobility of about 71 cm^2/Vs were successfully fabricated. The experimental results showed that the doping concentration and the grain size of the SPC poly-Si films increased with increasing PH_3(2% in H_2)/SiH_4 gas flow ratio, whereas the crystal quality of the material deteriorated. It was shown that the stress in the large-grained poly-Si thin films was the main reason for the deterioration of the material quality. The stress in the large-grained (> 20 μm) poly-Si films was found to be in excess of 1000 MPa, which leads to defects (for example dislocations) in the films. Advanced characterization techniques such as Raman, EBSD, TEM and HAADF-STEM were applied in this work to establish a

relationship between the stress and dislocations in poly-Si thin films. With respect to device applications, it was desirable to control the stress and defects in large-grained poly-Si thin films and strike the right balance between the grain size and the material quality.

N-type SPC polycrystalline silicon thin films with large grains and high crystal quality were successfully fabricated on planar glass by controlling the stress and intra-grain misorientation in the films. The stress was successfully engineered to values below 130 MPa through the control of the a-Si:H deposition temperature and the PH_3(2% in H_2)/SiH_4 gas flow ratio. The best poly-Si crystal quality was obtained for a-Si:H films deposited at 410 °C, using a low PH_3(2% in H_2)/SiH_4 gas flow ratio of 0.02. This SPC poly-Si film was found to have the least tensile stress (128 MPa) and a low intra-grain misorientation of ~1°. Furthermore, the impact of the n^+ emitter doping concentration on the structural and electrical properties of poly-Si thin-film solar cells was studied in detail. A relative improvement in the efficiency by 46 % for *p*-type poly-Si thin-film solar cells was demonstrated through the improvement of the material quality of the n^+ emitter layer.

Furthermore, a significant effort was made in this work to increase the deposition rate of PECVD a-Si:H films without impacting the material quality of the resulting SPC poly-Si films. A high deposition rate of 146 nm/min was achieved through the control of the SiH_4 gas flow and the RF power density. A highly conformal deposition of a-Si:H over the large glass sheet area of 1200 cm^2

using high-rate PECVD was achieved. A relationship between the SiH_4 gas flow and the RF power density was established. A linear increase in the deposition rate up to 146 nm/min was achieved by keeping the ratio of SiH_4 gas flow to RF power density constant at about 2.4 sccm/mWcm^{-2}. This ratio was also found to affect the thickness uniformity of a-Si:H films and the material quality of the resulting SPC poly-Si films. A very high SPC poly-Si crystal quality with a thickness non-uniformity of less than ± 6% over 30×40 cm^2 was obtained. A further increase in the deposition rate to about 250 nm/min seems possible through the control of the SiH_4 gas flow and the RF power density, while maintaining a good thickness uniformity and a high crystal quality.

Finally, the thesis explored poly-Si thin films as a crystalline template for p-type β-$FeSi_2$, which is an earth abundant semiconductor material. *p*-β-$FeSi_2$(Al) was successfully integrated with *n*-type poly-Si on glass and its material and photovoltaic properties were studied. The formed Al-doped p^+ Si layer was shown to play a key role for the quality of the interface between the β-$FeSi_2$ film and the poly-Si film. A high-quality interface between β-$FeSi_2$(Al)/n-poly-Si was observed through the formation of a thin epitaxial p^+ Si layer on poly-Si during thermal treatment of the $FeSi_2$ layer. The interface quality was found to be the key challenging factor towards the integration and was found to degrade for thicker β-$FeSi_2$ films. A promising open-circuit voltage (V_{oc}) of 320 mV with pseudo fill factor (*pFF*) of 67 % was obtained for the *p*-type β-$FeSi_2$/p^+ Si/n^- Si/n^+ Si/SiN/ glass thin-film solar cell test structure, with a scope of further improvement by interfacial engineering and thickness optimization.

8.2 Original contributions

The major original contributions of this thesis are:

- Commissioning of a PECVD cluster tool and establishing a stable baseline process for the fabrication of poly-Si thin-film solar cells. The PECVD cluster tool was the backbone of this research and the baseline diodes were building blocks for the research of other members in the Poly-Si thin-film solar cell group.
- Fabrication of very-large-grained (> 30 μm) poly-Si thin films and characterization of their structural and electrical properties.
- Establishment of advanced characterisation tools such as EBSD and Raman to map large-grained poly-Si thin films and identify the source of stress in the films.
- Demonstration of improvement in the material quality of the poly-Si thin films through the control of stress in the films.
- Impact of the n^+ emitter layer on the performance of the *p*-type poly-Si thin-film solar cell was established. It was demonstrated that an optimization of the electrical and structural properties of the n^+ emitter layer leads to a significant improvement in the performance of the poly-Si thin-film solar cell.
- Development of a recipe to achieve high deposition rates in the PECVD system. A relationship between the SiH_4 gas flow and the RF power density was established. A linear increase in the deposition rate up to 146

nm/min was achieved by keeping the SiH_4 gas flow to RF power density ratio constant at about 2.4 sccm/mWcm^{-2}. a-Si:H films deposited at a rate of 146 nm/min were found to be highly conformal (non- uniformity < 6%) over a large area glass sheet of 1200 cm^2.

- SPC poly-Si thin-film material formed from high rate deposited a-Si:H films was demonstrated to be of higher quality than that obtained from low rate deposited a-Si:H films.
- For the first time, SPC poly-Si thin films were successfully integrated with the earth abundant semiconductor material β-$FeSi_2$. A solar cell test structure using *p*-type β-$FeSi_2$ and *n*-type poly-Si thin films was fabricated. The solar cell test structures showed promising photovoltaic characteristics with V_{oc} and *pFF* values of 320 mV and 67%, respectively.

8.3 Future work

This thesis has successfully demonstrated that the material quality of *n*-type SPC poly-Si thin films does not depend on the grain size but on the grain shape. In addition, for a typical poly-Si thin-film solar cell consisting of three individual layers (n^+ emitter, p^- absorber, p^+ BSF, it was shown that an improvement in the material quality of just the n^+ emitter layer significantly improves the performance of the poly-Si thin-film solar cells. However, it is not known yet how each individual layer affects the overall material quality and the performance of the poly-Si thin-film solar cells. Thus, further work is required based on the knowledge of the present work, to further advance this PV technology. Several topics are suggested that deserve further investigations.

8.3.1 Impact of absorber and BSF layers on the performance of SPC poly-Si thin-film solar cells

In this work, it was shown that the variation in phosphorus concentration in a-Si:H films impacts the material quality of the resulting n^+ poly-Si thin films. Furthermore, the electrical and material quality of the n^+ emitter layer was found to significantly impact the performance of the *p*-type poly-Si thin-film solar cells. However, the impact of boron doping in the a-Si:H films on the grain size and material quality of the *p*-type SPC poly-Si thin films is not yet known. Therefore, it will be rewarding to investigate the effect of the boron doping concentration on the material quality of the *p*-type poly-Si thin films, followed by a systematic study to understand the impact of the absorber and BSF layers on the performance

of poly-Si thin-film solar cells. A detailed study on the effects of boron doping on the electrical and structural (grain size, shape and orientation, stress) properties of *p*-type SPC poly-Si thin films is required to understand and improve the overall material quality of the SPC poly-Si thin-film solar cells.

8.3.2 Poly-Si thin film solar cells using high-rate PECVD a-Si:H films

A highly conformal deposition of a-Si:H films over a comparatively large glass sheet area of 1200 cm^2 was achieved using high-rate PECVD. Specifically, a deposition rate of 146 nm/min was achieved. A significant further enhancement of the a-Si:H deposition rate is achievable by further optimization of the PECVD/VHF-PECVD process parameters, such as RF power, process pressure, gas flow and RF frequency. A very high deposition rate of up to 500 nm/min seems feasible. In addition, in this work the material quality of a separately deposited SPC poly-Si thin absorber layer using high-rate PECVD was evaluated. It is highly advisable to fabricate SPC poly-Si thin-film solar cells using the high-rate PECVD a-Si:H films and test their PV performance.

8.3.3 Transfer of the experiments to textured glass sheets

Most of the optical characterization techniques cannot be used on textured substrates. In addition, variations in the textured surfaces affect the measurement data, which can have significant influence on the interpretation of the result. Thus, to obtain the consistency in measurements and data, most experiments of this thesis were performed on planar glass. However, SPC poly-Si thin-film solar cells require an efficient light trapping scheme to significantly improve the J_{sc}. One

way to achieve this is to deposit the solar cells onto textured glass sheets. Therefore, it is highly recommended to transfer the experiments performed in this work to textured glass sheets (for example AIT glass).

8.3.4 Metallization of β-$FeSi_2$/poly-Si thin-film solar cells

In this work, the highly absorbing earth abundant semiconductor β-$FeSi_2$ was integrated with SPC poly-Si thin films, giving p-type β-$FeSi_2$/p^+ Si/n^- poly-Si/n^+ poly-Si thin-film solar cell test structures with promising photovoltaic properties. It is highly recommended to metalize the solar cell test structure and characterize the cell using EQE and I-V testing. The EQE study of these cells will help to understand the losses in the structure and the contribution from the β-$FeSi_2$ film. Further optimization of the thickness of the poly-Si thin films is required to improve the PV performance of the test structure.

List of Publications Resulting from this Thesis

- Journal Publications
- Conference Publications

Journal papers

[1] **A. Kumar**, P.I. Widenborg, G.K. Dalapati, C. Ke, G.S. Subramanium, A.G. Aberle, Controlling stress in large-grained solid phase crystallized *n*-type poly-Si thin films to improve crystal quality (status: major revision at Journal of Crystal Growth & Design).

[2] **A. Kumar**, F. Law, G.K. Dalapati, G.S. Subramanium, P.I. Widenborg, H.R. Tan, A.G. Aberle, Synthesis and Characterization of Large-Grain Solid-Phase Crystallized Polycrystalline Silicon Thin Films, *J. Vac. Sci. Technol*. A **32**, 061509 (2014).

[3] **A. Kumar**, H. Hidayat, C. Ke, S. Chakraborty, G.K. Dalapati, P.I. Widenborg, C.C. Tan, S. Dolmanan, A.G. Aberle, Impact of the n^+ emitter layer on the structural and electrical properties of p-type polycrystalline silicon thin-film solar cells, *Journal of Applied Physics* 114 (2013) 134505.

[4] **A. Kumar**, G.K. Dalapati, H. Hidayat, F. Law, H.R. Tan, P.I. Widenborg, B. Hoex, C.C. Tan, D.Z. Chi, A.G. Aberle, Integration of β-$FeSi_2$ with poly-Si on glass for thin-film photovoltaic applications, *RSC Advances* 3 (2013) 7733-7738.

[5] G.K. Dalapati, **A. Kumar**, C.C. Tan, S.L. Liew, P. Sonar, H.L. Seng, H.K. Hui, S. Tripathy, D. Chi, Impact of Al passivation and Co sputter on the structural property of β-$FeSi_2$ for Al-doped β-$FeSi_2$/*n*-Si(100) based solar cells application, *ACS Applied Materials & Interfaces* 5 (2013) 5455-5460.

[6] H. Hidayat, **A. Kumar**, F. Law, C. Ke, P.I. Widenborg, A.G. Aberle, Impact of rapid thermal annealing temperature on non-metallised polycrystalline silicon thin-film diodes on glass, *Thin Solid Films* 534 (2013) 629-635.

[7] S. Virasawmy, N. Palina, P.I. Widenborg, **A. Kumar**, G.K. Dalapati, H.R. Tan, A.A.O. Tay, B. Hoex, Direct laser doping of poly-silicon thin films via

laser chemical processing, *IEEE Journal of Photovoltaics* 3 (2013) 1259-1264.

[8] F. Law, H. Hidayat, **A. Kumar**, P. Widenborg, J. Luther, B. Hoex, On the transient amorphous silicon structures during solid phase crystallization, *Journal of Non-Crystalline Solids* 363 (2013) 172-177.

[9] H. Hidayat, P.I. Widenborg, **A. Kumar**, F. Law, A.G. Aberle, Static large-area hydrogenation of polycrystalline silicon thin-film solar cells on glass using a linear microwave plasma source, *IEEE Journal of Photovoltaics* 2 (2012) 580-585.

[10] H. Hidayat, **A. Kumar**, Y. Huang, F. Law, K. Cangming, P.I. Widenborg, A.G. Aberle, Doping concentration measurements on highly doped polycrystalline silicon thin films on glass for photovoltaic applications (2013, manuscript under major revision at *IEEE Journal of Photovoltaics*).

[11] C. Ke, S. Chakraborty, **A. Kumar**, P.I. Widenborg, A.G. Aberle, I.M. Peters, Investigation of interdigitated metallization patterns for polycrystalline silicon thin-film solar cells on glass (2014, manuscript under review at *IEEE Journal of Photovoltaics*).

Conference papers

[1] **A. Kumar**, P.I. Widenborg, G.K. Dalapati, G.S. Subramanian, A.G. Aberle, Impact of deposition parameters on the material quality of SPC poly-Si thin films using high-rate PECVD of a-Si:H, submitted to *Photovoltaic Technical Conference - Thin Film & Advanced Silicon Solutions -2014*, Aix-en-Provence, France (accepted).

[2] **A. Kumar**, P.I. Widenborg, F. law, H. Hidayat, G.K. Dalapati, A.G. Aberle, Study of large-grained *n*-type polycrystalline silicon thin films made by the

solid phase crystallization method, *Proc. 39th IEEE Photovoltaic Specialists Conference*, Tampa, Florida, 2013, pp. 0586-0588.

[3] H. Hidayat, **A. Kumar**, F. Law, P.I. Widenborg, A.G. Aberle, Electro-chemical capacitance voltage measurements as a novel doping profiling method for polycrystalline silicon thin-film solar cells on glass, *Proc. 27th European Photovoltaic Solar Energy Conference*, Frankfurt, Germany, 2012, pp. 2434-2437.

[4] **A. Kumar**, H. Hidayat, F. Law, P.I. Widenborg, A.G. Aberle, Impact of n^+ emitter layer on the performance of poly-Si thin-film solar cells, *Technical Digest of the 22nd International Photovoltaic Science and Engineering Conference (PVSEC-22)*, Hangzhou, China, Nov 2012.

[5] **A. Kumar**, P.I. Widenborg, H. Hidayat, Q. Zixuan, A.G. Aberle, Impact of rapid thermal annealing and hydrogenation on the doping concentration and carrier mobility in solid phase crystallized poly-Si thin films, *MRS Online Proceedings Library*, 1321 (2011).

Appendices

- Table summarizing the number of samples used in chapter 3
- Table summarizing the number of samples used in chapter 4
- Table summarizing the number of samples used in chapter 6

Table: *List and name of samples used in the study of growth and Characterization of large grained n^+ poly-Si thin films (chapter 3)*

Sample no	*SiH_4 flow (sccm)*	*PH_3 flow (sccm)*	*Temperature (°C)*	*Power ($mWcm^2$)*	*Pressure (Pa)*
SPC 13_1	40	1	410	34	106
SPC 13_2	40	2.5	410	34	106
SPC 13_3	40	5	410	34	106
SPC 13_4	40	7.5	410	34	106
SPC 13_5	40	10	410	34	106
SPC 13_6	40	14	410	34	106
SPC 13_7	40	18	410	34	106

Table: *List and name of samples used in study of the improved material quality of n^+ poly-Si thin Film through stress engineering (chapter 4)*

Sample no	*SiH_4 flow (sccm)*	*PH_3 flow (sccm)*	*Temperature (°C)*	*Power (mW/cm^2)*	*Pressure (Pa)*
SPC 13_8	10	1	380	8	106
SPC 13_9	10	2.5	380	8	106
SPC 13_10	10	0.2	380	8	106
SPC 13_11	10	0.2	410	8	106
SPC 13_12	10	1	410	8	106
SPC 13_13	10	2.5	410	8	106

Table: *List and name of the samples used in the study of spc poly-Si absorber layers from high-rate deposited a-Si:H films (Chapter 6).*

Sample no	*SiH_4 flow (sccm)*	*RF power density (mW/cm^2)*	*Deposition rate (nm/min)*
HRD 1.1	60	67	18
HRD 1.2	80	67	29
HRD 1.3	100	67	40
HRD 1.4	120	67	48
HRD 1.5	160	67	63
HRD 1.6	200	67	71
HRD 1.7	225	67	75
HRD 1.8	200	67	71
HRD 1.9	200	100	92
HRD 1.10	200	133	81
HRD 1.11	200	167	69
HRD 1.12	200	200	67
HRD 1.13	250	100	91
HRD 1.14	250	133	107
HRD 1.15	300	133	125
HRD 1.16	300	167	107
HRD 1.17	350	130	130
HRD 1.18	400	167	146
HRD 1.19	400	133	135